ABSTRACT

KLEIN, MARY ALTHEA.

Substituted Carbonyl-Linked Bis(dioxolene) Complexes: Is a Carbonyl an Effective Ferromagnetic Coupler?

(Under the direction of Dr. David A. Shultz)

Bis-semiquinone complexes have been successfully synthesized and characterized to give triplet ground states from the use of typical coupling units. The typical coupling unit ethenylidene has produced compounds with ground state triplets, *i.e.* trimethylenemethane (TMM). Upon substitution of oxygen onto the ethenylidene coupler of TMM, to give oxyallyl, the degeneracy of the two non-bonding molecular orbitals is broken, which allows configuration interaction to take place between the ground configuration singlet and the excited configuration singlet. Therefore, it is conceivable that oxyallyl would produce a ground state singlet but computational methods have computed a triplet ground state.

We propose to use oxyallyl as the linker between two semiquinones to produce a ground state triplet. Previous work using oxyallyl as the linker was unsuccessful in producing the bis-semiquinone complex without the use of an oxidizing agent, which eventually decomposed the complex. We will use the same semiquinone backbone but substitute a more electron-donating group, methoxy, onto the phenyl ring increasing the oxidizability to produce the bis-semiquinone complex. Another approach in increasing the oxidizability is to use a less electronegative metal, manganese, on the complex. Once the bis-semiquinone is synthesized then characterization will enable us to determine the ground state of the bis-semiquinone and the type of spin coupling taking place between the two electrons.

SUBSTITUTED CARBONYL-LINKED BIS(DIOXOLENE) COMPLEXES: IS A CARBONYL AN EFFECTIVE FERROMAGNETIC COUPLER?

by

MARY ALTHEA KLEIN

A thesis submitted to the Graduate Faculty of
North **C**arolina **S**tate **U**niversity
in partial fulfillment of the requirements for the
Degree of Master of Science

CHEMISTRY

Raleigh, North Carolina
2003

APPROVED BY:

_____
David A. Shultz
Chair of Advisory Committee

_____ _____
Dennis W. Wertz Tatyana I. Smirnova

DEDICATION

I dedicate this work to my parents Kenneth and Deedee Klein. You have always told me I can do anything I put my mind to, and for that, I wish to express my gratitude to the both of you. If I had to "choose" all over again, I would still "choose" you! I love you both "more than where the number stops." I also want to dedicate this work to my grandparents, Angelo and Effie Kyrmas, and Mary Jane and Leonard Klein. You have been just as supportive and a staple in my life as my parents. You have always been there and your love means so much to me. Without all these people I would not have had as many opportunities in my life or the strength to get through the challenges that came with those opportunities.

I love you all so very much!!

BIOGRAPHY

Mary Althea Klein, born April 11, 1978 in Reading, Pennsylvania to father Kenneth Charles Klein, mother Deedee Klein, and sibling Christopher Kermit Klein. Mary has successfully completed the Muhlenberg school district requirements for grades kindergarten through 12th, graduating with a 3.91GPA and ranking 12th in her class. She has also received honor awards while attending Muhlenberg including National Honor Society, an academic achievement award, and a service award.

Mary attended West Chester University of Pennsylvania and received a bachelor of science in the field of chemistry with a GPA of 3.11. She endured a rigorous chemistry program approved by the American Chemical Society and was accepted to the Pennsylvania Equine Toxicology Research Laboratory for an internship. Her accolades include being part of two different research projects one of which she was a Merck scholar. While at West Chester she was able to balance school with initiation into the Zeta Eta Chapter of Alpha Xi Delta where she served a year as secretary to the executive board.

Mary decided to attend North Carolina State University in hopes to gain a better understanding and background in the discipline of chemistry. Under the direction of Dr. David A. Shultz, she has successfully synthesized new materials and has been able to characterize these materials using unique instrumentation such as electron paramagnetic resonance and super-conducting quantum interference device. She successfully fulfilled the requirements for a master of science degree on March 20, 2003.

ACKNOWLEDGEMENTS

I have always been told that I can accomplish anything I put my mind to. Well, I have put my mind toward striving to earn a higher degree in the chemistry field and I have been able to accomplish that mission. I would not have been able to do such a mission without the support of my family, friends, colleagues, professors, and most of all advisors. To all these people I wish to express my courage, love, ambition, and most of all my gratitude toward their understanding, patience, and support.

I would like to thank my parents Kenneth and Deedee Klein, my grandparents Angelo and Effie Kyrmas, and Mary Jane and Leonard Klein, and my brother Christopher Klein for their continuous support throughout my student career. Your support carried miles away. I would also like to thank Joshua Yohannan for all his encouragement and love, and taking me out on those "sweet tooth" runs. He believed in me when I didn't believe in myself and he never let me quit. Mister man you are truly a good person. Thanks to my best friends from home, even though you guys were hundreds of miles away you still managed to visit, call, email, and stay my best friends. Thank goodness for the summer beach trip!

I would also like to give thanks to my advisors at West Chester University of Pennsylvania, Dr. John Townsend and Dr. Melissa Cichowicz for their recommendations and their graduate school horror stories. Special thanks to some of the Chemistry department staff at NCSU, you made life here a bit easier. Crissy Williams for all your help in understanding what needed to be done and by what date. Glenn Hennessee for computer information, pilot fish stories, and office chats. Cynthia Wertz for her patience with teaching and professor conflicts.

Last but not least, I would like to thank Dr. David A. Shultz and the past and present Shultz group members. Dr. Shultz was always patient, even with my so called "stupid" questions, and was able to explain things in a manner that books will never be able to do. This is what makes him a great professor and advisor. To those that are part of the Shultz group thank you for all contributions in helping me better understand chemistry and life beyond Pennsylvania. Rosario Fico, Kathryn Preuss, Krishna Kumar, Scot Bodnar, Christopher Mussari, Candice Brannen, Jessica Queen, R. Joesph Bousquet "Joey Biscuit", Sofi Bin-Salamon, Kira Bostrikova, Joseph Sloop, and Tashni-Ann Coote.

TABLE OF CONTENTS

	Page
LIST OF FIGURES	viii
LIST OF TABLES	xiii
LIST OF SCHEMES	xiv

CHAPTER I: BIRADICALS

I.1. Biradical Introduction.	1
I.2. Orbital Approximation.	1
I.3. The Pauli Exclusion Principle.	2
I.4. Spin State Energies.	5
I.5. Hund's Rule.	14
I.6. Spin Coupling.	14
I.7. Valence Bond Model vs. Molecular Orbital Theory.	15
I.8. Common Coupling Units.	21
I.9. Previous Studies on Oxyallyl and Some Oxyallyl Derivatives.	25
Chapter I References	33

CHAPTER II: MAGNETOMETRY

II.1. Introduction to Magnetism and Types of Magnetism.	35
II.2. Electron Paramagnetic Resonance (EPR).	45
II.3. Super-conducting Quantum Interference Device (SQUID).	54
Chapter II References	54

CHAPTER III: SYNTHESIS AND CHARACTERIZATION OF OXYALLYL TYPE BIS-SEMIQUINONES

III.1. The Semiquinone Radical Anion. 56

III.2. Semiquinone-Metal Interactions. 66

III.3. Previous Studies on OXA Derivatives and the Stability of Carbonyl-Linked Bis-Semiquinones. 69

III.4. Results, Discussion, and Conclusions to Producing the First Isolable Carbonyl-Linked Bis-Semiquinone. 82

Chapter 3 References 100

EXPERIMENTALS 102

Experimental References 115

LIST OF FIGURES

Figure I.1. Orthogonality of two p-orbitals with overlap density designated by the shaded region. 3

Figure I.2. Four combinations of spins for two electrons in two orbitals; paired α's, paired β's, and two combinations of paired $\alpha\beta$. 4

Figure I.3. An increase in the exchange integral stabilizes the triplet state and destabilizes the singlet state. 10

Figure I.4. Simple depiction of energy differences within, 2**k**, and between the zwitterionic excited state configurations ($^{1}EC_{1,2}$) and the open-shell ground configurations ($^{1,3}GC$), j^{o}-j, and their wavefunctions. 11

Figure I.5. Configuration interaction of a two-electron two-orbital system. 13

Figure I.6. Simple diagram depicting Hund's rule and electron spin coupling. 15

Figure I.7. VB model using α and β spin designation for TMM and TME. 17

Figure I.8. VB model using the "starred" designation for TMM and TME. 18

Figure I.9. Disjoint or non-coextensive FOs of TME. 19

Figure I.10. Non-disjoint or coextensive FO's of TMM. 20

Figure I.11. Common coupling units ethenylidene, phenylene, cyclobutadienylidene coupling two methylene radical moieties. 22

Figure I.12. Ethenylidene as an antiferromagnetic and ferromagnetic CU when two methylene radical moieties are attached in a 1,1-connection and 1,2-connection. 23

Figure I.13. Phenylene as an antiferromagnetic and ferromagnetic CU when two methylene radical moieties are attached *ortho*, *para*, and *meta* to one another. 24

Figure I.14. Cyclobutadienyledene as an antiferromagnetic and ferromagnetic CU when two radical moieties are attached in a 1,2-connection and 1,3-connection. 24

Figure I.15. Three states of TMM T_0, S_1, and S_2. 26

Figure I.16. The triplet state and two singlet states of open-shell oxyallyl, and the closed-shell zwitterionic oxyallyl. 26

Figure I.17. MO energy level diagram for oxyallyl and TMM with spin densities. 27

Figure I.18. Energy level diagram of TMM and OXA considering configuration interaction. 28

Figure I.19. Biradicals studied in the determination of triplet and singlet state C=O bond lengths. 30

Figure I.20. Computed C-O bond lengths of oxyallyl. 31

Figure I.21. Stretching frequencies of triplet and singlet cyclopentanone-2,5-diyl and closed-shell bicylco[2.1.0]pentan-5-one. 32

Figure II.1. Inverse $\chi_{para.}$ as a function of temperature for a paramagnet. 38

Figure II.2. Inverse χ as a function of Temperature. For $\theta = 0$ ideal paramagnetic behavior is exists, $\theta > 0$ ferromagnetic interactions exists, and $\theta < 0$ antiferromagnetic interactions exist. 39

Figure II.3. Saturation magnetization values of different spin systems (g fixed at 2); • is S = 1, ♦ is S = 2, ■ is S = 3, and ▲ is S = 4. 42

Figure II.4. Types of magnetism including diamagnetism, paramagnetism, ferromagnetism, and antiferromagnetism. 44

Figure II.5. EPR detectable one-electron system. 45

Figure II.6. Exchange parameter J in relation with the ZFS parameters D and E. 46

Figure II.7. EPR detectable two-electron system where $M_s = \pm 1, 0$, and $\Delta M_s = 1$ transition. 47

Figure II.8. Energy separation of microstates in relation with the molecular geometry of an atom, triplet excited benzene, and triplet excited naphthalene. 49

Figure II.9. Simulated spectra for a triplet excited species with cubic symmetry ($D = 0$), axial symmetry ($D \neq 0$; $E = 0$), and rhombic symmetry ($D \neq 0$; $E \neq 0$). 51

Figure II.10. The "forbidden" $\Delta M_s = 2$ transition in relation to the $\Delta M_s = 1$ transition of a triplet species. 52

Figure III.1. A semiquinone product resulting from the one-electron reduction of an orthoquinone and the one-electron oxidation of a catecholate. 56

Figure III.2. The semiquinone's singly occupied molecular orbital (SOMO). 57

Figure III.3. TMM-type bis-semiquinone. 58

Figure III.4. Hückel coefficients of a bis-semiquinone with an ethenylidene coupling unit. 59

Figure III.5. Carbonyl-linked bis-semiquinone and resonance hybrids of the triplet ground state. 60

Figure III.6. Hückel coefficients of a bis-semiquinone with a carbonyl coupling unit. 61

Figure III.7. Sterically protected semiquinone (left) and bis-semiquinone (right). 62

Figure III.8. Potassium hydro-tris(3-cumenyl-5-methyl pyrazolyl)borate ligand ($Tp^{Cum, Me}$). 64

Figure III.9. Comproportionation of one equivalent of quinone and one equivalent of catecholate yielding two equivalents of semiquinone. 65

Figure III.10. Semiquinone production upon air oxidation of one equivalent of catecholate and one equivalent of metal ion. 65

Figure III.11. Antiferromagnetic and ferromagnetic exchange coupling between the *d*-orbitals and *p*-orbitals. 67

Figure III.12. Antiferromagnetic and ferromagnetic metal-ligand exchange coupling with a semiquinone. 68

Figure III.13. Two electroactive groups conjugated to an ethenlydiene coupling unit but not conjugated to one another. 70

Figure III.14. TMM-type bis-semiquinones, exchange parameters, J, and structural deviation parameters. 71

Figure III.15. Carbonyl-linked bis-arylnitrene. 73

Figure III.16. $(Tp^{Cum, Me}Zn)_2$-*t*-Bu. 73

Figure III.17. ORTEP representations of the crystal structures **(3.4)** and **(3.5)**. Cumenyl groups are omitted for clarity. 76

Figure III.18. Hypothetical carbonyl-linked quinonemethide-semiquinone. 78

Figure III.19. Comparison of bond lengths with 3,5-DBSQZn($Tp^{Cum, Me}$) and carbonyl-linked **(3.4)** and **(3.5)**. 79

Figure III.20. Delocalization of -1 formal charge of **(3.5)**. 79

Figure III.21. EPR spectra at (77K; THF) of oxidized carbonyl-linked **(3.4)** and **(3.5)** (bottom) and $\Delta M_s = 2$ transition (inset). Simulated EPR spectrum with $|\mathbf{D}/hc| = 0.01077cm^{-1}$ and $|\mathbf{E}/hc| = 0.0011cm^{-1}$. 81

Figure III.22. Experimental EPR spectrum (77K; MTHF) of a mixture of oxidized **(3.4)** and **(3.5)** (bottom) and the $\Delta M_s = 2$ transition near half field (inset). Simulated EPR spectrum with $|\mathbf{D_1}/hc| = 0.0108cm^{-1}$ and $|\mathbf{D_2}/hc| = 0.0126cm^{-1}$. 84

Figure III.23. Variable EPR studies on a mixture of **(3.4)** and **(3.5)** suggests ferromagnetic coupling of the two electron spins. 86

Figure III.24. ORTEP representation of the crystal structure **(3.8)**. Cumenyl groups are omitted for clarity. 88

Figure III.25. Comparison of bond lengths with 3,5-DBSQZn($Tp^{Cum, Me}$) and carbonyl-linked (3.8) where $\Sigma_{avg} |\Delta_i| = 0.203 \pm 0.04$Å. 89

Figure III.26. UV-Vis spectrum of **(3.8)** with bis-semiquinone $n \rightarrow \pi^*$ transition. 90

Figure III.27. Saturation magnetization data of **(3.8**) suggests ferromagnetic coupling between to the two electron spins. 91

Figure III.28. Variable SQUID magnetic data of **(3.8)**. 92

Figure III.29. UV-Vis spectrum of **(3.9)** with bis-semiquinone $n \rightarrow \pi^*$ transition. 94

Figure III.30. Saturation magnetization data of **(3.9)** suggests ferromagnetic coupling between to the two electron spins. 95

Figure III.31. Experimental EPR spectrum (77K; MTHF) of bis-semiquinone **(3.17)** (bottom) and the $\Delta M_s = 2$ transition near half field (inset). Simulated EPR spectrum with $|\mathbf{D}/hc| = 0.00919 cm^{-1}$ and $|\mathbf{E}/hc| = 0.000804 cm^{-1}$. 98

Figure III.32. Variable EPR studies on a mixture of **(3.17)** suggests ferromagnetic coupling of the two electron spins. 99

LIST OF TABLES

Table III.1. Important Bond Lengths (Å) for **(3.4)**. 77

Table III.2. Important Bond Lengths (Å) for **(3.5)**. 77

Table III.3. Important Bond Lengths (Å) for **(3.8)**. 88

LIST OF SCHEMES

Scheme III.I. Synthesis of bis-catechol **(3.3)**. 74

Scheme III.2. Failed synthetic attempt to produce $(Tp^{Cum, Me}Zn)_2$-*t*-Bu. 75

Scheme III.3. Alternate synthesis of bis-catechol **(3.3)**. 83

Scheme III.4. Successful synthetic attempt to produce **(3.8)**. 87

Scheme III.5. Attempted synthesis of **(3.9)**. 93

Scheme III.6. Synthesis of Bis-Catechol **(3.16)**. 96

Scheme III.7. Attempted synthesis of complex **(3.17)**. 97

CHAPTER I: BIRADICALS

I.1. Biradical Introduction.

Biradical molecules have been known since the early twentieth century but were not studied experimentally until the 1960's when Paul Dowd successfully observed the triplet state of trimethylenemethane, TMM.[1.1] Since Dowd's electron paramagnetic resonance experiments of TMM, other biradical molecules have been found to have singlet and triplet ground states. For example, tetramethyleneethane, TME, has a singlet ground state, and *meta*-xylylene has a triplet ground state.[1.2] *Meta*-xylylene, TMM, and TME are just a few of many molecules that have been used to make more stable biradical compounds. Some of these more stable biradical compounds are produced by substitution of TMM and *meta*-xylylene. Chapter one will focus on theories, rules, and principles to predict the ground state of biradicals.

I.2. Orbital Approximation.

Since the Schrödinger Equation for a multiple electron atom is mathematically challenging, a compromise is to use the orbital approximation. The wavefunction for an electron in orbital ψ, has energy E. The wavefunction for a many-electron atom is written as $\Psi(r_1, r_2, ...)$, where r_n are the Cartesian coordinates.[1.3] In the orbital approximation, it is assumed that there are no interactions, between the electrons and that each electron occupies its own orbital. In this case, the wavefunction for a many-electron atom is given by Eqn. I.1, where $\psi(r_1)$ is the one-electron orbital wavefunction.

$$\Psi(r_1, r_2, ...) = \psi(r_1)\psi(r_2)... \qquad \textbf{Eq. I.1}$$

Since the electrons move independently of each other, the energy of the system is the sum of the energies of the electrons, Eqn. I.2.

$$E_n = E_1 + E_2 \ldots \qquad \textbf{Eq. I.2}$$

Because we wish to focus on *bi*radicals, a two-electron system will be considered. If in a two-electron system the energy of the two electrons is summed, the Schrödinger Equation requires that the two wavefunctions $\psi(r_1)$ and $\psi(r_2)$ are multiplied. The product will then be the wavefunction of the two-electron system, $\Psi(r_1, r_2)$.

Eqn. I.1 describes the two electrons as being distinguishable. However, since it is known that any two electrons are indistinguishable there needs to be a wavefunction that describes this indistinquishability.[1.3, 1.4]

I.3. The Pauli Exclusion Principle.

There are four quantum numbers describing one electron in an atomic orbital. These quantum numbers are designated as: *n*, the principle quantum number; *l*, the angular momentum quantum number; m_l, the magnetic quantum number; and m_s, the spin quantum number. The Pauli exclusion principle, simply stated, expresses that two electrons must not possess the same four quantum numbers. If two electrons were to occupy the same orbital, then the two electrons must have opposite spin quantum numbers.

The <u>total</u> wavefunction must be antisymmetric with respect to the exchange of two electrons.[1.3, 1.4, 1.5] Unlike the orbital approximation, the total wavefunction accounts for both the orbital wavefunction and the spin wavefunction. First, the orbital wavefunction will be examined. A simple two-electron, two-orbital system can be described by Eqn. I.3 and Figure I.1.

$$\psi_{xy} = \varphi_x(1)\varphi_y(2) \qquad \textbf{Eq. I.3}$$

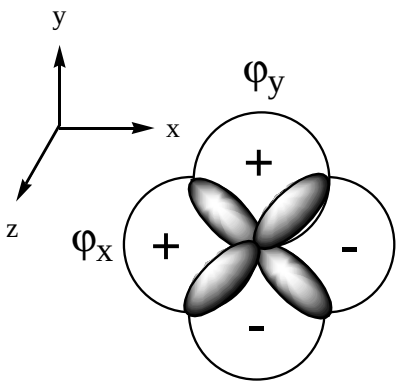

Figure I.1. Orthogonality of two p-orbitals with overlap density designated by the shaded region.

Again, there is the problem of being able to distinguish between the two electrons, as given by the square of Eqn. I.3: $\varphi^2_x(1)\varphi^2_y(2)$. Therefore, an acceptable orbital wavefunction would be one that gives $\psi_{xy} = \pm \psi_{xy}$ when operated upon by the permutation operator, P_{12}, a function that switches (permutes) electron labels. Symmetric and antisymmetric orbital wavefunctions are generated as linear combinations of Eqn. I.3 and its permutation gives Equations. I.4 and I.5.

$$\psi_{\text{orb, S}} = 0.707\left[\varphi_x(1)\varphi_y(2) + \varphi_y(1)\varphi_x(2)\right] \qquad \textbf{Eq. I.4}$$

$$\psi_{\text{orb, A}} = 0.707\left[\varphi_x(1)\varphi_y(2) - \varphi_y(1)\varphi_x(2)\right] \qquad \textbf{Eq. I.5}$$

Eqn. I.4 is a symmetric wavefunction, because when it is operated upon by P_{12}, it gives back the original wavefunction. Eqn. I.5 is an antisymmetric wavefunction, because upon being operated on by P_{12}, it gives back the negative of the original wavefunction. It can be seen from the symmetric and antisymmetric orbital wavefunctions that the electrons are indistinguishable.

An electron can take on the spin, α, which is spin "up", or β, which is spin "down". In a two-orbital, two-electron system there are four possible combinations of spin, Figure I.2.

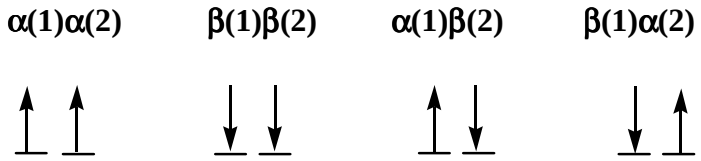

Figure I.2. Four combinations of spins for two electrons in two orbitals; paired α's, paired β's, and two combinations of paired αβ.

The first two spin combinations, shown in Equations I.6 and I.7, when operated upon by P_{12} give back their original wavefunction. However, the latter two combinations are neither symmetric nor antisymmetric. This poses the same problem as with the orbital wavefunction, Eqn. I.3. Since the two spins are distinguishable, linear combinations must be taken to produce a symmetric spin wavefunction and an antisymmetric spin wavefunction, Equations I.8 and I.9.

$$\psi_{\uparrow\uparrow,S} = \alpha(1)\alpha(2) \qquad \textbf{Eq. I.6}$$

$$\psi_{\downarrow\downarrow,S} = \beta(1)\beta(2) \qquad \textbf{Eq. I.7}$$

$$\psi_{\uparrow\downarrow,S} = 0.707[\alpha(1)\beta(2) + \beta(1)\alpha(2)] \qquad \textbf{Eq. I.8}$$

$$\psi_{\uparrow\downarrow,A} = 0.707[\alpha(1)\beta(2) - \beta(1)\alpha(2)] \qquad \textbf{Eq. I.9}$$

Eqn. I.8 is a symmetric wavefunction; because when it is operated upon with P_{12}, it gives back the original wavefunction. The wavefunction from Eqn. I.9 is an antisymmetric wavefunction; because upon being operated upon with P_{12}, it gives back the negative of the wavefunction. It can be seen from the symmetric spin wavefunction and antisymmetric spin wavefunction that the spins are indistinguishable; therefore, they are acceptable wavefunctions.

Now that both components of the total wave function have been examined and, as mentioned, the total wavefunction must be antisymmetric, four antisymmetric total wavefunctions can be produced, Equations I.10, I.11, I.12, and I.13.[3]

$$\Psi_{tot} = \psi_{\text{orb, A}}\psi_{\uparrow\uparrow,S} \qquad \textbf{Eq. I.10}$$

$$\Psi_{tot} = \psi_{\text{orb, A}}\psi_{\downarrow\downarrow,S} \qquad \textbf{Eq. I.11}$$

$$\Psi_{tot} = \psi_{\text{orb, A}}\psi_{\uparrow\downarrow,S} \qquad \textbf{Eq. I.12}$$

$$\Psi_{tot} = \psi_{\text{orb, S}}\psi_{\uparrow\downarrow,A} \qquad \textbf{Eq. I.13}$$

In Equations I.10, I.11, and I.12, the spatial wavefunction is the antisymmetric part of the total wavefunction, and these three Equations are components of a triplet state. In Eqn. I.13 the spin wavefunction is the antisymmetric part of the total wavefunction and is a singlet state. The spatial wavefunction is used to show the stabilization of the triplet state relative to the singlet state.

I.4. Spin State Energies.

As shown from the Pauli exclusion principle, a triplet state and a singlet state are produced from the orbital and spin wavefunctions. When two electrons are brought close together they repel, and it is the repulsion energy of these two electrons that will be used to

predict which state is more stable. The spatial wavefunctions will be used to determine the repulsion energies, since the orbitals dictate the position of the electrons.

The ground state configuration of an atom or molecule is dictated by the exchange parameter **J**, as shown in Eqn. I.14.

$$\mathbf{J} = J_F - J_{AF} \qquad \textbf{Eq. I.14}$$

In Eqn. I.14, the ferromagnetic contribution, J_F, considers the spin state coupling in the ground configuration, and the antiferromagnetic contribution, J_{AF}, considers the spin state coupling resulting from mixing of the ground configuration with an excited configuration.

First, the electron-electron repulsion energy of the ground singlet configuration will be calculated. The spatial wavefunction being used is from Eqn. I.4. To obtain the repulsion energy, the coulomb operator, e^2/r_{12}, where e is the charge on an electron and r_{12} is the distance between the two electrons, will be used as shown in Eqn. I.14.

$$E_{\text{singlet}} = \left\langle \psi_{\text{orb,S}} \left| \frac{e^2}{r_{12}} \right| \psi_{\text{orb,S}} \right\rangle \qquad \textbf{Eq. I.14}$$

or

$$E_{\text{singlet}} = \left\langle 0.707\left[\varphi_x(1)\varphi_y(2) + \varphi_y(1)\varphi_x(2)\right] \left| \frac{e^2}{r_{12}} \right| 0.707\left[\varphi_x(1)\varphi_y(2) + \varphi_y(1)\varphi_x(2)\right] \right\rangle \qquad \textbf{Eq. I.15}$$

If the symmetric spatial wavefunction is operated upon by the coulomb operator then Eqn. I.16 results.

$$\begin{aligned} E_{\text{singlet}} = 0.5\Bigg\langle & \left[\varphi_x(1)\varphi_y(2)\left|\frac{e^2}{r_{12}}\right|\varphi_x(1)\varphi_y(2)\right] + \left[\varphi_x(1)\varphi_y(2)\left|\frac{e^2}{r_{12}}\right|\varphi_y(1)\varphi_x(2)\right] \\ & + \left[\varphi_y(1)\varphi_x(2)\left|\frac{e^2}{r_{12}}\right|\varphi_x(1)\varphi_y(2)\right] + \left[\varphi_y(1)\varphi_x(2)\left|\frac{e^2}{r_{12}}\right|\varphi_y(1)\varphi_x(2)\right]\Bigg\rangle \end{aligned} \qquad \textbf{Eq. I.16}$$

The first and the fourth integral show electron 1 on orbital φ_x and electron 2 on orbital φ_y or electron 1 on orbital φ_y and electron 2 on orbital φ_x, respectively. This is the same as stating that one electron occupies one orbital and the other electron occupies the other orbital. By combining the similarly labeled electron orbitals of sets one and four the top part of Eqn. I.17 is yielded and the electron-electron repulsion energy is described as the coulomb integral, $\mathbf{j}_{xy}$.

$$E_{\text{singlet}} = 0.5\left\langle \left[\varphi_x(1)\varphi_x(1)\left|\frac{e^2}{r_{12}}\right|\varphi_y(2)\varphi_y(2)\right] + \left[\varphi_y(1)\varphi_y(1)\left|\frac{e^2}{r_{12}}\right|\varphi_x(2)\varphi_x(2)\right] + \left[\varphi_x(1)\varphi_y(1)\left|\frac{e^2}{r_{12}}\right|\varphi_x(2)\varphi_y(2)\right] + \left[\varphi_x(1)\varphi_y(1)\left|\frac{e^2}{r_{12}}\right|\varphi_x(2)\varphi_y(2)\right]\right\rangle \qquad \textbf{Eq. I.17}$$

Upon examination of sets two and three from Eqn. I.16 both electrons one and two are in both orbitals φ_y and φ_x simultaneously. This is possible, but only if the two electrons are in the *overlap region*, the dark region in Figure I.1. By combining the similarly labeled electron orbitals of sets two and three the bottom part Eqn. I.17 is yielded and the electron-electron repulsion in the overlap region is described as the exchange integral, $\mathbf{k}_{xy}$. Therefore, Eqn. I.17 can be modified to give Eqn. I.18.

$$E_{\text{singlet}} = \mathbf{j}_{xy} + \mathbf{k}_{xy} \qquad \textbf{Eq. I.18}$$

The energy of the ground configuration triplet can now be predicted using the same method as the energy of the singlet. The antisymmetric orbital wavefunction of the triplet will be used as shown in Eqn. I.19.

$$E_{\text{triplet}} = \left\langle \psi_{\text{orb, A}}\left|\frac{e^2}{r_{12}}\right|\psi_{\text{orb, A}}\right\rangle \qquad \textbf{Eq. I.19}$$

or

$$E_{\text{triplet}} = \left\langle 0.707\left[\varphi_x(1)\varphi_y(2) - \varphi_y(1)\varphi_x(2)\left|\frac{e^2}{r_{12}}\right|0.707\left[\varphi_x(1)\varphi_y(2) - \varphi_y(1)\varphi_x(2)\right]\right]\right\rangle \qquad \textbf{Eq. I.20}$$

If the antisymmetric orbital wavefunction is operated by the coulomb operator, Eqn. I.21 is yielded.

$$E_{\text{triplet}} = 0.5\left\langle \begin{array}{l} \left[\varphi_x(1)\varphi_y(2)\left|\frac{e^2}{r_{12}}\right|\varphi_x(1)\varphi_y(2)\right] - \left[\varphi_x(1)\varphi_y(2)\left|\frac{e^2}{r_{12}}\right|\varphi_y(1)\varphi_x(2)\right] \\ -\left[\varphi_y(1)\varphi_x(2)\left|\frac{e^2}{r_{12}}\right|\varphi_x(1)\varphi_y(2)\right] + \left[\varphi_y(1)\varphi_x(2)\left|\frac{e^2}{r_{12}}\right|\varphi_y(1)\varphi_x(2)\right] \end{array}\right\rangle \qquad \textbf{Eq. I.21}$$

Again, upon examination of Eqn. I.21 and combining like terms, the first and the fourth sets, show electron 1 is on orbital φ_x and electron 2 is on orbital φ_y or electron 1 is on orbital φ_y and electron 2 is on orbital φ_x, respectively. Examining integrals two and three shows that both electron's one and two are in both orbitals φ_y and φ_x simultaneously. By combining the similarly labeled electron orbitals of sets two and three the top part Eqn. I.22 is yielded, and again the electron-electron repulsion energy is described as the coulomb integral, $\mathbf{j}_{xy}$.

$$E_{\text{triplet}} = 0.5\left\langle \begin{array}{l} \left[\varphi_x(1)\varphi_x(1)\left|\frac{e^2}{r_{12}}\right|\varphi_y(2)\varphi_y(2)\right] - \left[\varphi_y(1)\varphi_y(1)\left|\frac{e^2}{r_{12}}\right|\varphi_x(2)\varphi_x(2)\right] - \\ \left[\varphi_x(1)\varphi_y(1)\left|\frac{e^2}{r_{12}}\right|\varphi_x(2)\varphi_y(2)\right] + \left[\varphi_x(1)\varphi_y(1)\left|\frac{e^2}{r_{12}}\right|\varphi_x(2)\varphi_y(2)\right] \end{array}\right\rangle \qquad \textbf{Eq. I.22}$$

Upon examination of sets two and three from Eqn. I.21, both electrons one and two are in both orbitals φ_y and φ_x simultaneously. Again, this is possible, but only if the two electrons are in the overlap region. By combining the similarly labeled electron orbitals of sets two and three the bottom part Eqn. I.22 is yielded and the electron-electron repulsion in

the overlap region is described as the exchange integral, $\mathbf{k}_{xy}$. Therefore, Eqn. I.22 can be modified to give Eqn. I.23.

$$E_{\text{triplet}} = \mathbf{j}_{xy} - \mathbf{k}_{xy} \qquad \textbf{Eq. I.23}$$

The gap between the triplet and singlet states can be measured from the difference in energies of the two states, ΔE_{ST}. This difference is shown to be $2\mathbf{k}_{xy}$, which means that the triplet state lies $2\mathbf{k}_{xy}$ below the singlet state.

$$\Delta E_{ST} = E_{\text{singlet}} - E_{\text{triplet}} = 2\mathbf{k}_{xy} \qquad \textbf{Eq. I.24}$$

Stating Eqn. I.24 verbally, there is less electron-electron repulsion when the system's electrons align parallel, ferromagnetic alignment, as in a triplet state. As the exchange integral becomes smaller, the difference between the singlet and triplet states becomes smaller, the electron-electron repulsion energy of two parallel spins is increased, Figure I.3. Therefore, the ferromagnetic contribution, J_F, to the system is $2\mathbf{k}_{xy}$.

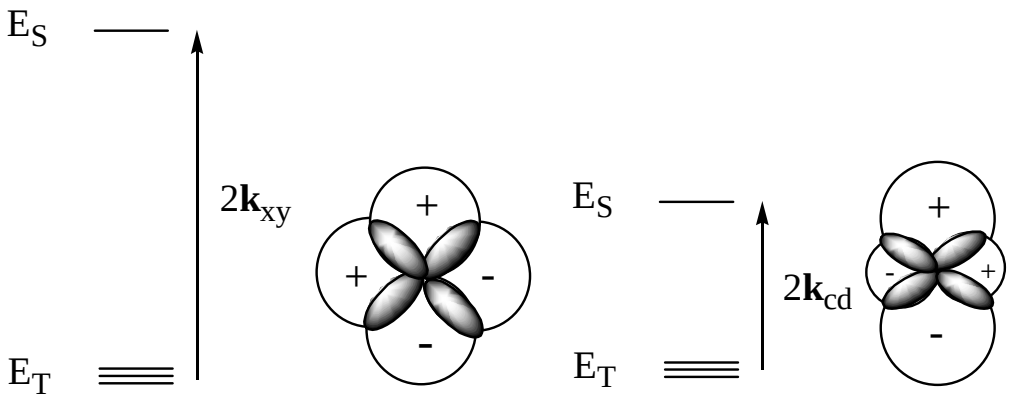

Figure I.3. An increase in the exchange integral stabilizes the triplet state and destabilizes the singlet state.

The antiferromagnetic contribution can now be considered. The antiferromagnetic contribution is given by Equation I.25.[1.4]

$$J_{AF} = \frac{\left\langle {}^1GC \middle| H \middle| {}^1EC \right\rangle^2}{j^\circ - j} \qquad \textbf{Eq. I.25}$$

In Eqn. I.25 $^1\mathbf{GC}$ is described by Eqn. I.4, $^1\mathbf{EC_1}$ and $^1\mathbf{EC_2}$, will be described shortly, j° is the one-center columbic repulsion between the two electrons in the *same* orbital, and j is the two-center columbic repulsion between the two electrons in *different* orbitals. Figure I.4 is an energy level diagram describing the energy differences within each configuration and the energy differences between each configuration.

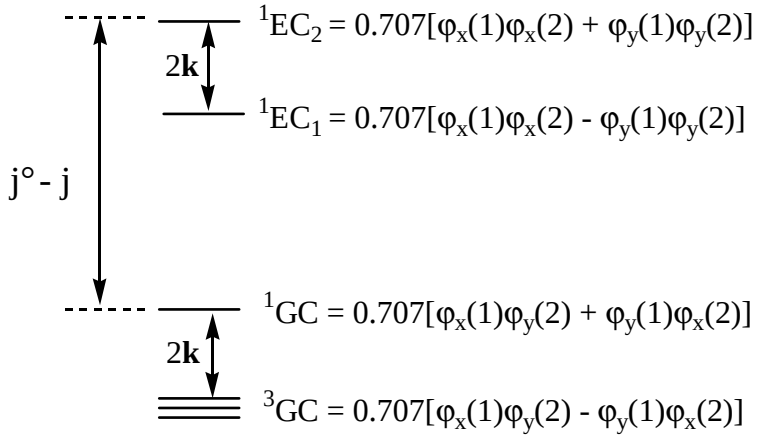

Figure I.4. Simple depiction of energy differences within, 2**k**, and between, $j^o - j$, the zwitterionic excited state configurations ($^1EC_{1,2}$) and the open-shell ground configurations ($^{1,3}GC$), and their wavefunctions.

The energy of the excited singlet configuration is described by Equation I.26, where ^1EC_i is described by Eqn. I.27 and I.28. These equations represent the zwitterionic closed-shell singlet state. There is no closed-shell triplet state.

$$E_{\text{singlet, } EC} = 0.5\left\langle {}^1EC_i \left| h(1) + h(2) + \frac{e^2}{r_{12}} \right| {}^1EC_i \right\rangle \qquad \textbf{Eq. I.26}$$

where,

$$^1EC_1 = \left\langle 0.707\left[\varphi_x(1)\varphi_x(2) - \varphi_y(1)\varphi_y(2)\right]\right\rangle \qquad \textbf{Eq. I.27}$$

$$^1EC_2 = \left\langle 0.707\left[\varphi_x(1)\varphi_x(2) + \varphi_y(1)\varphi_y(2)\right]\right\rangle \qquad \textbf{Eq. I.28}$$

and

$$E_{^1EC_1} = 0.5\left\langle \left[\varphi_x(1)\varphi_x(2) - \varphi_y(1)\varphi_y(2)\right] \left| h(1) + h(2) + \frac{e^2}{r_{12}} \right| \left[\varphi_x(1)\varphi_x(2) - \varphi_y(1)\varphi_y(2)\right] \right\rangle \qquad \textbf{Eq. I.29}$$

$$E_{^1EC_2} = 0.5\left\langle \left[\varphi_x(1)\varphi_x(2) + \varphi_y(1)\varphi_y(2)\right] \middle| h(1) + h(2) + \frac{e^2}{r_{12}} \middle| \left[\varphi_x(1)\varphi_x(2) + \varphi_y(1)\varphi_y(2)\right] \right\rangle \quad \textbf{Eq. I.30}$$

The electrostatic portions of these energies are given by Eqn. I.31 and Eqn. I.32.

$$E_{^1EC_1} = j^\circ - k_{xy} \quad \textbf{Eq. I.31}$$

$$E_{^1EC_2} = j^\circ + k_{xy} \quad \textbf{Eq. I.32}$$

However, only $^1\mathbf{EC_2}$ will mix with the ground singlet state configuration.[1.5] The energy difference between $^1\mathbf{EC_2}$ and $^1\mathbf{GC}$ is described by Eqn. I.33.

$$\Delta E_{SS} = j^\circ - j \quad \textbf{Eq. I.33}$$

Equation I.33 is the denominator of Eqn. I.25. The numerator of Eqn. I.25 is described by Eqn. I.34.

$$\left\langle {}^1EC \middle| h(1) + h(2) + \frac{e^2}{r_{12}} \middle| {}^1GC \right\rangle^2 \quad \textbf{Eq. I.34}$$

Neglecting the power of two for the moment,

$$E_{\text{singlet, mixing}} = 0.5\left\langle \varphi_x(1)\varphi_x(2) + \varphi_y(1)\varphi_y(2) \middle| h(1) + h(2) + \frac{e^2}{r_{12}} \middle| \varphi_x(1)\varphi_y(2) + \varphi_y(1)\varphi_x(2) \right\rangle \quad \textbf{Eq. I.35}$$

Expansion of Eqn. I.35 gives Eqn. I.36.

$$E_{\text{singlet, mixing}} = 2\left(\beta_{xy} + l\right) \quad \textbf{Eq. I.36}$$

where β, the resonance integral, is described by Eqn. I.37,

$$\beta_{xy} = \left\langle \varphi_x(1) \middle| h(1) \middle| \varphi_y(1) \right\rangle \quad \textbf{Eq. I.37}$$

and l is the hybrid coulomb integral described by Eqn. I.38,

$$l = \left\langle \varphi_x(1)\varphi_y(1) \middle| \frac{1}{r_{12}} \middle| \varphi_y(1)\varphi_y(2) \right\rangle \quad \textbf{Eq. I.38}$$

The antiferromagnetic contribution can be related to these results to give Eqn I.39.

$$J_{AF} = \frac{4(\beta_{xy} + l)^2}{j^\circ + j_{xy}} \qquad \textbf{Eq. I.39}$$

The exchange parameter **J** can now be described by Equation I.40.

$$\mathbf{J} = 2k_{ab} - \frac{4(\beta_{xy} + l)^2}{j^\circ - j_{xy}} = J_F - J_{AF} \qquad \textbf{Eq. I.40}$$

If the energy difference in $j^o - j$ is small then configuration interaction can take place as shown in Figure I.5.

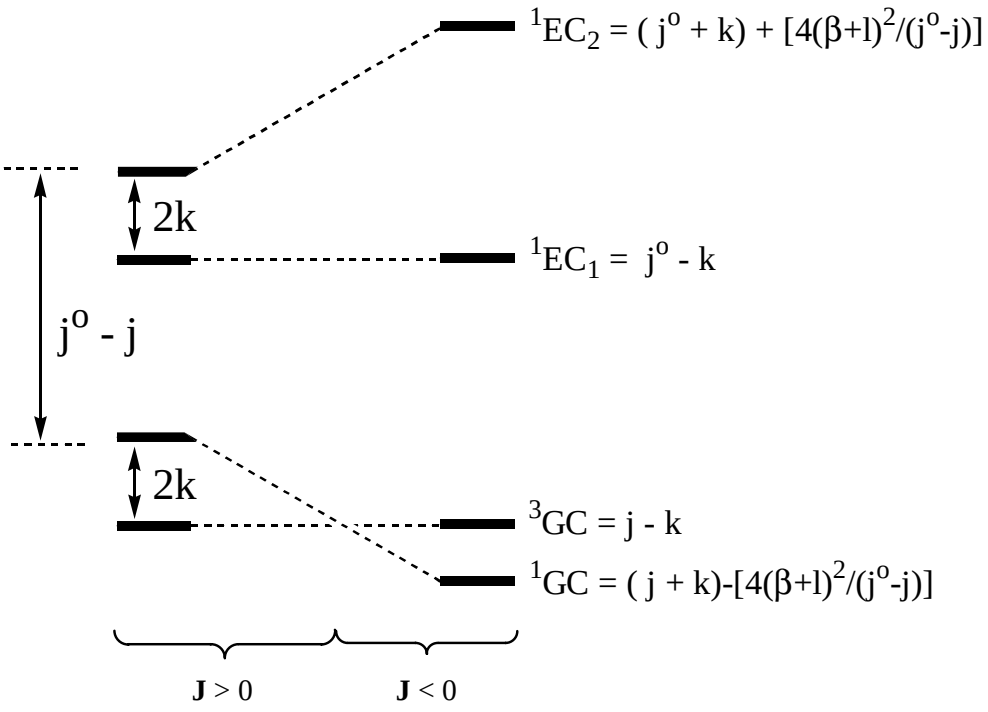

Figure I.5. Configuration interaction of a two-electron two-orbital system.

By using computational methods and/or experiments, the exchange parameter, **J**, can be determined. From this, the components of the ferromagnetic and antiferromagnetic contributions can be determined.

I.5. Hund's Rule.

Hund stated that the spin multiplicity, 2S+1, must be maximized for the ground state of two electrons in a degenerate set of orbitals. Maximum spin multiplicity is dictated by the total spin, S. If two electron spins posses the same spin quantum numbers, $\alpha(1)\alpha(2)$ or $\beta(1)\beta(2)$, their spins will be parallel. If they posses different spin quantum numbers, $\alpha(1)\beta(2)$ or $\alpha(2)\beta(1)$, their spins will be anti-parallel. For parallel spins S, will equal one; and for anti-parallel spins, S will equal zero, as shown in Figure I.6.

The same statements apply to Hund's Rule as derived from the Pauli exclusion principle. As the electrons are brought close in distance to one another, the electron-electron repulsion energy will get larger. Therefore, by maximizing the spin multiplicity, there will be less electron-electron repulsion; and the triplet state will be more stabilized.

I.6. Spin Coupling.

If the electrons are paired in a parallel fashion, triplet state, then the electrons are ferromagnetically coupled. If the electrons are paired in an antiparallel fashion, singlet state, then the electrons are antiferromagnetically coupled, as shown in Figure I.6.

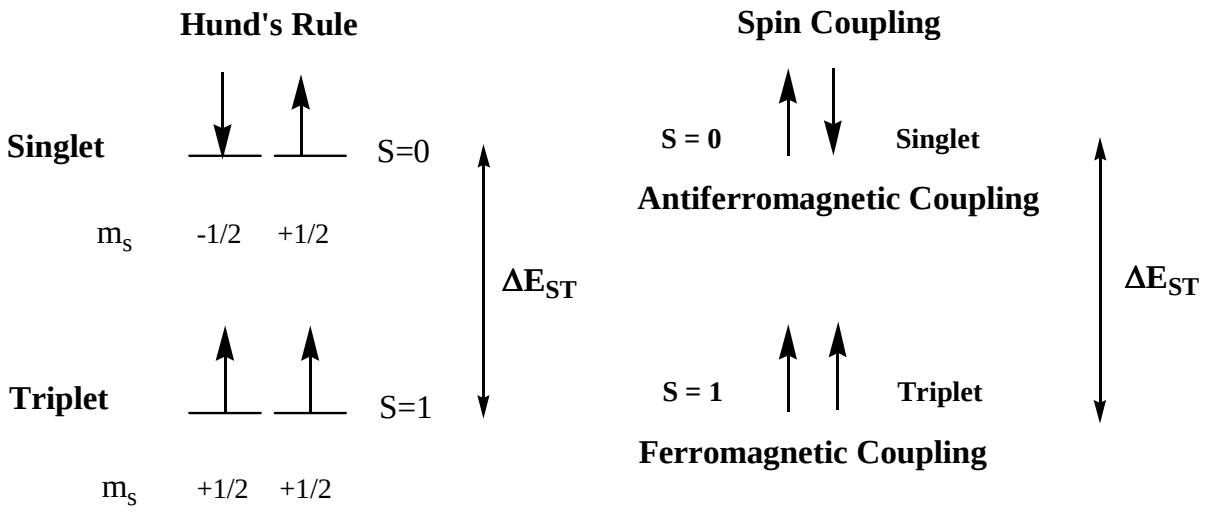

Figure I.6. Simple diagram depicting Hund's rule and electron spin coupling.

When the ground state is a triplet, if ΔE_{ST} is large, the two electrons are strongly ferromagnetically coupled. When ΔE_{ST} is small, the two electrons are weakly ferromagnetically coupled. The same can be concluded when the ground state is a singlet. If ΔE_{ST} is large, the two electrons are strongly antiferromagnetically coupled; or if ΔE_{ST} is small, the two electrons are weakly antiferromagnetically coupled.

I.7. Valence Bond Model vs. Molecular Orbital Theory.

The Pauli exclusion principle and Hund's rule have predicted ground states for atoms; however, there needs to be a way to predict ground states for *molecules*. Both the valence bond (VB) model and molecular orbital (MO) theory are useful in predicting ground states of molecules. The VB model minimizes the electron-electron repulsion by placing one electron on each *p*-π atomic orbital of a molecule. MO theory assumes that each atomic orbital (AO)

combines to make an MO, and the electrons that are not involved in a π-bond are in non-bonding MO's (NBMO).

The definitions of Kekulé and non-Kekulé molecules needs to be introduced to understand both the VB and MO approaches. A Kekulé molecule can be defined as a molecule whose structure, through resonance, shows all atoms involved in π-bonding. Therefore, a non-Kekulé molecule is a molecule whose structure, even through resonance, has at least two atoms not involved in π-bonding.[1.6]

The VB model assumes that one electron occupies the *p*-π atomic orbital on each carbon so that in the system the electron-electron repulsion is minimized.[1.8] There are two ways to use VB model in the determination of the ground state of a molecule. In a Kekulé molecule where there is full π-conjugation each adjacent atom has opposite spins. This spin polarization leads to a pattern of αβαβαβαβ.,, again where α is spin up and β is spin down. The VB model maximizes the amount of αβ combinations, which represents a bond. If any biradical molecule is considered and each atom is assigned α and β spins, by taking the difference in the amount of α and β spins and dividing by two the spin multiplicity can be determined as shown in Eqn. I.41.

$$S = \frac{\Sigma\alpha - \Sigma\beta}{2} \qquad \textbf{Eq. I.41}$$

If the amount of α spins is greater than the amount of β spins by two, the molecule will posses a ground state triplet. If the amount of α spins and β spins are equal, the molecule will posses a ground state singlet. Figure I.7 shows the triplet and singlet ground states of TMM and TME using α and β spin designation.

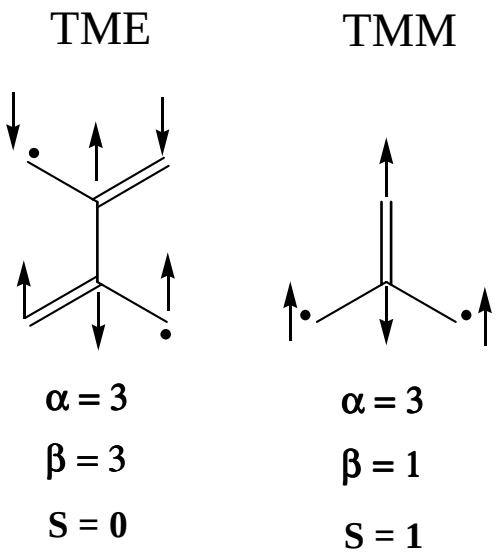

Figure I.7. VB model using α and β spin designation for TMM and TME.

Another way to approach the VB model is by "starring" alternate atoms in a non-Kekulé molecule. The molecules in Figure I.7 are used to show this "starring" approach in Figure I.8. If the carbon atoms containing α spins are starred and the carbon atoms containing β spins are not starred; then by modifying Eqn. I.41, the ground states of these molecules can be determined from Eqn. I.42.[1.2]

$$S = \frac{\Sigma N^{*} - \Sigma N}{2} \qquad \textbf{Eq. I.42}$$

In Eqn. I.42, N^{*} is the amount of starred atoms and N is the amount of unstarred atoms. If the amount of N^{*} is greater than the amount of N by two, the molecule will posses a triplet ground state. If the amount of N^{*} and N are equal, then the molecule will posses a singlet ground state.

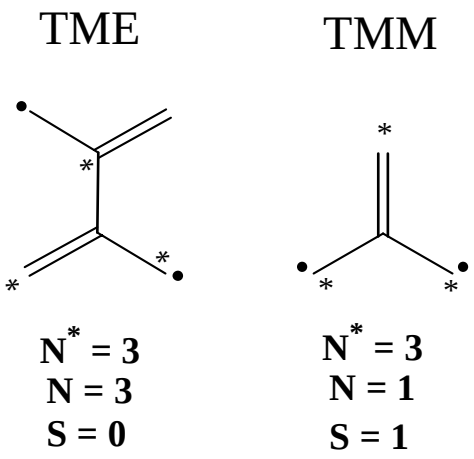

Figure I.8. VB model using the "starred" designation for TMM and TME.

The spin designation and the "starred" designation lead to the same conclusion. A difference of two gives a ground state triplet molecule.

MO theory looks at the AO's that are involved in π-bonding and attempts to maximize the spin density. The electrons that are not involved in π-bonding are placed in NBMO. Borden and Davidson found that the NBMO's or SOMO's of a non-Kekulé molecule could be determined, without doing Hückel calculations, using a zero-sum rule.[1.8] The zero-sum rule states that the sum of the coefficients of the starred atoms and the adjacent unstarred atoms must sum to zero.[1.2, 1.8]

However, the zero-sum rule will not be valid for all molecules, and the fragment orbitals (FO) of these molecules will be taken into consideration. For non-Kekulé molecules where the unstarred atom's coefficients in at least one of the FOs are nonzero, the molecule is said to be disjoint. Another way to state the former sentence is to say that if the two FOs

when superimposed do not share common electronic volumes then they are non-coextensive or "disjoint". [1.8] The FOs of the molecule TME are non-coextensive, Figure I.9.[1.2, 1.8, 1.9]

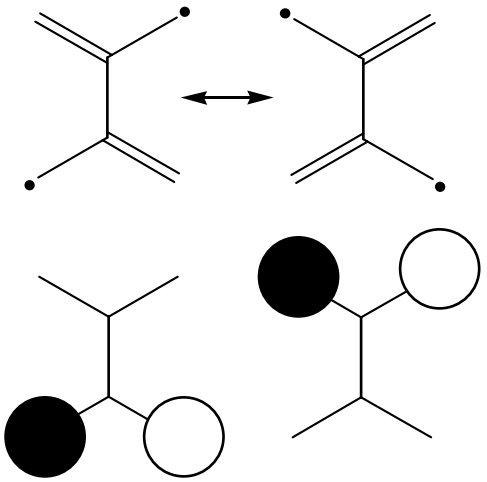

Figure I.9. Disjoint or non-coextensive FOs of TME.

On the other hand, if the unstarred atoms in the FOs of a non-Kekulé molecule are zero in both FOs, the molecule is said to be "non-disjoint". [1.2, 1.8] Another way to state the former sentence is to say that if a molecule's FOs when superimposed share common electronic volumes they are coextensive or non-disjoint. The FOs of the molecule TMM are coextensive, Figure I.10.[1.2 , 1.8, 1.9]

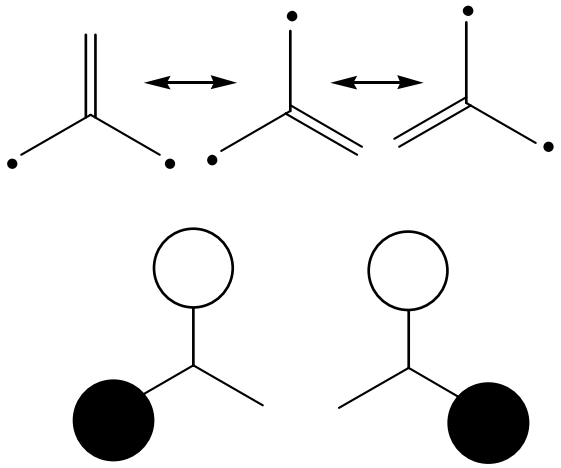

Figure I.10. Non-disjoint or coextensive FO's of TMM.

A simpler way to determine whether a non-Kekulé molecule is disjoint or non-disjoint is by determining N^* and N. As the VB model showed with the star designation for the determination of the ground state, if the difference in the amount of N^* and N is nonzero, the molecule will be non-disjoint, like TMM. If the difference in the amount of N^* and N is zero, the molecule will be disjoint, like TME.[1.2, 1.8, 1.9]

The difference in energy of the triplet and singlet states, ΔE_{ST}, can be estimated depending on whether a non-Kekulé molecule is disjoint or non-disjoint.[1.2, 1.8] The Pauli Exclusion Principle summarizes that when two electrons are brought close in distance to one another and the electron-electron repulsion increases in energy, the triplet state is stabilized. For a disjoint molecule such as TME, two electrons would not simultaneously occupy the same AOs. When two electrons do not simultaneously occupy the same AO, the singlet state and triplet state will have the same energy. On the other hand, with a non-disjoint molecule

such as TMM, the two electrons could possibly occupy the same AOs simultaneously. When two electrons occupy the same AOs simultaneously, the electron-electron repulsion energy is increased. For a non-disjoint molecule, the ΔE_{ST} will be larger than the ΔE_{ST} for a disjoint molecule.[1.2, 1.8, 1.9]

The VB model worked in the determination of the ground state for a non-Kekulé molecule, while MO theory worked in the determination of the size of ΔE_{ST}. Together the two approaches can be used to estimate the size of ΔE_{ST} of the ground configuration in a disjoint or non-disjoint molecule.

I.8. Common Coupling Units.

Throughout the years many non-Kekulé molecules have been prepared using common coupling units (CU). A CU will be defined as a bridge that connects two or more radical moieties. Some common CUs include ethenylidene, phenylene, and cyclobutadienylidene, as shown in Figure I.11. A CU can be couple two electron spins ferromagnetically antiferromagnetically depending on their position on the CU.

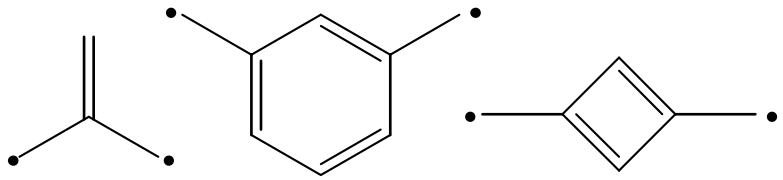

Ethenylidene **Phenylene** **Cyclobutadienylidene**

Figure I.11. Common coupling units ethenylidene, phenylene, cyclobutadienylidene coupling two methylene radical moieties.

As mentioned in the previous section, TMM contains two methylene radical moieties that are bridged by an ethenylidene CU in a 1,1-connection. Both experimentally and theoretically, TMM is found to have a triplet ground state, where $\Delta E_{ST} \approx 15$ kcal/mol, which means that ethenylidene is a ferromagnetic CU.[1.1, 1.2, 1.8, 1.9] On the other hand, when two methylene radical moieties are connected in a 1,2-connection, ethenylidene acts as an antiferromagnetic CU, as shown in Figure I.12. The NBMOs of the 1,2-connection are disjoint; therefore, the ground state would be predicted to be a singlet.

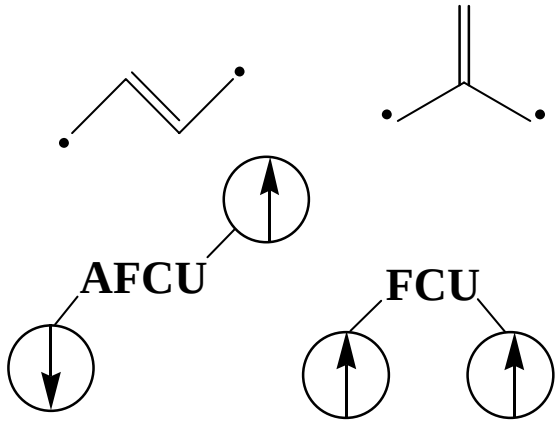

Figure I.12. Ethenylidene as an antiferromagnetic and ferromagnetic CU when two methylene radical moieties are attached in a 1,1-connection and 1,2-connection.

Another CU that is often used is phenylene. When two methylene radical moieties are positioned *ortho* or *para* to one another then phenylene acts as an antiferromagnetic CU. When the two methylene radical moieties are positioned *meta* to one another then phenylene acts as a ferromagnetic CU giving the well-studied triplet ground state molecule *meta*-xylylene.[1.2, 1.10] Figure I.13 shows phenylene as an antiferromagnetic and ferromagnetic CU.

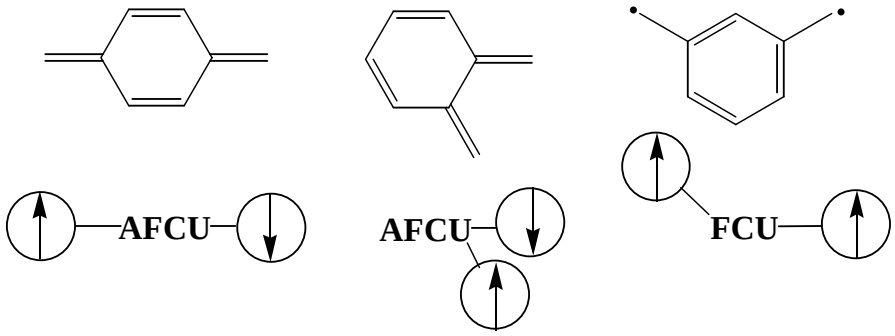

Figure I.13. Phenylene as an antiferromagnetic and ferromagnetic CU when two methylene radical moieties are attached *ortho*, *para*, and *meta* to one another.

Two methylene radical moieties bridged by cyclobutadienyledene in a 1,2-connection give, experimentally and theoretically, a triplet ground state.[1.2, 1.11] Cyclobutadienyledene can act as a ferromagnetic or antiferromagnetic coupler, as shown in Figure I.14.

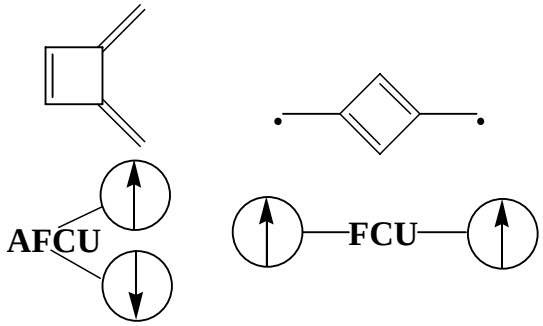

Figure I.14. Cyclobutadienyledene as an antiferromagnetic and ferromagnetic CU when two radical moieties are attached in a 1,2-connection and 1,3-connection.

Ethenylidene, phenylene, and cyclobutadienyledene are also used in the production of larger more stable biradical molecules. Altering the CUs by substitution of a heteroatom, steric shielding, or joining multiple CUs can result in a more stable biradical.[1.2] Examples of these include those produced and characterized by Dr. David A. Shultz.[1.13, 1.14] These molecules have shown either ferromagnetic or antiferromagnetic coupling.

I.9. Previous Studies on Oxyallyl and Some Oxyallyl Derivatives.

We propose to determine if a carbonyl group can act as an effective ferromagnetic coupler.[1.14] As in TMM, ethenylidene acts as a very good ferromagnetic coupler. So would substitution of an oxygen atom on the ethenylidene CU still produce at ground state triplet? The type of bonding that will occur and the MOs will be taken into account for the theoretical determination of the ground state for a carbonyl-linked biradical.

The triplet state of TMM has delocalized bonding over all three methylenes. One of the two singlet states has localized π-bonding of one of the methyl groups to the central carbon and the other singlet state has delocalized π-bonding between two of the methyl groups, as shown in Figure I.15.[1.8]

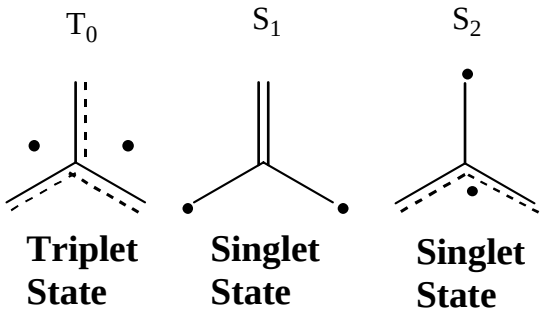

Figure I.15. Three states of TMM T_0, S_1, and S_2.

If oxygen is substituted in place of one of the methylene groups, to give oxyallyl, shown in Figure I.16, then the singlet state, S_1, containing π-bonding to the substituted oxygen may become more stabilized than the triplet state. This stabilization is due to the C=O π-bonds being stronger than the C=C π-bonds.

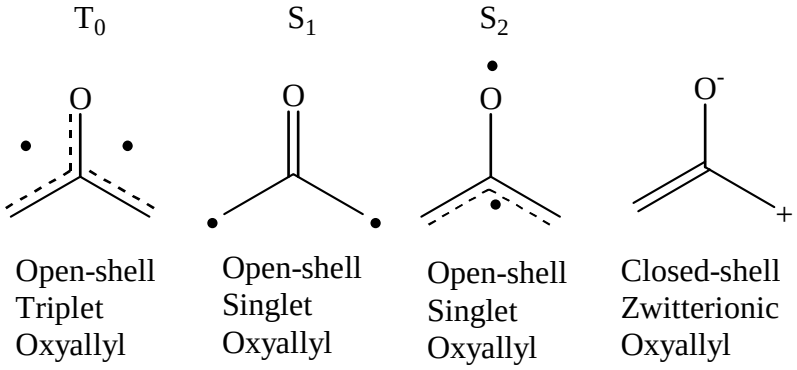

Figure I.16. The triplet state and two singlet states of open-shell oxyallyl, and the closed-shell zwitterionic oxyallyl.[1.16]

If the two NBMOs of TMM are considered, the NBMO with the greater amount of electron density where the oxygen atom is substituted will be lowered in energy. The other NBMO will remain unchanged since this NBMO contains a node where the oxygen is substituted. Figure I.17 shows the degeneracy lifting using a simple Hückel energy diagram.

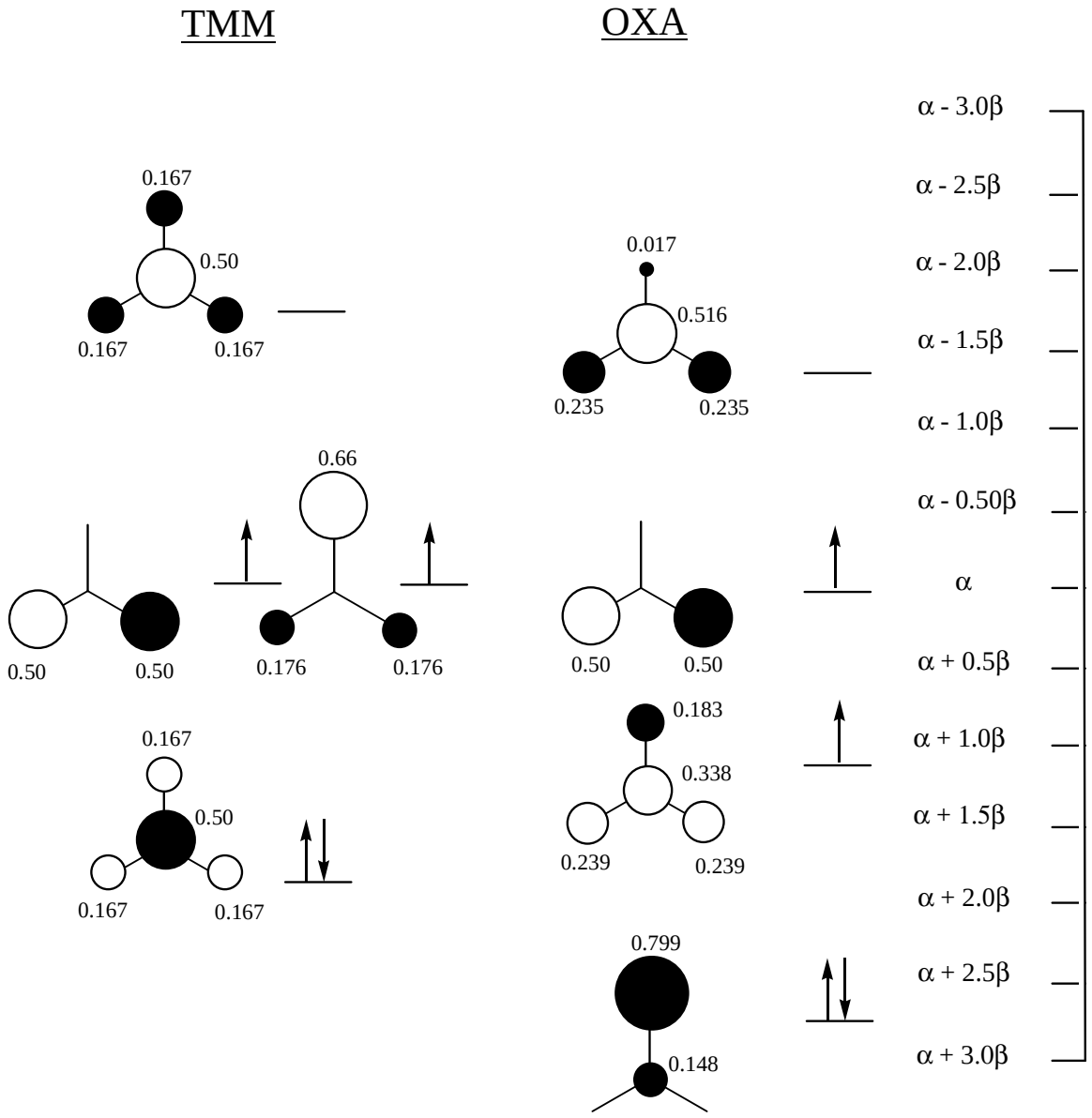

Figure I.17. MO energy level diagram for oxyallyl and TMM with spin densities.

As discussed in Section I.6, TMM would be predicted to have a large ΔE_{ST} since the two NBMOs are coextensive. Upon substitution of oxygen to give OXA the amount of orbital overlap between the two NBMOs increases. Since overlap density dictates the size of the exchange integral, **k**, it can be inferred that ΔE_{ST} for oxyallyl will be larger than TMM's ΔE_{ST}.

However, there is the possibility that the closed-shell zwitterionic OXA configuration can mix with the open-shell singlet state of OXA, producing a ground state singlet. This possibility arises from the energy difference in the two NBMO's of OXA. There is now a stronger interaction between the ground configuration singlet and the excited configuration singlet lowering the energy of the ground configuration singlet below the ground state triplet, as shown in Figure I.18.

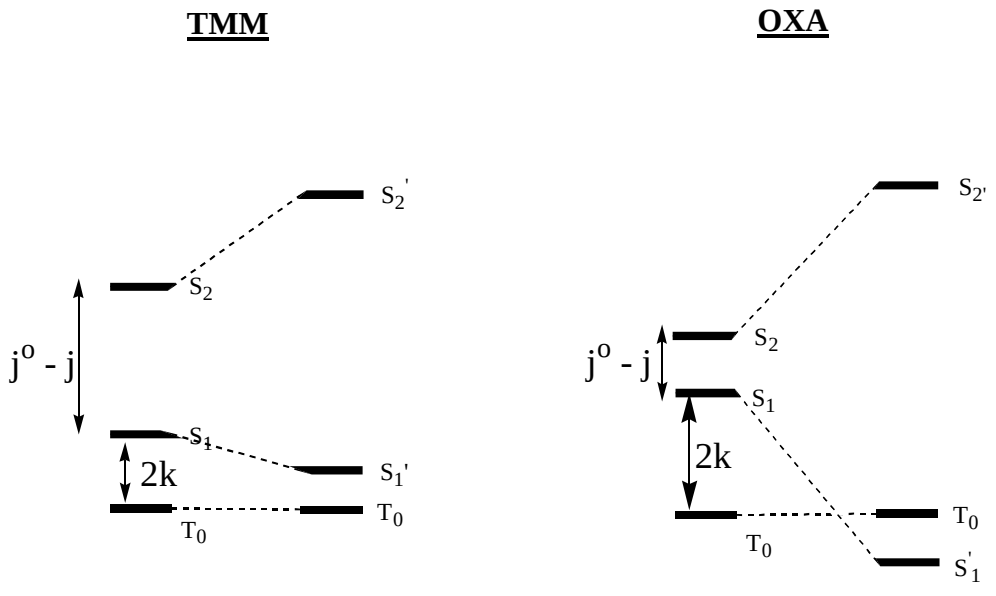

Figure I.18. Energy level diagram of TMM and OXA considering

There has been no experimental evidence to prove that OXA prefers a ground state triplet. The few computational methods done show that OXA prefers a ground state triplet. The largest ΔE_{ST} is calculated to be about 4.4 kcal/mol.[1.15] It is unclear whether these methods consider configuration interaction.

The biradical oxyallyl is a very reactive molecule that has been found to be an intermediate in some reactions.[1] In 1984 Borden, *et al*. were able to compute the ground state of oxyallyl as a $^3B_2$ with a small $\Delta E_{ST} \approx 6$ kcal/mol using the highest levels of theory at the time.[1.18] In the 1990's Lahti, *et al*. as well as Borden, *et al*. questioned whether higher levels of theory would reverse the favoring of a $^3B_2$ ground state, since oxyallyl's ΔE_{ST} was small in comparison to TMM's $\Delta E_{ST} \approx 15$ kcal/mol, and whether the ground state would prefer open-shell triplet or a closed-shell zwitterionic state, Figure I.16. [1.15, 1.19] Borden, *et al*. decided to use higher levels of theory to compute oxyallyl's ΔE_{ST} while Lahti *et al*. decided to study the effects of substitution on oxyallyl derivatives specifically studying bond lengths to determine the ground state of cyclobutanone-1,3-diyl and cyclopentanone-2,5-diyl.[1.15] Lahti *et al*. compared computational results of studies done on cyclopentanene-2,5-diyl.[1.19] The computed C-O bond lengths of triplet states and singlet states for cyclobutanone-1,3-diyl and cyclopentanone-2,5-diyl shown in Figure I.19, since these two molecules would be expected to show delocalization in the triplet state.

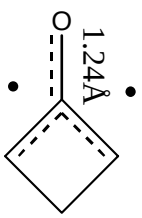

Triplet Cyclobutanon-2,4-diyl

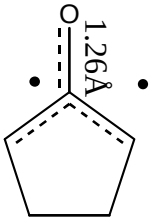

Triplet Cyclopentanone-2,5-diyl

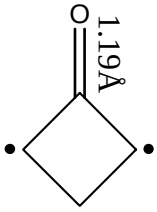

Singlet Cyclobutanon-2,4-diyl

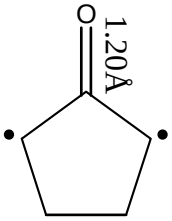

Singlet Cyclopentanone-2,5-diyl

Figure I.19. Biradicals studied in the determination of triplet and singlet state C=O bond lengths.

The C-O bond length of the triplet cyclobutanone-1,3-diyl was computed to be 1.24Å, where the singlet cyclobutanone-1,3-diyl C-O bond length was computed to be 1.19Å. The triplet cyclopentanone-2,5-diyl C-O bond length was computed to be 1.26Å, where the singlet cyclopentanone-2,5-diyl C-O bond length was computed to be 1.20Å. They were also able to compute the C-C bonds both in the singlet, 1.46Å, and the triplet, 1.45Å, states. Upon inspection of the C-O bond lengths and C-C bond lengths they concluded that from the short C-O bonds and long C-C bonds the oxyallyl would not be best represented by a zwitterionic structure, usually longer bond lengths, but instead by a C^{+}-O^{-} bond shortened by strong columbic attractive forces. They were also able to compute ground states for both cyclobutanone-1,3-diyl, -3.7 kcal/mol, and cyclopentanone-2,5-diyl, -5.8 kcal/mol, where negative ΔE_{ST} corresponds to ground state singlet. [1.19] In 1995 Borden used

more advanced levels of theory to compute the singlet-triplet gap of cyclopentanone-2,5-diyl. He determined the same magnitude of ΔE_{ST} for cyclopentanone-2,5-diyl as as well as the stability of the open-shell singlet and triplet compared with the closed-shell form.[1.16]

Borden *et al*. computed the C-O bond lengths for oxyallyl. They were in accordance with the C-O bond lengths that Lahti computed. The C-O bond length of the singlet oxyallyl was computed to be 1.214Å and the triplet C-O bond length was computed to be 1.254Å. The C-C bond lengths were also in accordance with those found by Lahti where the singlet C-C bond length was computed to be 1.471Å and the triplet C-C bond length 1.444Å, as shown in Figure I.20.[1.15] They were also able to compute a range of ΔE_{ST} values from 4.4 kcal/mol to –5.1 kcal/mol where a negative ΔE_{ST} corresponds to a ground state singlet.[1.15]

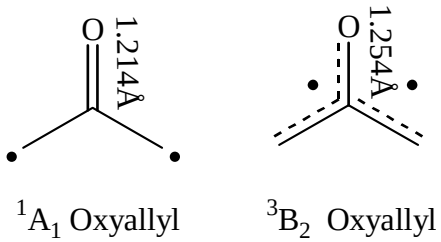

Figure I.20. Computed C-O bond lengths of oxyallyl.

Since C-O π-bonds have a distinct infrared stretching frequency Borden proposed using a simple characterization technique, infrared spectroscopy, to distinguish the triplet cyclopentanone-2,5-diyl from the singlet cyclopentanone-2,5-diyl.[1.16] Computational

methods were used to determine the triplet state and singlet state stretching frequencies of biradical cylcopentanone-2,5-diyl and the stretching frequency of closed-shell bicylclo[2.1.0]pentan-5-one, shown in Figure I.21. The lower C=O stretching frequency calculated for the triplet is due to the delocalized π-bonding which will increase the C=O bond length which decreases the force constant consequently decreasing the stretching frequency.[1.16]

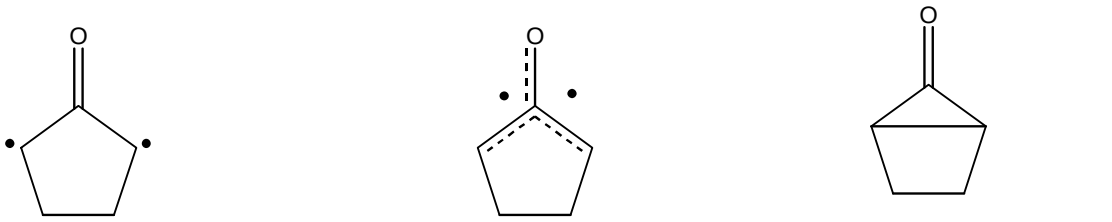

Singlet Cyclopentanone-2,5-diyl
ν = 1736 cm^{-1}

Triplet Cyclopentanone-2,5-diyl
ν = 1387 cm^{-1}

Bicyclo[2.1.0]pentan-5-one
ν = 1830 cm^{-1}

Figure I.21. Stretching frequencies of triplet and singlet cyclopentanone-2,5-diyl and closed-shell bicylco[2.1.0]pentan-5-one.

From the three stretching frequencies calculated by Borden it should be easy to determine from infrared spectroscopy whether the singlet or triplet state of biradical cylcopentanone-2,5-diyl or bicyclo[2.1.0]pentan-5-one was generated.

These few experiments and computational methods are the extent to which OXA has been studied. Experimental evidence that suggests that a carbonyl-linker can act as a ferromagnetic coupling unit will be further discussed in Chapter 3.

Chapter I References.

1.1 Dowd, P. *J. Am. Chem. Soc.* **1966**, *88*, 2587. Dixon,D. A.; Dunning, T. A.; Eades, R. A.; Kleier, D. A. *J. Am. Chem. Soc.* **1981**, *103*, 2878.

1.2 Rajca, A. *Chem. Rev.* **1994**, *94*, 871.

1.3 Atkins, P. *Physical Chemistry*; W.H. Freeman and Company: New York, 1998.

1.4 Castellan, G. W. *Physical Chemistry*; Benjamin/Cummings: California, 1986. Borden, W. T. *Diradicals*; John Willey and Sons: New York, 1982.

1.5 Bodnar, S. H.; *Ph.D. Dissertation*; N.C. State, 2002.

1.6 Wertz, D. *Symmetry, Molecular Orbital Theory, and Optical Spectroscopy of Inorganic Chemistry*; pending.

1.7 Meislich, H.; Nechanmkin, H.; Sharefkin, J. *Schaum's Outline of Theory and Problems of Organic Chemistry*; McGraw-Hill: New York, 1991.

1.8 Lahti, P. *Magnetic Properties of Organic Materials*; Marcel Dekker, Inc.: New York, 1999.

1.9 Borden, W. T.; Davidson, E. R. D. *J. Am. Chem. Soc.* **1977**, *99*, 4587.

1.10 Fort, R. C., Jr.; Getty, S. J.; Hrovat, D. A.; Lahti, P. M.; Borden, W. T. *J. Am. Chem. Soc.* **1992**, *114*, 7549.

1.11 Snyder, G. J.; Dougherty, D. A. *J. Am. Chem. Soc.* **1991**, *107*, 1774. Snyder, G. J.; Dougherty, D. A.; *J. Am. Chem. Soc.* **1989**, *111*, *3927*.

1.12 Borden, W. T.; Iwamura, H.; Berson, J. A. *Acc. Chem. Res.* **1994**, *27*, 109.

1.13 Shultz, D. A.; Bodnar, S. H.; Kumar, R. K.; Kampf, J. W. *J. Am. Chem. Soc.*

1999, *121*, 10664. Shultz, D. A.; Hollomon, M. G.; *Chem. Mat.* **2000**, *12*, 580. Shultz, D. A.; Bodnar, S. H.; Kampf, J. W. *ChemComm* **2001**, 93. Caneschi, A.; Dei, A.; Lee, H.; Shultz, D. A.; Sorace, L. *Inorg. Chem.* **2001**, *40*, 408. Shultz, D. A.; Fico, R. M.; Boyle, P. D.; Kampf, J. W. *J. Am. Chem. Soc.* **2001**, *123*, 10403.

1.14 Shultz, D. A.; Bodnar, S. H.; Kumar, R. K.; Lee, H.; Kampf, J. W. *Inorg. Chem.* **2001**, *40*, 546.

1.15 Coolidge, M. B.; Yamashita, K.; Morokuma, K.; Borden, W. T.; *J. Am. Chem. Soc.* **1990**, *112*, 1751.

1.16 Powell, H. K.; Borden, W. T.; *J. Org. Chem.* **1995**, *60*, 2654.

1.17 Shaad, L. J.; Hess, B. A. *J. Org. Chem.* **1981**, *46*, 1909. Hirano, T.; Kumagai, T.; Miyashi, T. *J. Org. Chem.* **1991**, *56*, 1907. Matlin, A. R.; Lahti, P. M.; Appella, D. *J. Am. Chem. Soc.* **1999**, *121*, 2164.

1.18 Osamura, Y.; Borden, W. T.; Morokuma, K. *J. Am. Chem. Soc.* **1984**, *106*, 5112.

1.19 Ichimura, A. S.; Lahti, P. M.; Matlin, A. R.; *J. Am. Chem. Soc.* **1990**, *112*, 2868.

CHAPTER II: MAGNETOMETRY

II.1. Introduction to Magnetism and Types of Magnetism.

Magnetization is dependent on the types of electrons, paired, unpaired, or both that a material possesses and on the magnitude of an applied field. When a field is applied the orientation that the electrons take, with or against the field, will help in the determination of which class of magnetism the sample may belong. There are many different classes of magnetism but this chapter will mainly focus on diamagnetism, paramagnetism, ferromagnetism, and antiferromagnetism.

Magnetization is described by Eqn. II.1, where H is the applied field and χ_{tot}, the proportionality constant, is the total magnetic susceptibility given in units of emu/mole, where $\chi_{tot} = \chi_{dia} + \chi_{para}$.[2.1]

$$M = \chi_{tot} H \qquad \textbf{Eq.II.1}$$

Magnetization can also be expressed in terms of the number of molecules and the magnetic moments of each thermally populated state, as shown in Eqn. II.2.

$$M = \frac{Ng^2\mu_B{}^2 S(S+1)H}{3kT} \qquad \textbf{Eq.II.2}$$

where,

$$\chi_{tot} = \frac{Ng^2\mu_B{}^2 S(S+1)}{3kT} \qquad \textbf{Eq.II.3}$$

and,

$$E_n = Sg\mu_B H \qquad \textbf{Eq.II.4}$$

In the resulting equations, E_n is the energy of each thermally populated state, *k* is Boltzmann's constant, 1.38 x 10^{-23} JK^{-1}, *N* is Avogadro's number, 6.022 x 10^{23} mol^{-1}, μ_B is

the Bohr magneton, 9.27 x 10^{-24} JT^{-1}, g is Landé constant, 2.0023, T is the absolute temperature, and S (or M_s) is the total spin.[2.1, 2.2]

When the material has no unpaired electrons or the electronic shells are completely filled the material is said to be diamagnetic.[2.1] Most molecules have some number of paired electrons and therefore a diamagnetic susceptibility, χ_{dia}. Pascal proposed that χ_{dia} be represented by Eqn. II.5, where n_i is the number of atoms of each type, χ_i is the contribution to the susceptibility of each of the diamagnetic atoms, and λ is a bond correction.[2.2]

$$\chi_{dia.} = \lambda + n_i \chi_i \qquad \textbf{Eq.II.5}$$

As seen from Eqn. II.5, the χ_{dia} is independent of the applied field and temperature so it can easily be separated out from the temperature dependent susceptibilities.[2.2] Pascal was successful in determining the diamagnetic susceptibilities of some atoms and these constituent susceptibilities are known as Pascal's constants. In Eqn. II.1, when a material that is predominately diamagnetic the total magnetic susceptibility is negative and relatively small: -10^{-6} to -10^{-7} emu g^{-1}.[2.1]

In a paramagnet the unpaired electrons are rapidly orienting, reorienting, and non-interacting so there is no permanent or spontaneous magnetic moment. Once a field is applied, the rapidly reorienting unpaired electrons align with the applied field. Unlike χ_{dia}, the paramagnetic susceptibility, χ_{para}, is dependent on temperature and χ_{para} varies inversely with respect to temperature, as shown in Eqn. II.6.[2.1, 2.2]

$$\chi_{para} = \frac{C}{T} \qquad \textbf{Eq.II.6}$$

Eqn. II.6 is known as the Curie Law where T is the absolute temperature and the Curie constant, **C**, is dependent on the total spin, **S**, as shown in Eqn. II.7.[2.1, 2.2]

$$C = \frac{Ng^2 \mu_B{}^2 S(S+1)}{3k} \qquad \textbf{Eq.II.7}$$

In Eqn. II.1 when the material that is predominantly paramagnetic the total magnetic susceptibility is positive and relatively large: 10^{-4} to 10^{-6} emu g^{-1}.[2.1] χ_{para} is often reported as μ_{eff}, the effective magnetic moment, described in Eqn. II.8 and Eqn. II.9.

$$\mu_{eff} = \left(\frac{3k}{N}\right)^{1/2} (\chi T)^{1/2} \qquad \textbf{Eq.II.8}$$

or

$$\mu_{eff} = \left[g^2 S(S+1)\right]^{1/2} \mu_B \qquad \textbf{Eq.II.9}$$

A plot of inverse χ as a function of temperature yields a straight line. The slope of the line is the inverse Curie constant, where the Curie constant is described in Eqn. II.7.

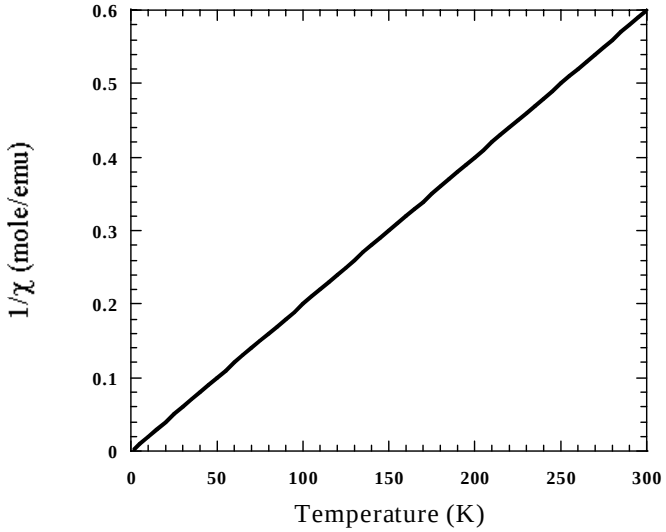

Figure II.1. Inverse $\chi_{para.}$ as a function of temperature for a paramagnet.

Materials that contain spin-orbit coupling, zero field splitting, and/or intermolecular interactions do not follow the Curie Law so the Curie-Weiss Law was devised, Eqn. II.10.[2.1, 2.2]

$$\chi = \frac{C}{T - \theta} \qquad \textbf{Eq.II.10}$$

The Weiss constant, θ, has units of temperature. The relation between θ, the spin in the system, S, the energy gap between the ground state and lowest excited state, *J'*, and the nearest neighbors, *z*, is shown in Eqn. II.11.[2.3]

$$\theta = \frac{zJ'\mathrm{S}(\mathrm{S}+1)}{3k} \qquad \textbf{Eq.II.11}$$

The sign and magnitude of θ can be extracted from the plot of inverse χ as a function of temperature, as shown in Figure II.1. With ideal paramagnetic behavior θ = 0 so the Curie Law is observed. Neglecting zero-field splitting, when θ < 0, antiferromagnetic interactions exist, and when θ > 0, then ferromagnetic interactions exist, as shown in Figure II.2.[2.2, 2.3]

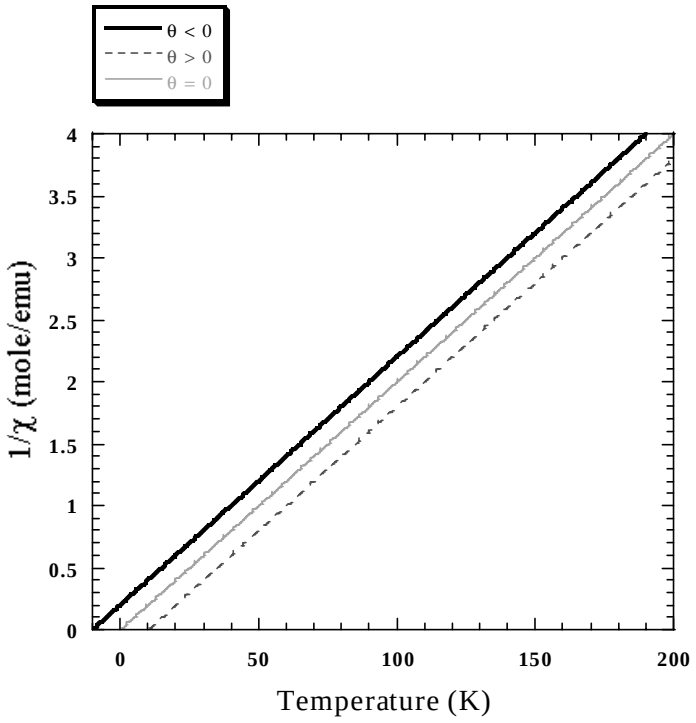

Figure II.2. Inverse χ as a function of Temperature. For θ = 0 ideal paramagnetic behavior is exists, θ > 0 ferromagnetic interactions exists, and θ < 0 antiferromagnetic interactions exist.

The magnetic moment is a key component in the determination of the number of unpaired electrons and the exchange coupling of the system. Measuring the magnetic moment of the sample allows us to extract the saturation magnetization and the susceptibility of the sample. The saturation magnetization values are obtained when the temperature is held constant, usually 2-4 K, and the field is swept. Thus far we have taken into consideration only the samples that obey Curie Law. For example, Eqn. II.6 and Eqn. II.10 portrays Curie Law behavior only when H/T < 0.7 T/K. This can be proved using the Brillouin function as shown in Eqn. II.12.

$$B_s(x) = \frac{1}{S}\left[\left(S+\frac{1}{2}\right)\coth\left[\left(S+\frac{1}{2}\right)x\right] - \frac{1}{2}\coth\frac{x}{2}\right] \qquad \textbf{Eq.II.12}$$

where

$$x = \frac{g\mu_B H}{kT} \qquad \textbf{Eq.II.13}$$

and

$$M = Ng\mu_B S B_s(x) \qquad \textbf{Eq.II.14}$$

If two limiting behaviors are considered one where $g\mu_B H/kT >> 1$ and $g\mu_B H/kT << 1$ then it can be proven that Eqn. II.2 portrays Curie Law behavior when H/T < 0.7 T/K. If the first scenario is considered, where $g\mu_B H/kT >> 1$, then Eqn. II.15 and Eqn. II.16 are generated and H/T >> 0.7 T/K.

$$B(x) = \frac{1}{S}\left[\left(S+\frac{1}{2}\right) - \frac{1}{2}\right] \approx 1 \qquad \textbf{Eq.II.15}$$

and

$$M_{sat} = Ng\mu_B S \qquad \textbf{Eq.II.16}$$

When the magnetization is equal to $Ng\mu_B S$ then the sample no longer exhibits Curie law behavior, and the sample is saturated. In this window the spins are at there maximum alignment and it is said that saturation magnetization has been reached. When H/T is large (high values of applied field and low temperature) the best determination of the spin value can be obtained.[2.2]

If the second scenario is considered where $g\mu_B H/kT << 1$ then Eqn. II.17 is generated.[2.3] In this region where H/T < 0.7 T/K the sample obeys Curie law behavior. A plot of magnetization as a function of H/T yields the slope (S + 1)/3.[2.2]

$$B(x) = \frac{(S+1)x}{3} \qquad \textbf{Eq.II.17}$$

Figure II.3 displays both regions where the Curie law is obeyed and where saturation magnetization dominates. The initial curvature of the graph follows the Curie law. This region is used to obtain χ-values by holding the applied field constant while the temperature is swept. The χ-values are independent of field and can be fitted to the van Vleck expression, Eqn. II.18. Again, the exchange coupling parameter can be extracted to determine ferromagnetic or antiferromagnetic coupling.

$$\chi T = \frac{2Ng^2\beta^2}{k\left[3 + e^{-2J/kT}\right]} \qquad \textbf{Eq.II.18}$$

When the curve has a slope equal to zero, the spins are at their maximum alignment. Since magnetization depends on the total spin, each system will have different saturation magnetization values, as shown in Figure II.3.

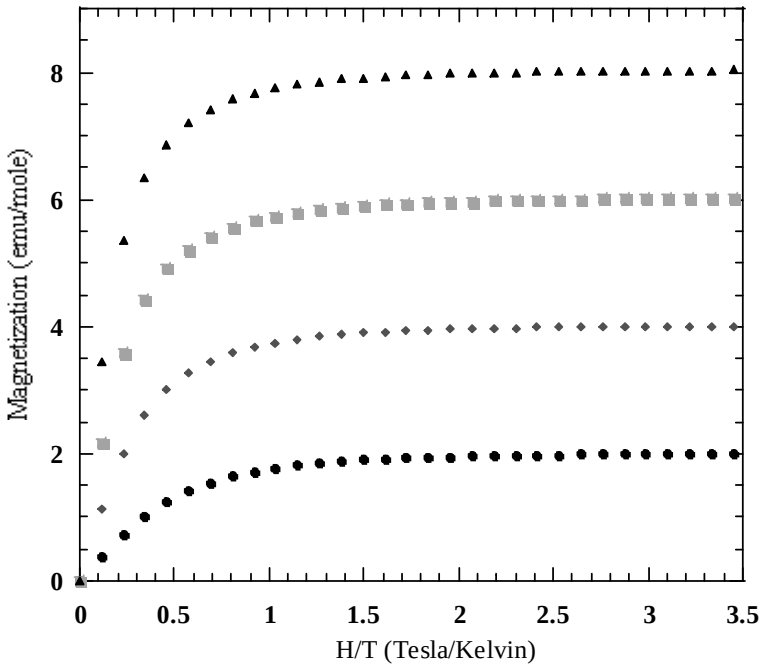

Figure II.3. Saturation magnetization values of different spin systems (g fixed at 2); • is S = 1, ♦is S = 2, ■ is S = 3, and ▲ is S = 4.

The last two types of magnetism to be discussed in this chapter deal with long range magnetic order.[2.4] Ferromagnets exhibit long-range magnetic order in a bulk magnetic behavior. In a ferromagnet the spins are often grouped together in domains.[2.4] Within each domain the spins are aligned parallel without the presence of an external field but the domains themselves are not necessarily aligned. Application of an applied field will cause the domain walls to break and the spins will align parallel with each other in one large domain giving bulk ferromagnetism.

In an antiferromagnet long-range magnetic order is also exhibited but the spins are aligned antiparallel in three dimensions throughout the material and are often grouped together in domains. When a field is applied the spins will align antiparallel and the domain walls will break to form one big domain with no net magnetic moment. Ferromagnets and antiferromagnets above a certain temperature, T_c for a ferromagnet and T_N for an antiferromagnet, exist as paramagnets. These temperatures are characteristic of the material so they will vary.[2.4] Figure II.4 depicts the different types of magnetism previously discussed.

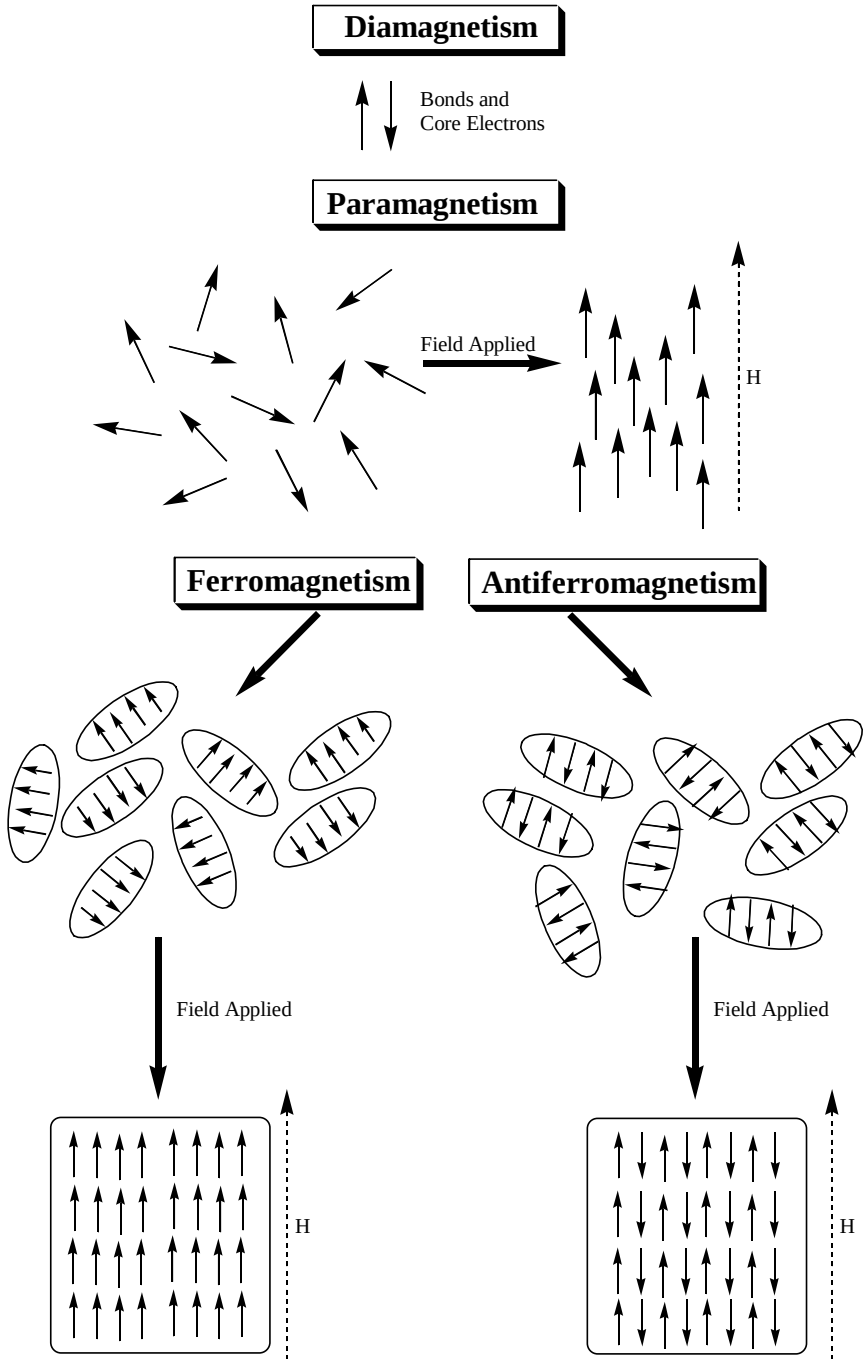

Figure II.4. Types of magnetism including diamagnetism, paramagnetism, ferromagnetism, and antiferromagnetism.

II.2. Electron Paramagnetic Resonance (EPR).

Electron paramagnetic resonance (EPR) allows the detection of the interactions of electron spins with each other (nuclear and electron) and with the interaction of electron spins with an applied field, known as the Zeeman effect.[2.5] The Zeeman effect is described by the energy of a magnetic moment in an applied field as proportional to the applied field and the spin of the system, $E_n = M_s g \mu_B H$.[2.2] For any molecule to be detectable by EPR an absorption must occur. This absorption can occur when a frequency of energy (usually microwave frequency for EPR) matches the energy separation between spin states ($\Delta M_s = \pm M_s$). Typically the frequency is held constant while the applied field is swept. The energy at which the applied field splits the spin states and the frequency of energy coincide, determines where the field strength at which an absorption will occur. The selection rule for EPR is $\Delta M_s = \pm 1$. Therefore, in a simple one-electron system the α spin state rises in energy and the β lowers in energy, as shown in Figure II.5, where $M_s = \pm ½$.

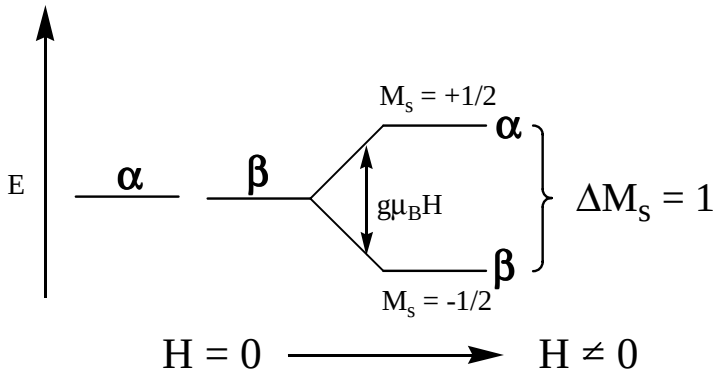

Figure II.5. EPR detectable one-electron system.

As discussed in Chapter 1 the exchange coupling, **J**, between the two electrons lifts the degeneracy of the singlet and triplet state. Zero field splitting (ZFS) lifts the degeneracy of the triplet microstates and that can be detected by EPR. Only the triplet state is EPR active since the singlet state has no spin. The magnitude of the ZFS interaction can be expressed using the spin Hamiltonian $\hat{H} = \hat{S}\bullet\mathbf{D}\bullet\hat{S}$, where **D** is described as the difference in energy between the lowest lying microstate and the average of the higher two microstates.[2.5, 2.6, 2.7] Figure II.6 shows the exchange coupling in relation with the ZFS parameters **D** and **E**, where **E** is described as energy difference between the two lowest lying microstates.

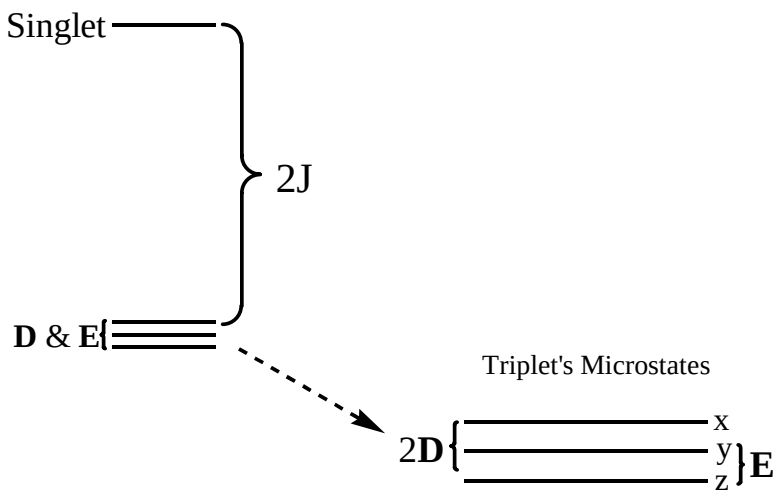

Figure II.6. Exchange parameter J in relation with the ZFS parameters D and E.

For a biradical system the two electrons can be aligned either parallel or antiparallel. If the two electrons are aligned antiparallel then the multiplicity is a singlet [2(0) + 1 = 1]. If the two electrons are aligned parallel then the multiplicity is a triplet [2(1) + 1 = 3]. For the EPR active triplet there are two allowed transitions since $M_s = \pm 1, 0$. A $\Delta M_s = 2$ transition will be further discussed later. Figure II.7 shows the $\Delta M_s = 1$ transitions using solid line double headed arrows.[2.5, 2.6, 2.7]

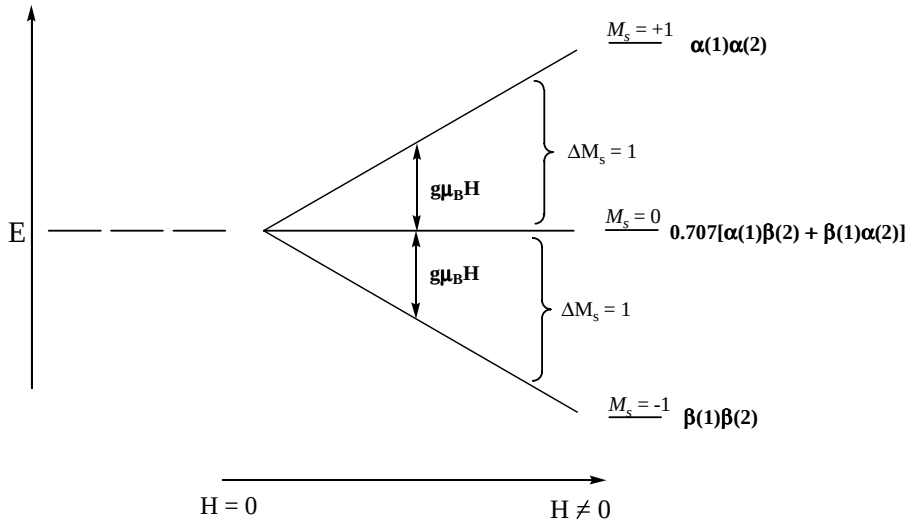

Figure II.7. EPR detectable two-electron system where $M_s = \pm 1, 0$, and $\Delta M_s = \pm 1$ transition.

The energy diagram depicted in Figure II.7 shows the degeneracy of the triplet microstates when no field is applied and the lifting of the degeneracy once a field is applied. However, this diagram only depicts the energy of the electrons as a function of applied

magnetic field. ZFS interactions need to be taken into consideration. For organic systems, ZFS is due to dipole-dipole interactions between the two-electron spins.[2.5, 2.7]

Molecular geometries that give rise to anisotropic electron distributions, will dictate the energy separations of the triplet microstates at zero field.[2.5] This energy separation is described by the ZFS parameters **D** and **E**.[2.5, 2.7] Figure II.8 depicts the ZFS parameters in relation to the molecular geometries of an atom, triplet excited benzene, and triplet excited naphthalene.

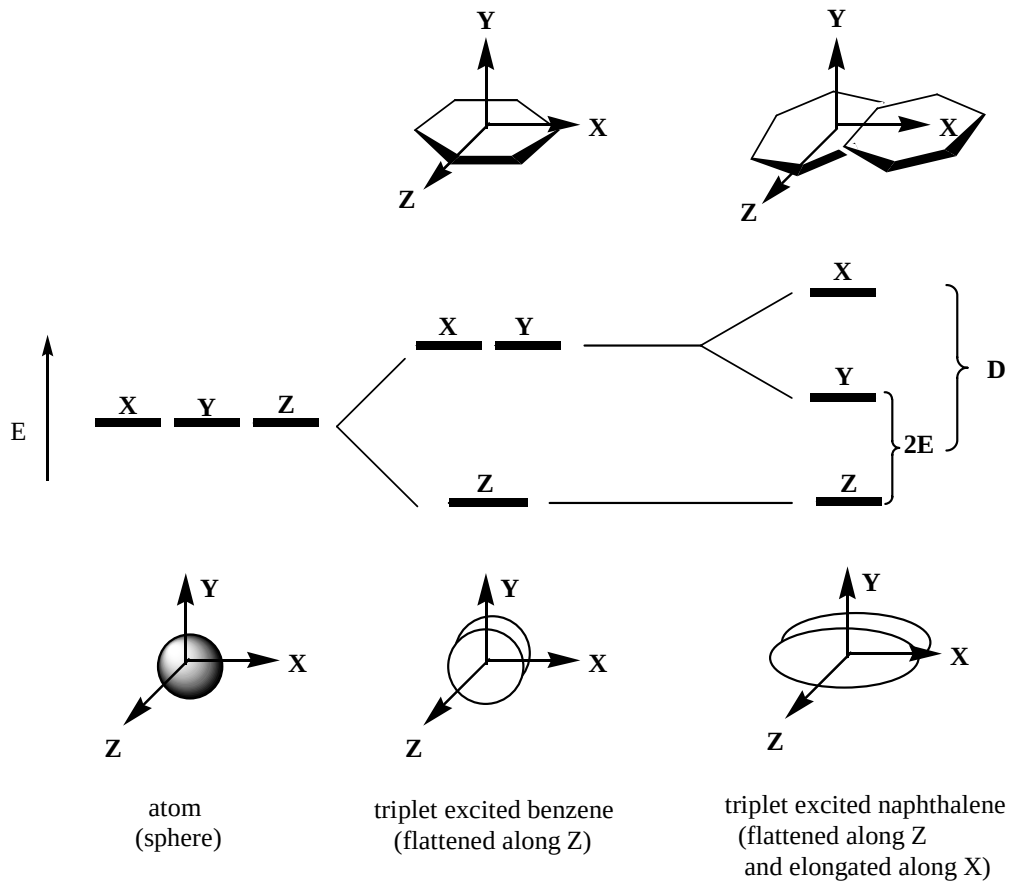

Figure II.8. Energy separation of microstates in relation with the molecular geometry of an atom, triplet excited benzene, and triplet excited naphthalene.

Figure II.8 depicts compression and elongation along certain axes in which the two electrons are confined to a certain plane, **XY**, **XZ**, or **YZ**. In an atom there is no minimizing the repulsive dipole-dipole interaction between the unpaired electrons because there is no direction along which the electrons can move further apart. In benzene compression along the **Z**-axis allows minimizing of the dipole-dipole interaction in the **XY** plane resulting in a lower energy Z state. In naphthalene compression along the **Z**-axis and elongation along the **X**-axis maximizes dipole-dipole interaction along the **YZ** plane resulting in a splitting of the

two highest energy states. The sign of the ZFS parameter **D** is dictated by the compression of along the **Z**-axis, or elongation along the **Z**-axis, to yield a positive value. Therefore, the geometrical shape of the spin distribution can be estimated from both the sign and magnitude of **D** and **E**.[2.5, 2.6]

The three triplet species in Figure II.8 can be characterized to have three different types of symmetry; cubic, axial, and rhombic. An atom possesses cubic symmetry ($x = y = z$) but ZFS is nullified by virtue of the high symmetry. For a triplet species to have axial ($x = y \neq z$) symmetry the species must possess three-fold or higher rotational symmetry, and a magnetically isotropic plane perpendicular to the symmetry axis, as with benzene (D_{6h}).[2.5] When a triplet species with axial symmetry is placed in an external applied field this field is aligned, for example, with the **Z**-axis of the species, and only the electrons in the **XZ**- or **YZ**-planes will be split by the field. The electrons in the **XY**-plane will not be affected since they are perpendicular with the applied field. With axial symmetry there are two allowed transitions but only one will be seen since they are at the same field strength. The ZFS would be dictated by the **D** parameter only ($E = 0$).

For a triplet species to have rhombic symmetry ($x \neq y \neq z$) the species must possess lower symmetry elements than a species of axial symmetry, for example naphthalene (D_{2h}). The ZFS would be dictated by both parameters **D** and **E**. Each symmetry type will result in three distinctly different EPR spectra, where the number of signals increases as the symmetry is lowered, as shown in Figure II.9. Each signal represents where the magnetic field is oriented along one of the axes of the system.[2.5, 2.7]

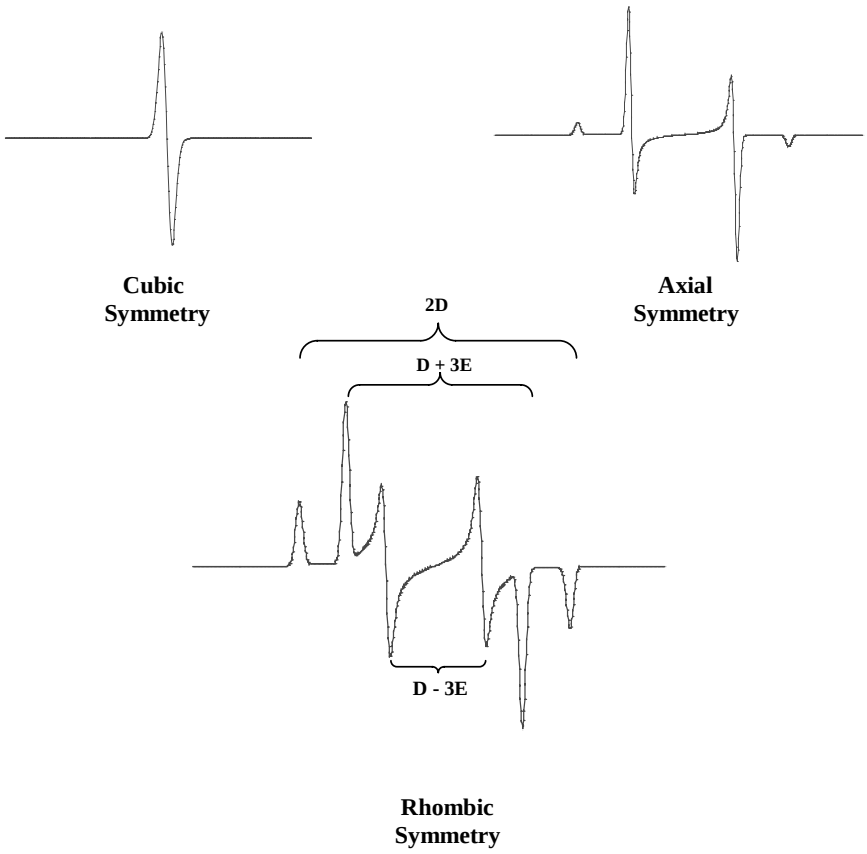

Figure II.9. Simulated spectra for a triplet excited species with cubic symmetry (D = 0), axial symmetry (D ≠ 0; E = 0), and rhombic symmetry (D ≠ 0; E ≠ 0).

A species with axial symmetry has six allowed transition, but as shown in Figure II.9, there are only four. This is due to the degeneracy of two of the axes. A species with rhombic symmetry has six allowed transition and as shown in Figure II.9, there are six displayed due to all the axes being different.[2.5]

All the previously mentioned transitions occur at high fields and correspond to the allowed $\Delta M_s = 1$ transitions.[2.3, 2.7] Depiction of the allowed $\Delta M_s = 1$ transitions are shown in Figure II.10 denoted as the solid line double headed arrow. At lower fields the "forbidden" (= weak) $\Delta M_s = 2$ transitions are sometimes observed.[2.7]

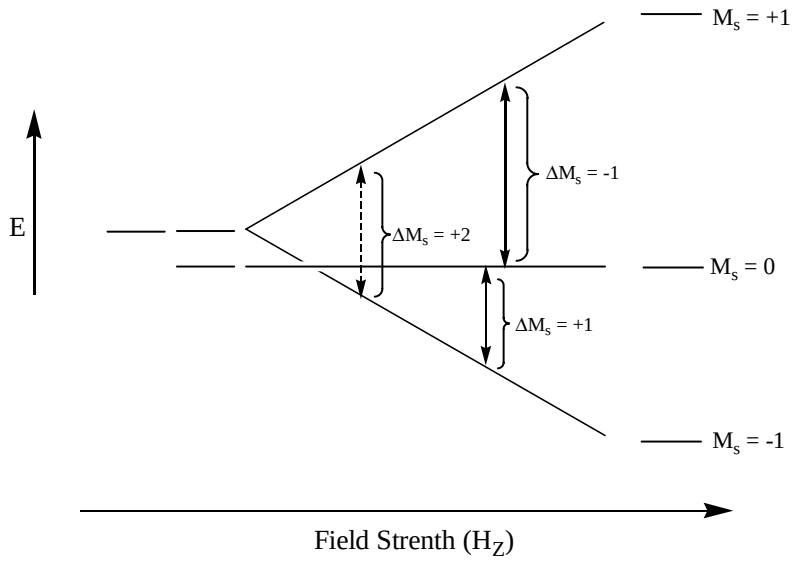

Figure II.10. The "forbidden" $\Delta M_s = 2$ transition in relation to the $\Delta M_s = 1$ transition of a triplet species.

There are two types of EPR techniques used in the Shultz group, frozen solution or fluid solution. Fluid solution EPR is useful in the determination of hyperfine coupling constants in a molecule. Hyperfine coupling is exhibited when electron spins couple to nuclear spins. Triplet species can be difficult to detect by EPR when the molecules are

rapidly reorienting in fluid solution. The $\Delta M_s = 1$ transitions will only be detected when the ZFS parameters **D** and **E** are sufficiently small, where $\mathbf{E} \approx 0$.[2.7] In fluid solution the rapidly reorienting molecules lead to line broadening in the EPR spectrum. This line broadening can make the spectrum appear as an $M_s = ½$ system.

Frozen solution EPR (or "powder" EPR), recorded at 77 K, allows for a rigid non-tumbling system, where ZFS can be observed. Frozen solution samples also allow for detection of the "forbidden" $\Delta M_s = 2$ transition at nearly half the center field of the $\Delta M_s = 1$ transitions.[2.7]

The spin-spin interaction of a triplet species can sometimes be detected using variable temperature EPR. The ground state can be assessed by the measurement of the change in spectral intensity versus inverse temperatures. Typically, the $\Delta M_s = 2$ transition is used to acquire the spectral intensity because it is easily integrated and there is no doublet impurity signal.[2.4] The proportional relationship between the spectral intensity, **I**, and χ allows for the use of the Curie law, as discussed in Section II.2. One very important aspect of determining the ground state of a molecule that has been left out thus far is the population of states as the temperature is increased. Since only the triplet state is EPR active it is useful to describe the relative population of the triplet state as shown in Eqn. II.17.

$$\mathbf{I} = \frac{C}{T}\left(\frac{3\exp\left(\frac{-2J}{kT}\right)}{1+3\exp\left(\frac{-2J}{kT}\right)}\right) \qquad \textbf{Eq.II.17}$$

Equation II.12 is described as a Boltzmann distribution and the sign of the exchange parameter can be acquired. When $\mathbf{J} < 0$, the magnitude can be determined. For $\mathbf{J} \geq 0$ a linear

relationship results and ferromagnetic interactions and/or degeneracy of the states (singlet and triplet) can be suggested.

II.3. Super-conducting Quantum Interference Device (SQUID).

The super-conducting quantum interference device (SQUID) magnetometer measures the magnetic moment of very small quantities of sample. Magnetic moment can be defined as the force acting on a system in an applied magnetic field from which the number of unpaired electrons can be determined.[2.8] SQUID is based on the Josephson junction, which is very sensitive to the changes in magnetic flux.[2.9] This sensitivity allows for very high accuracy in measuring the magnetic moment of a sample. The Josephson junction is coupled to super-conducting coils through which the sample is moved in the direction of the applied field. The coils will then detect any deviation of the flux, which is converted as an output voltage. This output voltage is then converted into the effective magnetic moment of the sample.[2.9] All data obtained from SQUID can be fit to the equations in Section II.1.

Chapter II References.

2.1 O'Conner, C. J. *Prog. Inorg. Chem.* **1982**, *29*, 203.

2.2 Carlin, R. L. *Magnetochemistry*; Springer-Verlag: New York, 1986.

2.3 Kahn, O. *Molecular Magnetism*; VCH: New York, 1993.

2.4 Bowl, A. K.; *Master's Thesis*; N.C. State, 1998.

2.5 Sandberg, K.; *Ph.D. Dissertation*; N.C. State, 1998.

2.6 Bodnar, S. H.; *Ph.D. Dissertation*; N.C. State, 2002

2.7 Weil, J. A. Bolton, J. R. Wertz, J. E. *Electron Paramagnetic Resonance Elementary Theory and Practical Applications*; John Wiley & Sons: New York, 1994.

2.8 Atkins, P. *Physical Chemistry*; W.H. Freeman and Company: New York, 1998.

2.9 McElfresh, M. *Fundamentals of Magnetism and Magnetic Measurements: Featuring Quantum Design's Magnetic Property Measurement System*; Quantum Design: San Diego, 1994.

CHAPTER III: SYNTHESIS AND CHARACTERIZATION OF OXYALLYL TYPE BIS-SEMIQUINONES

III.1. The Semiquinone Radical Anion.

Radical anion orthosemiquinones chelated to metal centers are of major interest in the field of magnetochemistry. A radical anion orthosemiquinone, herein known as a semiquinone, is simply a one-electron reduction product of an orthoquinone or a one-electron oxidation product of a catecholate, as shown in Figure III.1.

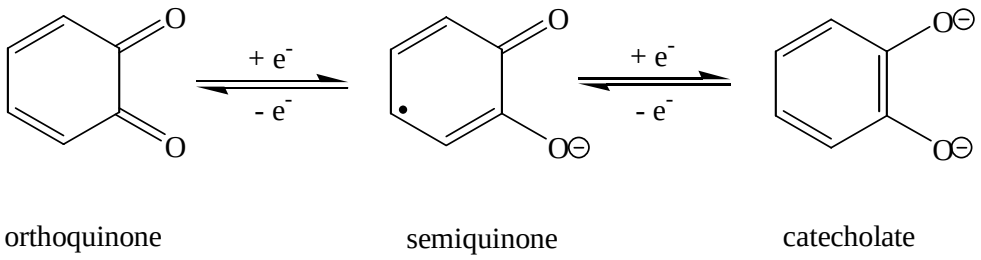

orthoquinone semiquinone catecholate

Figure III.1. A semiquinone product resulting from the one-electron reduction of an orthoquinone and the one-electron oxidation of a catecholate.

To understand the importance behind using a semiquinone in the study of multispin metal complexes, spin distribution will first be considered. Because resonance does not accurately portray spin distribution in this molecule, molecular orbitals (MO) will be used to determine spin densities. As discussed in Chapter I, MO theory looks at the atomic orbitals (AO) that are involved in π-bonding. The π-electrons that are not involved in π-bonding are

placed in non-bonding molecular orbitals (NBMO). The NBMO or singly occupied MO (SOMO) for a semiquinone is depicted in Figure III.2.

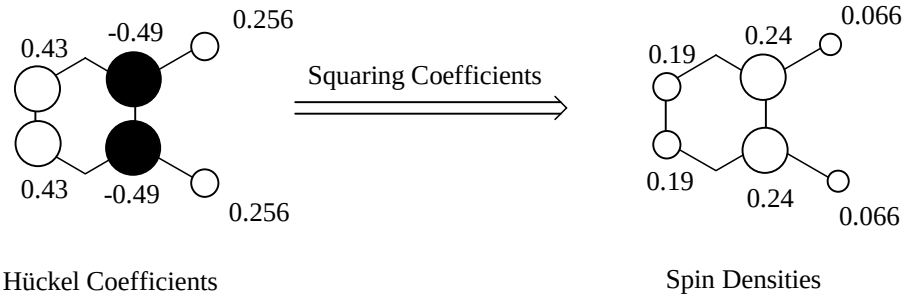

Figure III.2. The semiquinone's singly occupied molecular orbital (SOMO).

Hückel theory predicts the magnitude and sign of the coefficients for a semiquinone, shown on the left in Figure III.2. We need to consider only those atoms that have a nonzero coefficient to have the unpaired spin density. Second, by squaring the Hückel coefficients the spin densities can be determined and are normalized to one,[3.1] as shown on the right in Figure III.2.

Knowing where the spin density resides is crucial in producing high-spin molecules with maximum interaction between two spin centers. Combining two semiquinones via a linker, as discussed in Chapter I, produces a bis-semiquinone. A generic trimethylenemethane-type (TMM-type) bis-semiquinone is shown in Figure III.3.

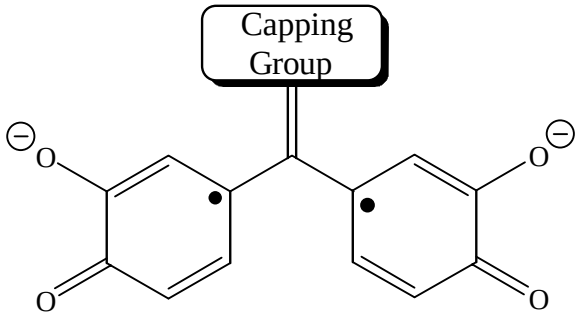

Figure III.3. TMM-type bis-semiquinone.

For a bis-semiquinone there are two NBMOs, which are linear combinations of the bonding and antibonding MO's of a semiquinone perhaps mixed with coupler orbitals. Again, using Hückel theory the coefficients of the atoms can be determined, and by squaring the coefficients the spin densities can be obtained. Shown in Figure III.4 are the NBMO's and their Hückel coefficients of a bis-semiquinone with the ethenylidene coupling unit.

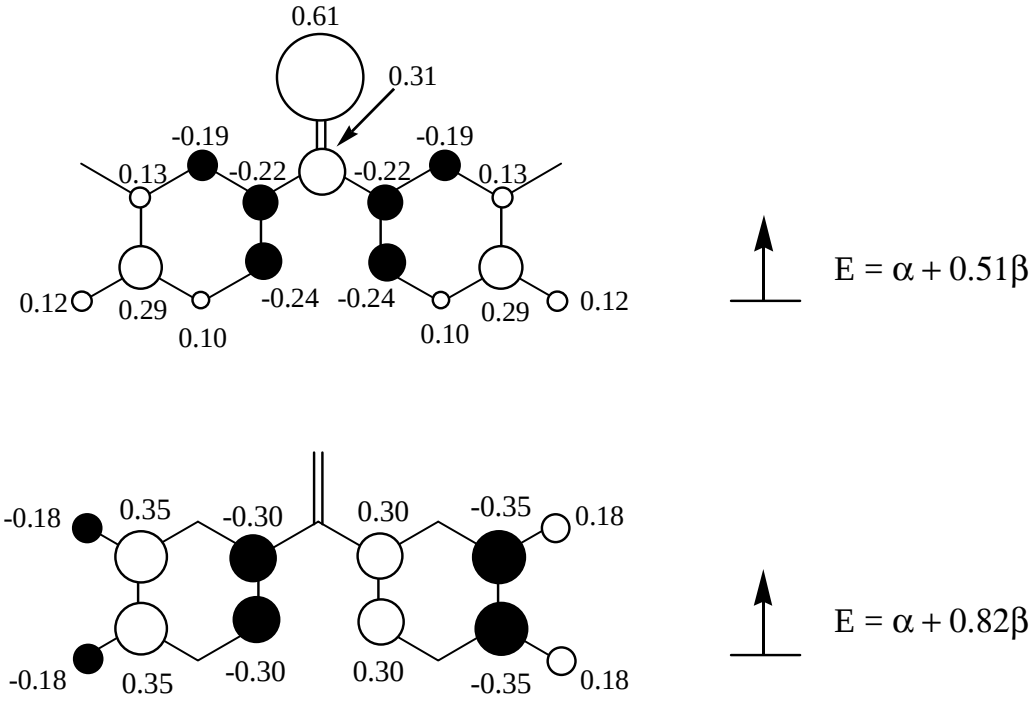

Figure III.4. Hückel coefficients of a bis-semiquinone with an ethenylidene coupling unit.

If the spin densities of the NBMO on the bottom in Figure III.4 are considered, no spin density resides in the ethenylidene coupling unit. However, the NBMO on the top shows about 46% of the spin residing in the coupling unit. Spin density in the coupling unit allows for an interaction between the two spins or exchange coupling to occur.

As discussed in Chapter I, the ethenylidene coupling unit in TMM was compared and contrasted to the carbonyl-coupling unit in oxyallyl (OXA). It was determined that substituting oxygen in place of one of the methylene groups, to give OXA, would lower the energy of the NMBO having electron density on oxygen. It was also shown the electron density of this NBMO shifted to other atoms in the molecule. Theoretically and computationally, oxyallyl alone is not a good candidate as a triplet ground state species.[3.2]

However, we propose that a carbonyl linked between two radical anion semiquinones will exhibit ferromagnetic coupling of the two electron spins. The reason for this is quite simple, carbonyls are well known to delocalize negative charge, as shown in Figure III.5.

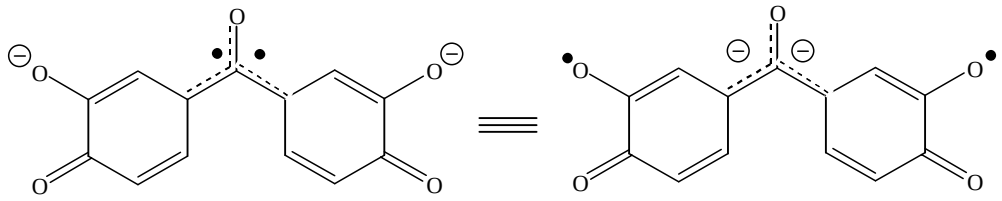

Figure III.5. Carbonyl-linked bis-semiquinone and resonance hybrids of the triplet ground state.

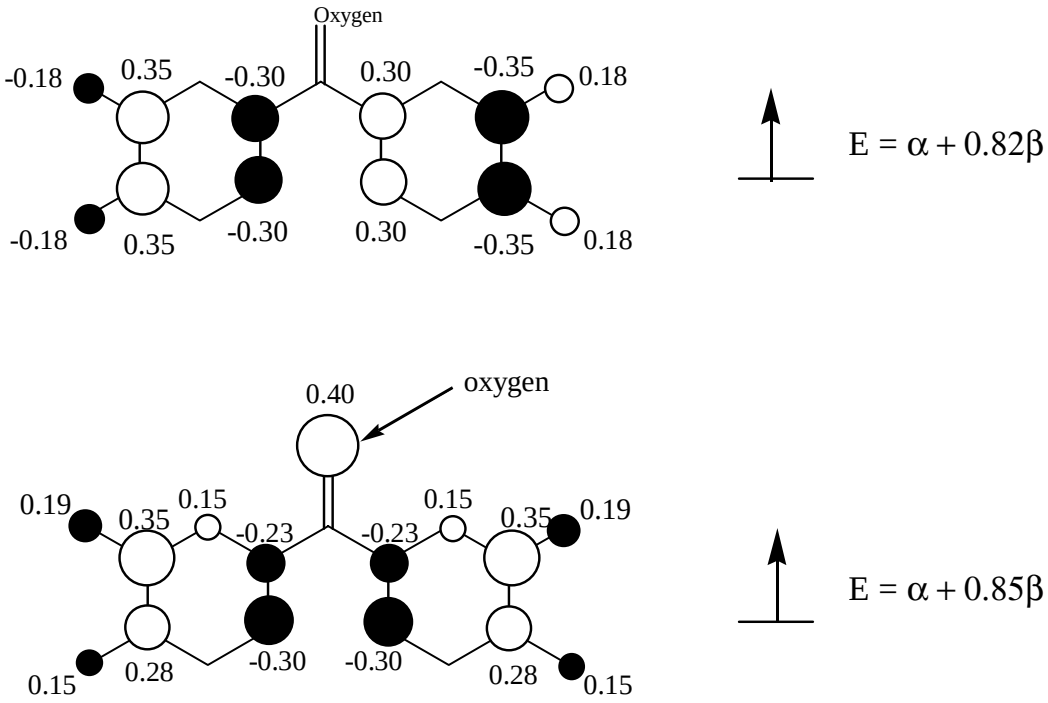

Figure III.6. Hückel coefficients of a bis-semiquinone with a carbonyl-coupling unit.

The energies of the NBMO's of the ethenylidene-linked bis-semiquinone will not dramatically change upon substitution of oxygen. The major reason for this is both bis-semiquinones possess C_{2v} symmetry, therefore, the NBMO's are again not part of a degenerate set. However, this does not mean that the NBMO with electron density where substitution takes place does not lower in energy because it does, as shown in Figure III.6. However, the SOMO-SOMO gap in Figure III.6 is less than that in Figure III.4.

Spin densities are useful and can be obtained using electron paramagnetic resonance. Hyperfine-coupling can be investigated, and, for biradicals, the zero-field splitting parameter D can be obtained, where D is related to the summation of all the products of spin densities

between two radical fragments. For a further understanding of estimating D for biradicals refer to the 1998 paper by Shultz and Sandberg.[3.3]

Now that spin distribution has been considered for the importance behind using semiquinones in the study of radicals, stability will be the next consideration. Semiquinones are fairly stable radicals; however, steric protection and chelation of a metal center is useful in preventing dimerization, other reaction pathways, and decomposition in ambient conditions. Figure III.7 shows two examples where steric protection and chelating a metal center allows for a more stable radical and biradical.

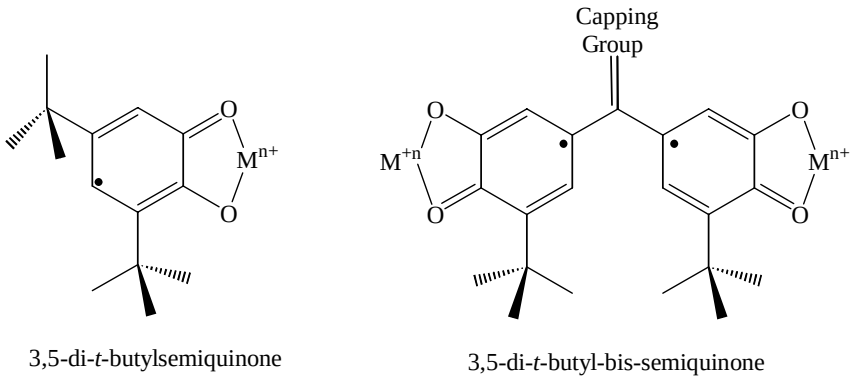

3,5-di-*t*-butylsemiquinone

3,5-di-*t*-butyl-bis-semiquinone

Figure III.7. Sterically protected semiquinone (left) and bis-semiquinone (right).

The sterically protected 3,5-di-*t*-butylsemiquinone, depicted on the left in Figure III.7, has been experimentally and theoretically studied.[3.4, 3.5] Upon chelating different first row transition metals to the semiquinone beautiful crystal structures and magnetic data have been obtained.[3.5] The use of first row transition metal ions will be further discussed in the next

section. The sterically protected 3,5-di-*t*-butyl-bis-semiquione, depicted on the right of Figure III.7, has been extensively studied within the Shultz group. The substitution of various linkers allows for further steric protection; however, may attenuate ferromagnetic interactions.

Another way to ensure steric protection to the bis-semiquinone is by using the bulky ancillary ligand hydrotris(3-*p*-cumenyl-5-methylpyrazolyl)borate, herein known as $Tp^{Cum, Me}$, shown in Figure III.8. This ligand has been previously synthesized by Ruf and Vahrenkampf.[3.4] Pierpont et al made complexes of Zn^{II}, Cu^{II}, and Co^{II} with $Tp^{Cum, Me}$ and 3,5-di-*t*-butylsemiquinone.[3.5] This ligand was chosen for two reasons. The first reason is that the ligand is large and encapsulating. The cumenyl groups provide a protective steric shielding to the semiquinone that allows for further stability and also attenuates the *inter*molecular magnetic interactions and aerobic oxidation to the semiquinone. The second reason for choosing this ligand is to allow for an overall charge neutral molecule. The semiquinone is a radical anion species so to balance the charges of the semiquinone (-1) and the transition metal (+2) another (-1) charge must be incorporated. The $Tp^{Cum, Me}$ qualifies for this condition as there are four bonds to the boron in the ligand, thus giving it a (-1) formal charge. The $Tp^{Cum, Me}$ ligand also helps in the crystallization of the bis-semiquinone complexes by locking the two semiquinones into place. This allows for fewer distortions within the crystal.

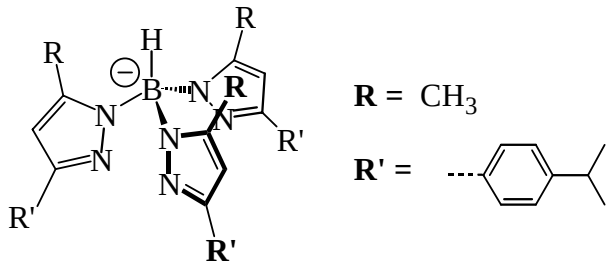

Figure III.8. Potassium hydro-tris(3-cumenyl-5-methyl pyrazolyl)borate ligand ($Tp^{Cum, Me}$).

Semiquinone complexes can be produced using several pathways. Two pathways in particular have produced high yields and upon crystallization produced x-ray and magnetic quality crystals.[3.4, 3.5] The first pathway uses the process of comproportionation. Comproportionation involves combining one equivalent of quinone with one equivalent of the doubly deprotonated catechol (catecholate) to produce two equivalents of a semiquinone, shown in Figure III.9.[3.6]

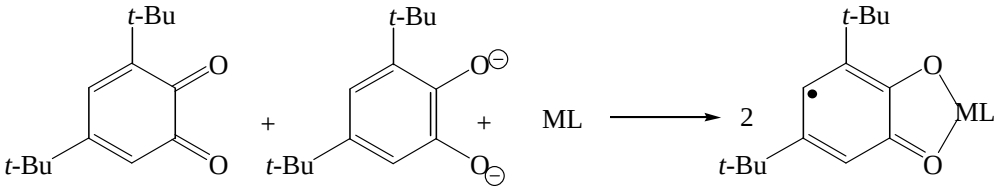

Figure III.9. Comproportionation of one equivalent of quinone and one equivalent of catecholate yielding two equivalents of semiquinone.

The second pathway involves air oxidation to the semiquinone upon the combination of one equivalent of catecholate to one equivalent of the metal ion, as shown in Figure III.10.[3.5, 3.6]

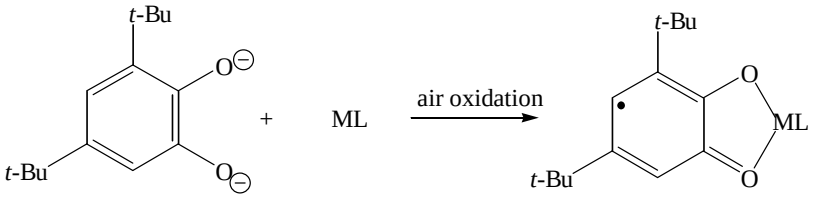

Figure III.10. Semiquinone production upon air oxidation of one equivalent of catecholate and one equivalent of metal ion.

Characterizing semiquinones can be achieved in several fashions. Infrared spectroscopy is a fast and useful tool in characterizing semiquinones. Semiquinones have a distinct C=O stretching frequency near 1445 cm^{-1}. This allows for a distinction between the

characteristic catecholate C-O stretch at 1250 cm^{-1} and the C=O quinone stretch at 1680cm^{-1}. The broad catechol O-H stretch is above 3100 cm^{-1}. Electronic absorption spectroscopy is useful tool in characterizing semiquinones since all semiquinones display absorption in the visible region of the spectrum. A fairly weak semiquinone $n \rightarrow \pi^*$ absorption around 800nm or 12,500cm^{-1} is another indication of semiquinones production. If suitable crystals are grown, x-ray crystallography can be used in elucidating bonds lengths of the semiquinone ring (dioxolene ring). Magnetometry data can be used to determine semiquinone production; however, collecting the data can be tedious. Bis-semiquinones can be detected by all the aforementioned techniques as well as electron paramagnetic resonance (EPR). These characterization techniques will be used later in this chapter to the determination of bis-semiquinones.

III.2. Semiquinone-Metal Interactions.

Thus far the importance behind using semiquinones in the study of radicals has been discussed. In this discussion the use of a transition metal ion attached to two ligands, a semiquinone and $Tp^{Cum, Me}$, produces a stable, magnetically interesting molecule. However, the semiquinone electron and the metal electrons can interact, herein known as metal-ligand exchange coupling. This exchange coupling can vary in magnitude and sign depending on the metal ion. Again, to determine this type of coupling the MOs need to be considered. The semiquinone's MOs and the metal's *d*-orbitals are close enough in energy to maximize mixing.[3.5] If the *p*-orbitals of the semiquinones SOMO are orthogonal to the metal orbital then ferromagnetic coupling results. If the *p*-orbitals of the semiquinones SOMO mix with the metal orbital (same symmetry) then antiferromagnetic coupling results. Figure III.11 is a simple cartoon depicting both types of semiquinone-metal exchange coupling.

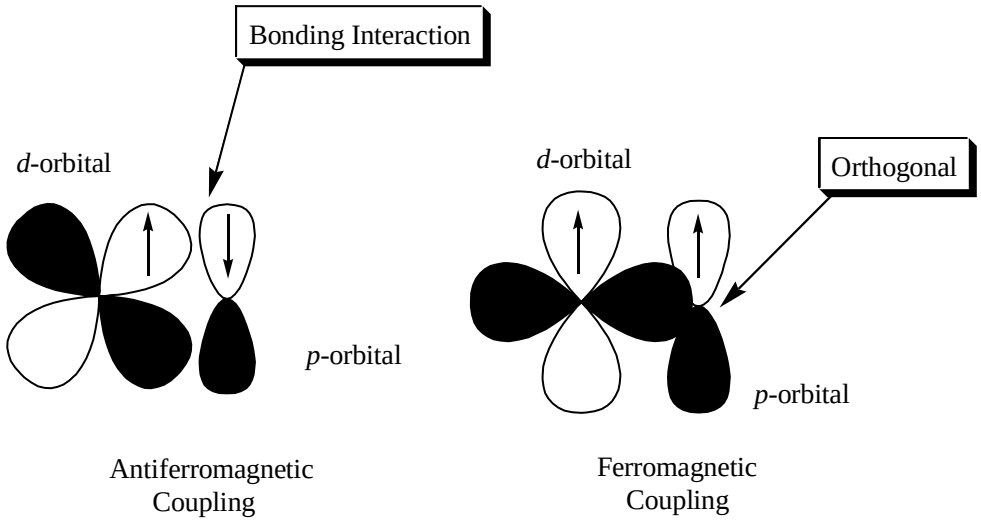

Figure III.11. Antiferromagnetic and ferromagnetic exchange coupling between the *d*-orbitals and *p*-orbitals.

Using the SOMO of 3,5-di-*t*-butylsemiquinone, calculated from Hückel theory, and the metal *d*-orbitals the metal-ligand exchange coupling can be determined for our compounds. The out-of-plane *p*-orbitals of the oxygen atom will be considered since they are part of the π-system. Again, those orbitals that are orthogonal with metal orbitals will give ferromagnetic metal-ligand exchange coupling, and those orbitals that mix will give antiferromagnetic metal-ligand exchange coupling. The semiquinone symmetry is C_{2v}, and the coordination geometry of $Tp^{Cum,Me}$ M(SQ) is trigonal bipyramidal, the local symmetry is C_s for the determination of the exchange coupling, as shown in Figure III.12.[3.7]

.

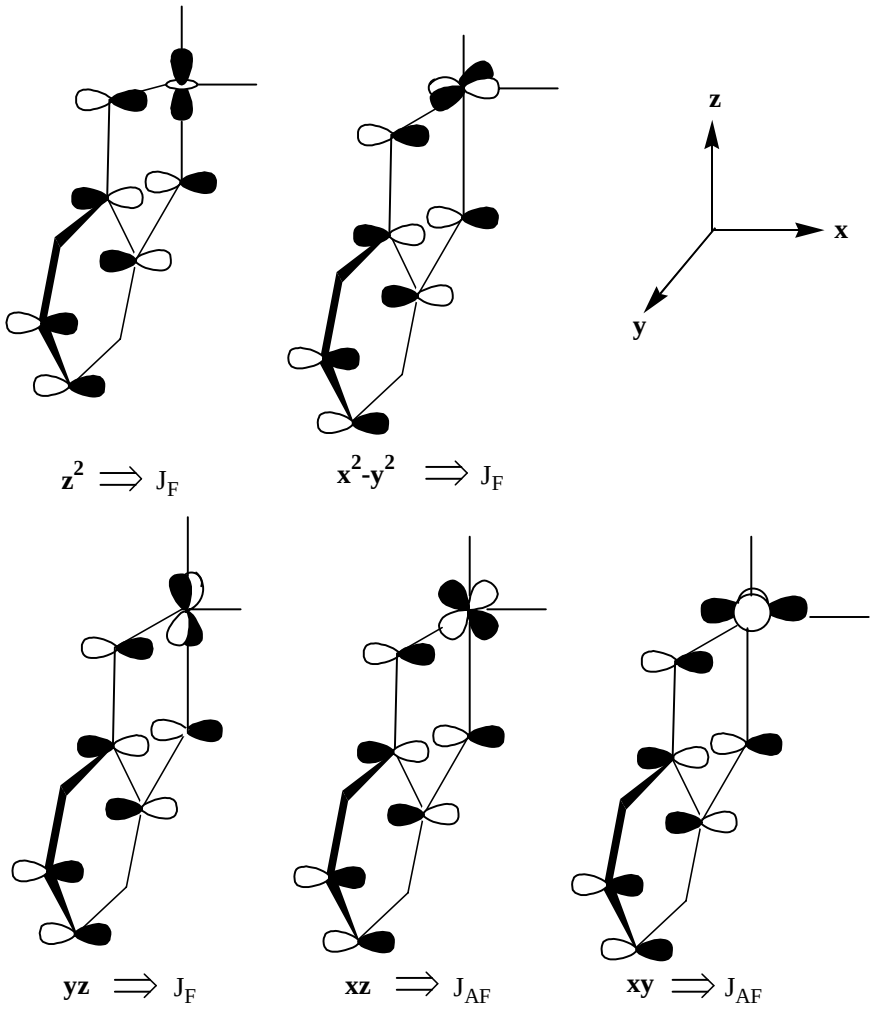

Figure III.12. Antiferromagnetic and ferromagnetic metal-ligand exchange coupling with a semiquinone.

As shown in Figure III.12, the z^2, x^2-y^2, and xy metal orbitals are orthogonal to the semiquinones *p*-orbitals. This orthogonality leads to a ferromagnetic exchange coupling. The metal orbitals xz and yz are symmetric to the semiquinones *p*-orbitals and contribute to an antiferromagnetic exchange coupling. The overall exchange parameter **J** can be expressed in terms of the two adjacent spin sites having *m* and *n* unpaired spins, as shown in Eqn. III.1.[3.7]

$$\mathbf{J} = \frac{1}{mn}\sum_{\mu=1}^{m}\sum_{\nu=1}^{n}\mathbf{J}_{\mu\nu} \qquad \text{Eq III.1}$$

Some examples of the nature of exchange coupling between metals and semiquinones are seen in $Tp^{Cum,Me}Cu(3,5\text{-}DBSQ)$ and the recently reported $(NN\text{-}SQ)MTp^{Cum,Me}$, where M^{II} is Mn, Ni, and Cu, and NN indicates nitronyl nitroxide. In the copper complex, there is a strong ferromagnetic exchange between the unpaired electron of the copper and the unpaired electron in the semiquinone was found to be $J = +52cm^{-1}$.[3.8] In the $(NN\text{-}SQ)MTp^{Cum,Me}$ complexes, an antiferromagnetic exchange decreases between the spins of the (NN-SQ) and M^{II} in the order $(NN\text{-}SQ)NiTp^{Cum,Me}$ ($J = -87.8cm^{-1}$) > $(NN\text{-}SQ)MnTp^{Cum,Me}$ ($J = -41.3cm^{-1}$) > $[NN\text{-}SQ(OMe)CuTp^{Cum,Me}$ ($J = +75.6cm^{-1}$).[3.6] The nature of the semiquinone-metal exchange coupling is useful in the prediction of χT values for spin systems where spin coupling between two semiquinones of most interest.

III.3. Previous Studies on OXA Derivatives and the Stability of Carbonyl-Linked Bis-Semiquinones.

Since Dowd successfully observed the triplet state of TMM in the 1960's, investigations into synthetically stable TMM-type biradicals has increased tremendously.[3.9] As discussed in Chapter I, a molecule whose NBMOs are non-disjoint will aid in the stabilization of the triplet state relative to the singlet state, *i.e.* TMM. Understanding what makes an effective CU is important in the understanding of how to design high-spin molecules. In the Shultz group, the design of high-spin molecules starts with a CU attached to two electroactive groups, for our purposes two dioxolene rings, as shown previously in Figure III.3.[3.10]

The dioxolene rings can display paramagnetic functionalities from the reduction or oxidization by one or more electrons, as shown earlier in Figure III.1. Figure III.13 shows

each dioxolene ring is in conjugation with the coupling unit but not in conjugation with each other. This insures that π-bond formation does not occur. Non-disjoint NBMO's are a product of cross-conjugated dioxolene rings. There are a lot of interesting properties that a molecule can take on when it is generated including mixed valency and, our interest, exchange coupling.[3.10]

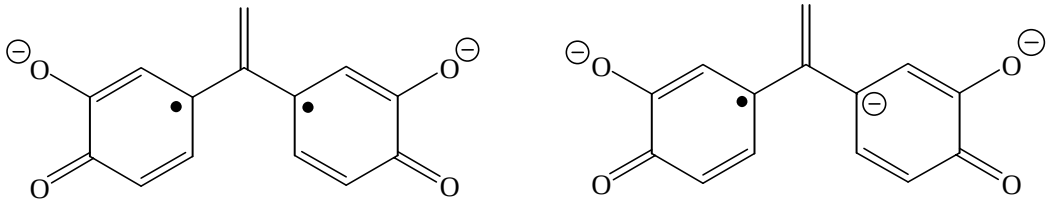

Exchange Coupled Species Mixed-Valent Species

Figure III.13. Two electroactive groups conjugated to an ethenlydiene coupling unit but not conjugated to one another.

The Shultz group has been very successful in the synthesis and characterization of TMM-type bis-semiquinones and the effect on the exchange coupling between two spins upon conformational changes. Examples of these TMM-type bis-semiquinones are shown in Figure III.14.[3.11]

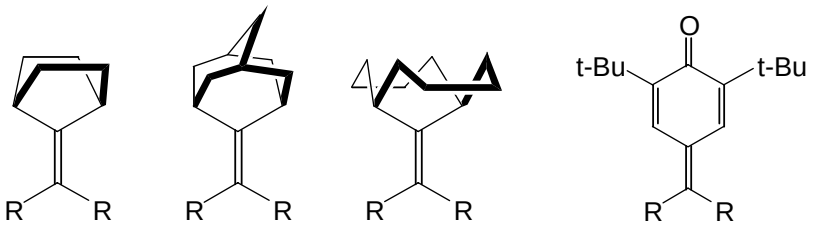

	A	**B**	**C**	**D**
Exchange Coupling, **J**, (cm^{-1})	+87	+24	-35	+209
Avg. $\Sigma\|\Delta_i\|$ (Å)	——	0.114 ± 0.001	0.102 ± 0.01	0.093 ± 0.01
$\|D\|$ (cm^{-1})	0.0098	0.0105	0.0124	0.0093

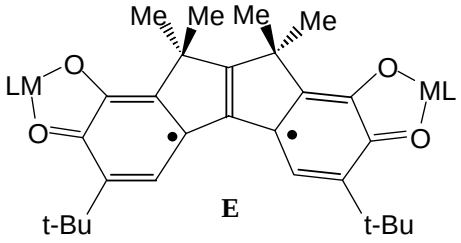

E

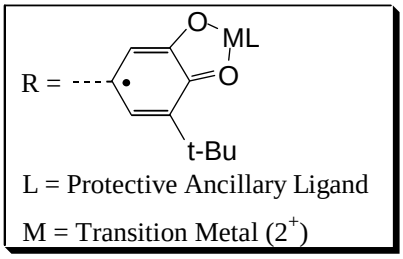

	E
Exchange Coupling, **J**, (cm^{-1})	+100
Avg. $\Sigma\|\Delta_i\|$ (Å)	——
$\|D\|$ (cm^{-1})	0.0068

Figure III.14. TMM-type bis-semiquinones, exchange parameters, J, and structural deviation parameters.

The capping group on the TMM-type CU sterically protects the spin density by preventing decomposition or polymerization. However, the relative bulkiness of a capping group attenuates the ferromagnetic exchange coupling. A variation in bulkiness can be seen in the CUs A through E shown in Figure III.14. In A, (norboryl)bis-semiquinone the bicyclic ring system is not as large as the bicyclic ring system in C, so less ferromagnetic interaction between the semiquinone rings is expected and observed for C. Less interaction between

semiquinones caused by less torsion of the semiquinone rings allows for stronger ferromagnetic exchange coupling and smaller D-values.[3.10, 3.12, 3.13] Therefore, by increasing the bulkiness of the capping group of the CU the singlet-triplet gap becomes smaller.

Now that bulkiness has been taken into consideration, we wish to determine the effect of heteroatom substitution of the CU. Linking C=O to two dioxolene rings will not sterically protect the spin density on the ring but will allow for planarity of the two rings. Planarity will increase the exchange coupling between the two electrons and decrease the D-value. Despite theoretical and computational studies done on OXA[3.2], we believe that attaching C=O to two semiquinones (radical anions) will result in a greater ferromagnetic coupling, due to the nature of C=O's electronegativity, than the observed exchange coupling of the TMM-type bis-semiquinones in Figure III.14.

Only two examples of experimental work on OXA derivatives have been reported to date. Lahti *et al*. have successfully prepared and observed a carbonyl-linked bis-arylnitrene, as shown in Figure III.15.[3.15] Their major finding was that the bis-arylnitrene gave a quintet EPR signal and a Curie Law plot was linear suggesting $\mathbf{J} > 0$ or degeneracy of the quintet and higher lying states. Unfortunately, nitrenes are unstable at ambient conditions so magnetic studies of this compound are quite impossible.

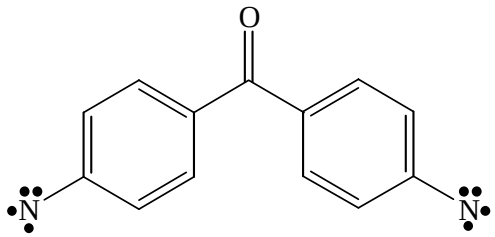

Figure III.15. Carbonyl-linked bis-arylnitrene.

Previous investigates linking a carbonyl to two dioxolene rings showed evidence of a triplet ground state; however, it was not isolable, Figure III.16.[3.14]

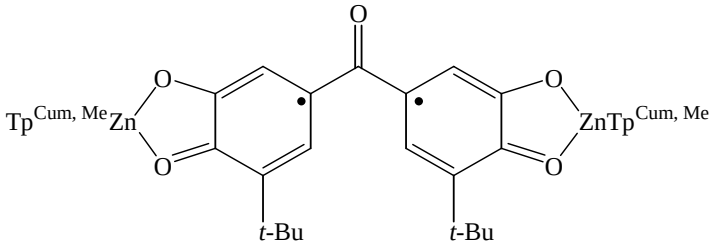

Figure III.16. $(Tp^{Cum,\ Me}Zn)_2$-*t*-Bu.

The synthesis of $(Tp^{Cum,\ Me}Zn)_2$-*t*-Bu begins with the preparation of the bis-catechol precursor, Scheme III.1.

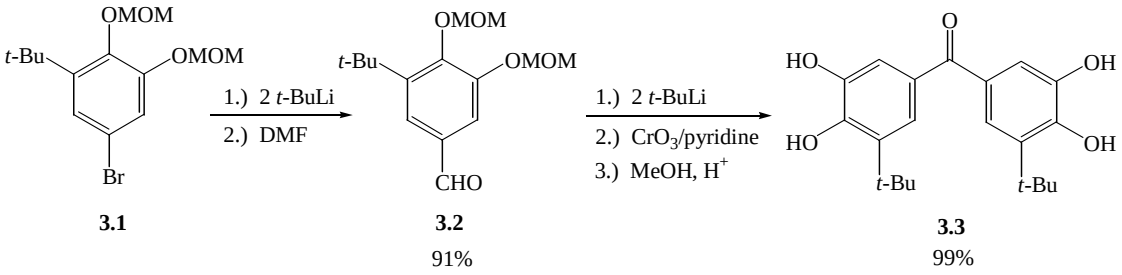

3.1 **3.2** 91% **3.3** 99%

Scheme III.I. Synthesis of bis-catechol **(3.3)**.

The bromide **(3.1)** is converted to the corresponding aldehyde **(3.2)** by a lithium-halogen exchange followed by reaction with dimethylformamide and work-up. The biscatechol is then obtained by addition of the appropriated amount of lithiated **(3.1)** to **(3.2)** followed by oxidation using Collin's Reagent to obtain the carbinol. The carbinol is then deprotected using standard conditions of a catalytic amount of concentrated hydrochloric acid in methanol to obtain the biscatechol **(3.3)** in good yield.

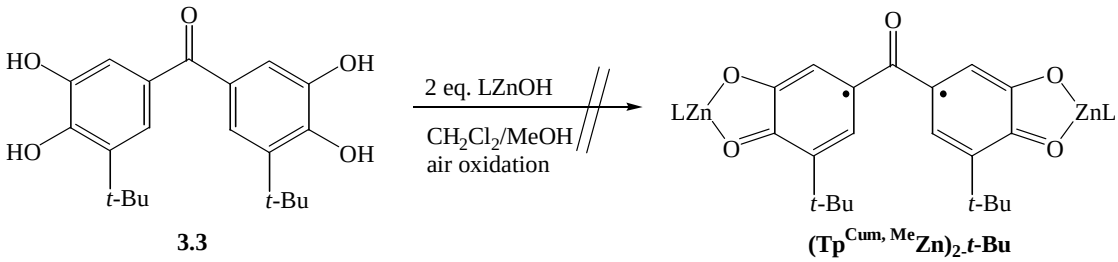

3.3 **$(Tp^{Cum, Me}Zn)_2$-*t*-Bu**

Scheme III.2. Failed synthetic attempt to produce $(Tp^{Cum, Me}Zn)_2$-*t*-Bu.

Unfortunately, the reaction of **(3.3)** with two equivalents of $Tp^{Cum, Me}$ ZnOH does not yield the target molecule $(Tp^{Cum, Me}Zn)_2$-*t*-Bu, Scheme III.2. This is evident from the lack of fine structure in the EPR spectrum at 77K, the appearance of OH stretching in the IR at 3635 cm^{-1}, the lack in appearance of C-O stretching indicative of bis-semiquinones, usually between 1420-1480 cm^{-1}, and a magnetic moment that is less than $1.7\mu_B$. Even though the bis-semiquinone was not generated, crystallization produced x-ray quality crystals. Two different types of crystals were obtained, pale green cubes and irregularly shaped blue crystals. The ORTEP diagrams and crystal bond length data of each crystal are seen in Figure III.17 and Tables III.1 and III.2.[3.14]

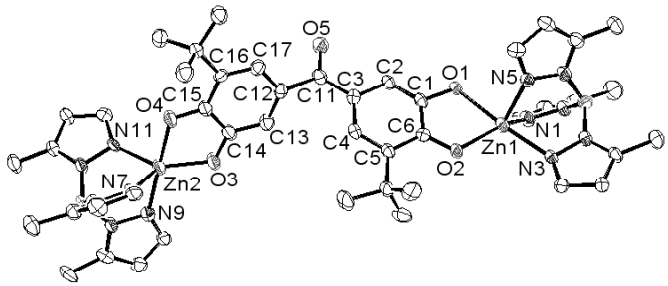

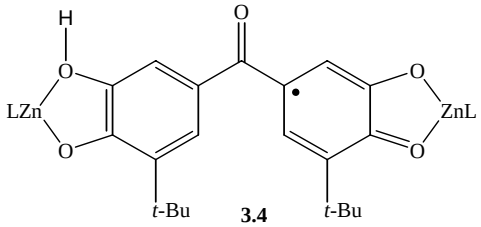

3.4

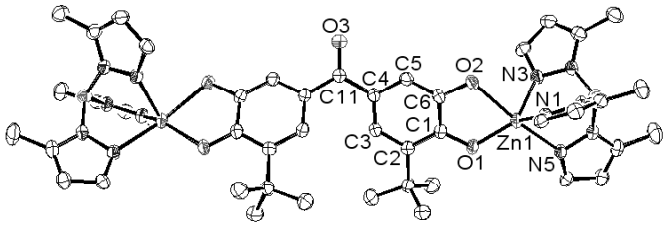

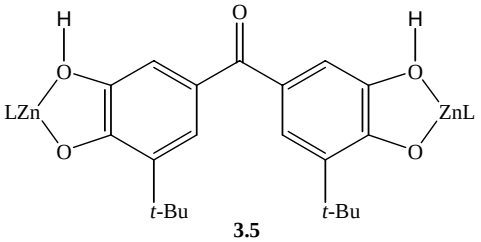

3.5

Figure III.17. ORTEP representations of the crystal structures **(3.4)** and **(3.5)**. Cumenyl groups are omitted for clarity.

Table III.1. Important Bond Lengths (Å) for **(3.4)**.

Bond	Length (Å)	Bond	Length (Å)
Zn1-O2	1.929(4)	Zn1-N1	2.049(6)
Zn1-N5	2.068(6)	Zn1-N3	2.175(5)
Zn1-O1	2.266(5)	Zn2-O3	1.977(5)
Zn2-N11	2.035(6)	Zn2-N7	2.049(6)
Zn2-O4	2.149(5)	Zn2-N9	2.217(6)
O1-C1	1.387(8)	O2-C6	1.323(7)
O3-C14	1.309(8)	O4-C15	1.298(8)
O5-C11	1.237(8)	C1-C2	1.372(9)
C1-C6	1.412(9)	C2-C3	1.413(9)
C3-C4	1.408(9)	C3-C11	1.445(9)
C4-C5	1.390(9)	C5-C6	1.431(9)
C11-C12	1.515(9)	C12-C13	1.372(9)
C12-C17	1.428(9)	C13-C14	1.416(9)
C14-C15	1.462(10)	C15-C16	1.441(9)
C16-C17	1.369(9)		

Table III.2. Important Bond Lengths (Å) for **(3.5)**.

Bond	Length (Å)	Bond	Length (Å)
Zn1-O1	1.915(3)	Zn1-N3	2.047(3)
Zn1-N1	2.050(3)	Zn1-N5	2.134(3)
Zn1-O2	2.282(3)	O1-C1	1.328(5)
O2-C6	1.377(5)	O3-C11	1.253(7)
C1-C6	1.421(6)	C1-C2	1.423(5)
C2-C3	1.397(6)	C3-C4	1.403(6)
C4-C5	1.405(6)	C4-C11	1.475(5)
C5-C6	1.374(6)		

Based on previous work of other bis-semiquinones[3.13], another possible complex, **(3.6)**, was a forerunner along with complexes **(3.4)** and **(3.5)**. However, based on bond lengths **(3.6)** is precluded.

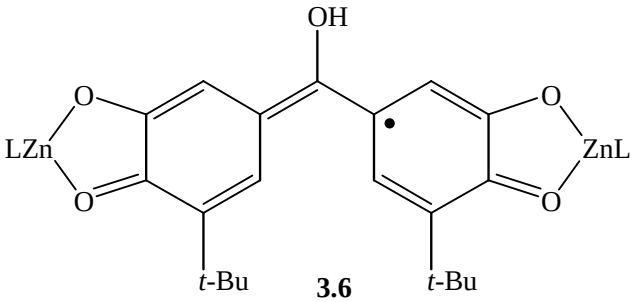

3.6

Figure III.18. Hypothetical carbonyl-linked quinonemethide-semiquinone.

It was concluded from the comparison with Pierpont's Zn($Tp^{Cum, Me}$)-3,5-$DBSQ^{3.5}$ bond lengths and the dioxolene ring bond lengths of carbonyl-linked **(3.4)** and **(3.5),** that the proton from each protonated catecholate group is on the less acidic oxygen, Figure III.19. This leaves the oxygen in the para-position with respect to the carbonyl having a –1 formal charge. Delocalization of the –1 formal charge into the dioxolene ring as evident from the bond lengths gives the resonance structures in Figure III.20.

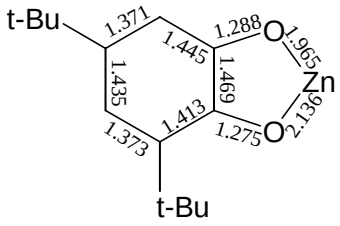

3,5-DBSQZn(Tp^{Cum,Me})

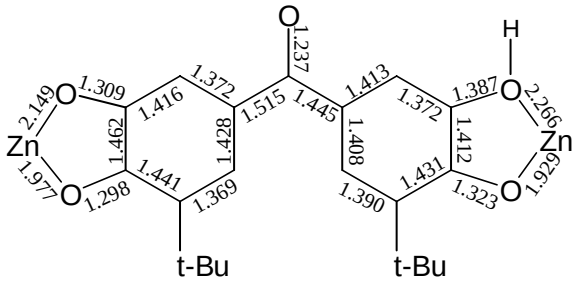

Semiquinone

Protonated Catecholate

3.4

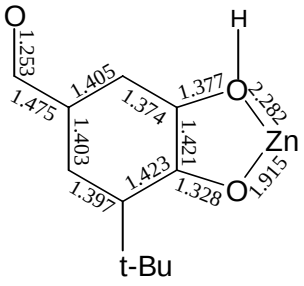

Protonated Catecholate

3.5

Figure III.19. Comparison of bond lengths with 3,5-DBSQZn(Tp$^{Cum, Me}$) and carbonyl-linked **(3.4)** and **(3.5)**.

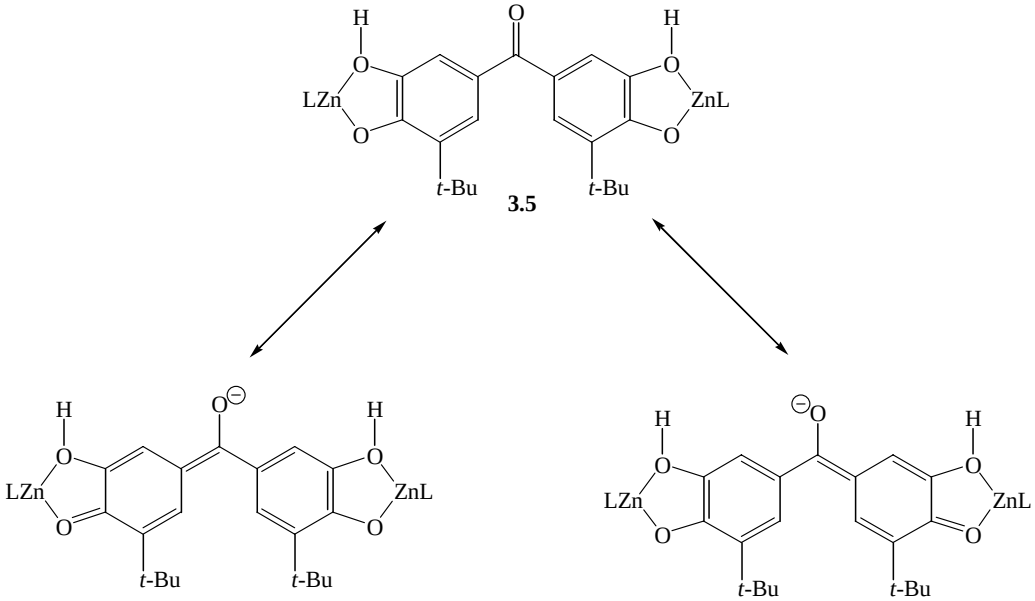

Figure III.20. Delocalization of –1 formal charge of **(3.5)**.

Complex **(3.4)** has crystallographic symmetry about the carbonyl C-O bond; therefore, only half of the complex is shown in Figure III.19. Structural deviation parameters can be calculated for the two crystal structures. A structural deviation parameter, $\Sigma|\Delta_i|$, can be defined as the sum of bond length deviations of the target molecule from a reference molecule. The $\Sigma|\Delta_i|$ will never be zero. The point of the deviation parameter is to give an idea of how a dioxolene ring's bond lengths compare to those of a known semiquinone dioxolene ring. If the bond lengths are similar then our dioxolene ring has "normal" semiquinone character. If the deviation is large then there are two possibilities that can exist: (1) the dioxolene ring is in a different oxidation state and/or (2) the dioxolene ring is a semiquinone that is delocalized into other parts of the compound. If the amount of delocalization is large then the deviation will be large and vice versa for a small amount of deviation.

In this case the target molecules/complexes are **(3.4)** and **(3.5),** and the reference is 3,5-DBSQZn($Tp^{Cum, Me}$), as shown in Figure III.19. The structural deviation parameter for complex **(3.5)** was determined to be $\Sigma|\Delta_i| = 0.361$Å. This is relatively large but expected since the dioxolene rings of **(3.5)** are not even in the same oxidation state as a semiquinone. Complex **(3.4)** has two structural deviation parameters because there are two different dioxolene rings, protonated catecholate and semiquinone. For the semiquinone part of complex **(3.4),** the deviation is $\Sigma|\Delta_i| = 0.120$Å, which is quite smaller than the deviation in **(3.5)**. This means that there is not much deviation from the bond lengths of 3,5-DBSQZn($Tp^{Cum, Me}$) and that there is some delocalization of the radical anion into the carbonyl CU. For the protonated catecholate part of complex **(3.4)**, the deviation is $\Sigma|\Delta_i| =$ 0.381Å. Again, this is quite a large deviation from the reference complex but expected.

Although crystal structures are interesting and useful, the main goal to this project was to produce the bis-semiquinone. Since air oxidation was not enough to produce the bis-semiquinone and a single EPR signal was observed at 77K for complex **(3.4)**, additional assistance was needed. Oxidation with PbO_2 yields evidence of a triplet ground state by frozen solution EPR, as shown in Figure III.21. Zero-field splitting parameters were calculated from spectral simulation to be $|D/hc| = 0.01077cm^{-1}$ and $|E/hc| = 0.0011cm^{-1}$.[3.16]

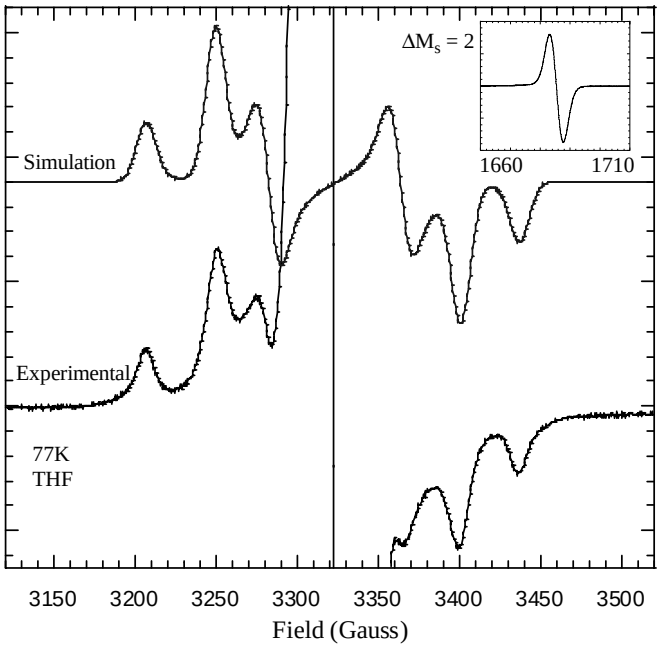

Figure III.21. EPR spectra at (77K; THF) of oxidized carbonyl-linked **(3.4)** and **(3.5)** (bottom) and $\Delta M_s = 2$ transition (inset). Simulated EPR spectrum with $|\mathbf{D}/hc| = 0.01077cm^{-1}$ and $|\mathbf{E}/hc| = 0.0011cm^{-1}$.

III.4. Results, Discussions, and Conclusions to Producing the First Isolable Carbonyl Linked Bis-Semiquinone.

Previous work has shown evidence of a carbonyl-linked bis-semiquinone triplet species upon oxidation with PbO_2. Unfortunately, the molecule $(Tp^{Cum, Me}Zn)_2$-*t*-Bu was not isolated, and no exchange coupling was obtained. Herein are recent studies into obtaining an isolable carbonyl-linked bis-semiquinone and efforts in collecting exchange coupling data. We propose putting a stronger electron-donating group, *i.e.* methoxy instead of *t*-butyl, onto the dioxolene ring. This will raise the energy of the semiquinones NBMO making it more oxidizable. We also propose to use a less electronegative metal center, i.e. manganese instead of zinc. The d-orbitals of manganese will be closer in energy to the semiquinone's NBMO which will allow for greater mixing of the orbitals. This will raise the energy of the semiquinone's NBMO making it more easily oxidizable.

Bis-catechol **(3.3)** was successfully synthesized as shown in Scheme III.1. However, **(3.3)** was synthesized using a somewhat different approach eliminating the need to synthesize **(3.2)**.

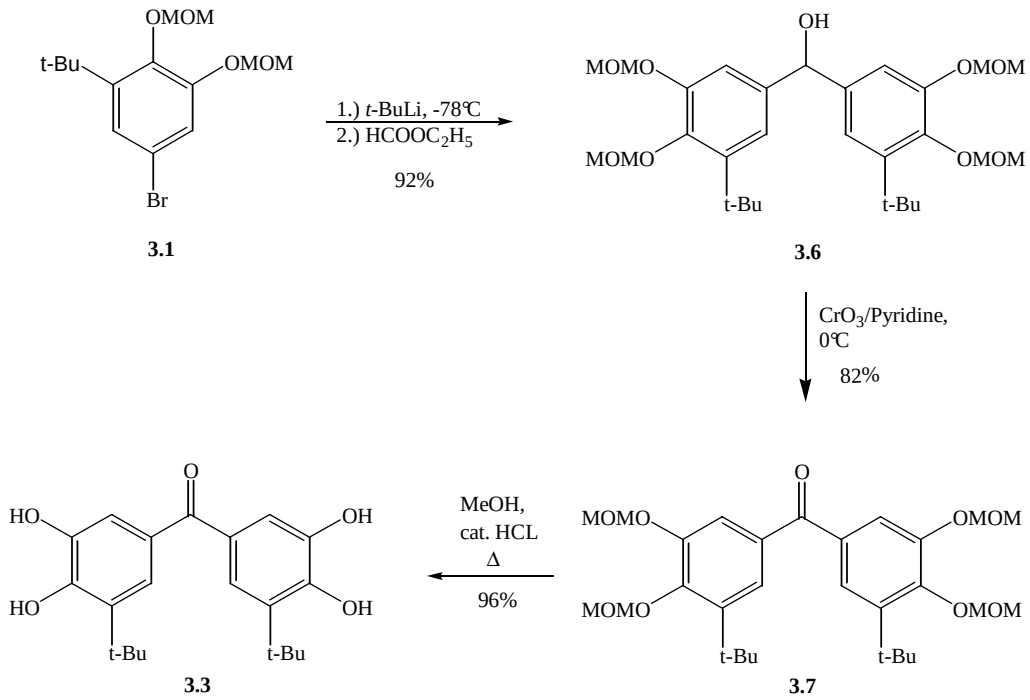

Scheme III.3. Alternate synthesis of bis-catechol **(3.3)**.

Bromide **(3.1)** undergoes a lithium-halogen exchange followed by reaction with the appropriate amount of ethyl formate to obtain the secondary alcohol **(3.6)**. As in Scheme III.1, the use of Collin's reagent gives the subsequent carbinol **(3.7)**, which is then deprotected using a catalytic amount of concentrated hydrochloric acid in methanol to obtain the bis-catechol **(3.3)** in good yield.

The bis-catechol **(3.3)** is then reacted with two equivalents of **LZn(OH)** as shown in Scheme III.2. From the lack of fine structure in the EPR at 77K, the appearance of O-H stretching in the IR at 3420 cm^{-1}, and lack in appearance of C-O semiquinone stretching we concluded that a mixture of (3.4) and (3.5) were again obtained. Upon oxidation with PbO_2

the triplet species grew in intensity while the monoradical/double quantum transition decreased in intensity, as shown in Figure III.22.

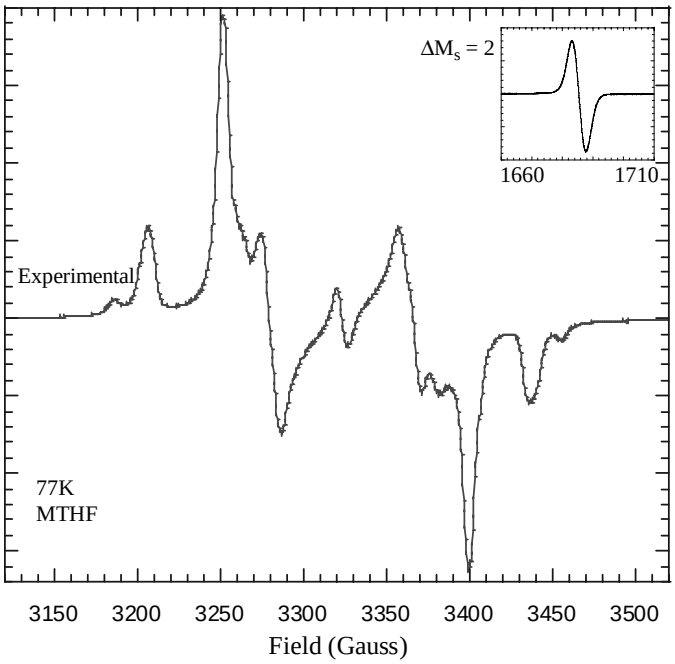

Figure III.22. Experimental EPR spectrum (77K; MTHF) of a mixture of oxidized **(3.4)** and **(3.5)** (bottom) and the $\Delta M_s = 2$ transition near half field (inset). Simulated EPR spectrum with $|\mathbf{D_1}/hc| = 0.0108 cm^{-1}$ and $|\mathbf{D_2}/hc| = 0.0126 cm^{-1}$.

The spectrum in Figure III.22 displays fine structure in the EPR and a growing $\Delta M_s = 2$ transition producing almost pure triplet species upon oxidation! Upon visual inspection of

the EPR spectrum several rotomers were formed at 77K. Since each rotomer has its own ZFS parameters there are several **D**- and **E**-values. However, only the **D**-values can be easily simulated (simulation 1 and simulation 2) since the x- and y-components overlap. The **D**-value for simulation 1 was determined to be $|\mathbf{D_1}/hc| = 0.0108cm^{-1}$, where $\mathbf{D_1}$ is the more predominant rotomer signal (inner). The **D**-value for simulation 1 was determined to be $|\mathbf{D_2}/hc| = 0.0126cm^{-1}$, where $\mathbf{D_2}$ is the rotomer with a less intense signal (outer).

Production of almost pure triplet species is evident that pure **LZn(OH)** needs to be used to ensure that chelation is effective. Not only does non-pure **LZn(OH)** give a mixture of complexes **(3.4)** and **(3.5)** but also gives a mixture of doubly protonated catecholate, monoradical, and biradical (upon oxidation). This is evident from the spectrum in Figure III.21 where the amount of monoradical is significantly larger than the amount of biradical. Due to the strong $\Delta M_s = 2$ transition near half field variable temperature EPR studies were conducted, and the results are shown in Figure III.23.

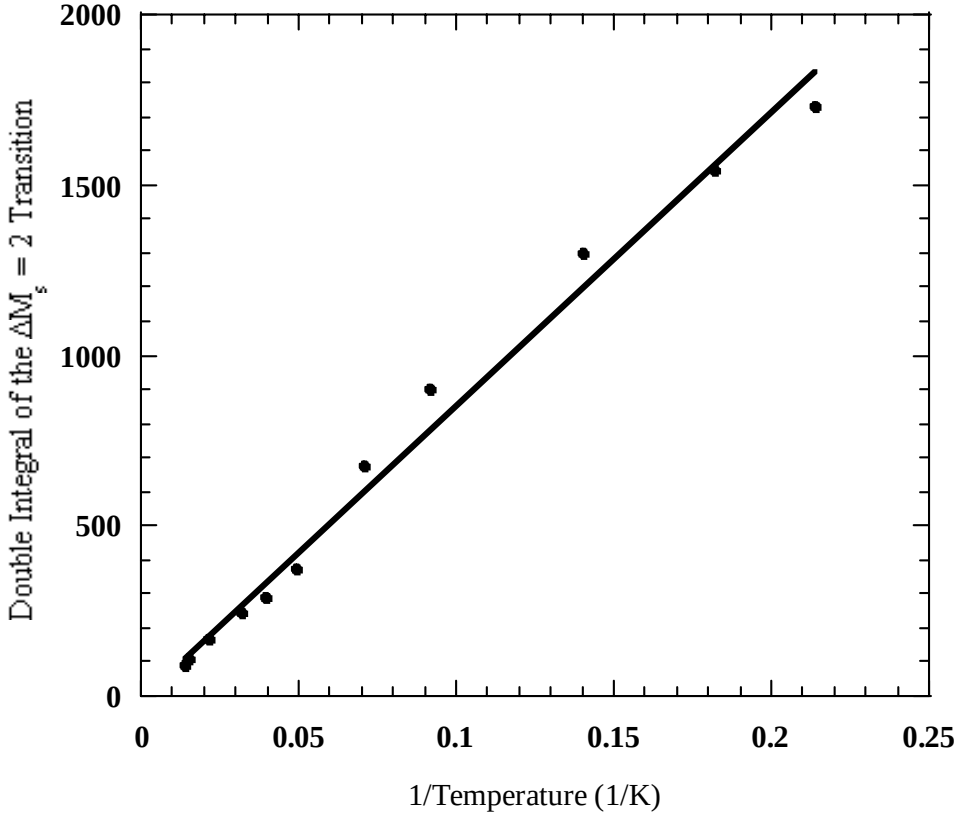

Figure III.23. Variable EPR studies on a mixture of **(3.4)** and **(3.5)** suggests ferromagnetic coupling of the two electron spins.

The linear relationship in Figure III.23 suggests that either the two electron spins are ferromagnetically coupled, **J** > 0, or there is a degeneracy of the singlet and triplet states. Unfortunately, no crystals were formed upon crystallization so no magnetic data was obtained.

The next step is to use a less electronegative metal center instead of zinc. Dr. Krishna Kumar successfully synthesized and obtained a crystal structure on **$(Tp^{Cum, Me}Co)_2$-*t*-Bu**, **(3.8)**, shown in Scheme III.4 and Figure III.24. Scheme III.4 displays the successful attempt to synthesize **$(Tp^{Cum, Me}Co)_2$-*t*-Bu** using the same standard conditions as previously mentioned.

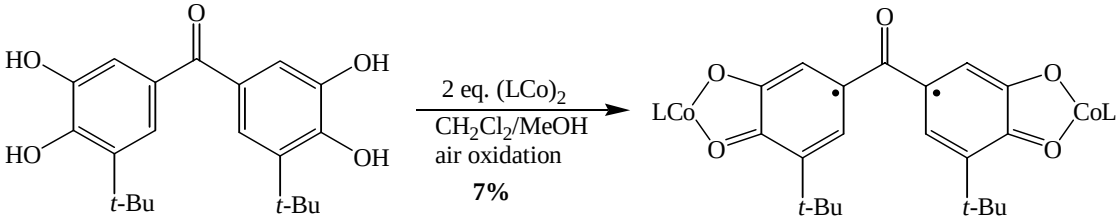

3.3 **3.8**

Scheme III.4. Successful synthetic attempt to produce **(3.8)**.

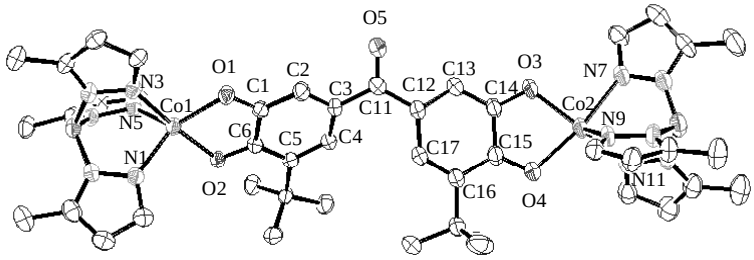

Figure III.24. ORTEP representation of the crystal structure **(3.8)**. Cumenyl groups are omitted for clarity.

Table III.3. Important Bond Lengths (Å) for **(3.8)**.

Bond	Length (Å)	Bond	Length (Å)
Co1-O2	2.057(4)	Co1-N1	2.051(6)
Co1-N5	2.132(6)	Co1-N3	2.058(5)
Co1-O1	1.976(5)	Co2-O3	1.989(5)
Co2-N11	2.067(6)	Co2-N7	2.131(6)
Co2-O4	2.043(5)	Co2-N9	2.044(6)
O1-C1	1.279(8)	O2-C6	1.268(7)
O3-C14	1.286(8)	O4-C15	1.272(8)
O5-C11	1.240(8)	C1-C2	1.441(9)
C1-C6	1.469(9)	C2-C3	1.365(9)
C3-C4	1.428(9)	C3-C11	1.498(9)
C4-C5	1.380(9)	C5-C6	1.444(9)
C11-C12	1.470(9)	C12-C13	1.387(9)
C12-C17	1.435(9)	C13-C14	1.391(9)
C14-C15	1.483(10)	C15-C16	1.439(9)
C16-C17	1.355(9)		

Complex **(3.8)** has does not have crystallographic symmetry about the carbonyl C-O bond so all the bond lengths are different. A structural deviation parameter, $\Sigma|\Delta_i|$, and again

if defined as the sum of bond length deviations of the target molecule from a reference molecule. In this case the target complex are **(3.8)** and the reference is 3,5-DBSQZn($Tp^{Cum, Me}$), as shown in Figure III.25. The structural deviation parameter for complex **(3.8)** was determined to as an average of both sides of the complex to be $\Sigma|\Delta_i| = 0.203 \pm 0.04$Å, which is quite large compared with the molecules in Figure III.14.

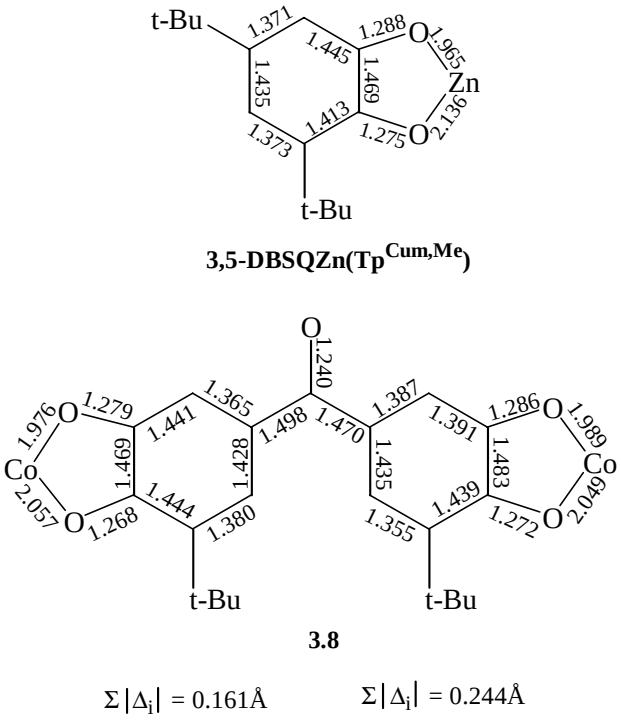

Figure III.25. Comparison of bond lengths with 3,5-DBSQZn($Tp^{Cum, Me}$) and carbonyl-linked (3.8) where $\Sigma_{avg}|\Delta_i| = 0.203 \pm 0.04$Å.

The complex nature of cobalt does not allow us to obtain EPR data. **(3.8)** was characterized using other characterization techniques. UV-Vis data was obtained and the typical n $\rightarrow \pi^*$ band for a semiquinone was observed between 12,000-14,000 cm^{-1}, as shown in Figure III.26.

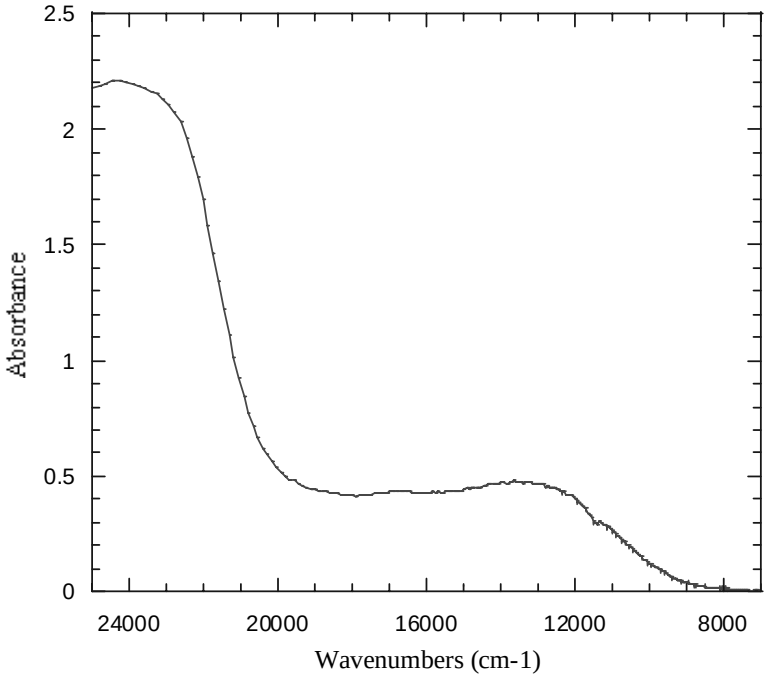

Figure III.26. UV-Vis spectrum of **(3.8)** with semiquinone n $\rightarrow \pi^*$ transition.

Magnetic data was obtained and the saturation magnetization and Curie Law plots are shown in Figures III.27 and III.28. As previously discussed, the two cobalts are antiferromagnetic coupled to the semiquinones rings and each cobalt contains three unpaired

spins. If the two electrons spins of the semiquinones are coupled ferromagnetically then upon saturation of the sample the plot will saturate to four Bohr magnetons, as shown in Figure III.27.

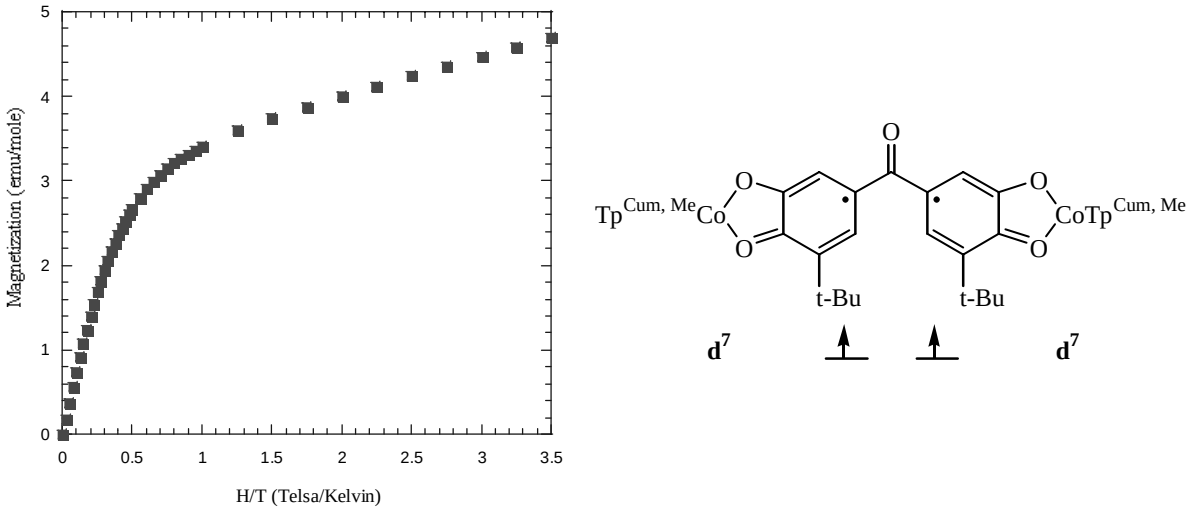

Figure III.27. Saturation magnetization data of **(3.8**) suggests ferromagnetic coupling between to the two electron spins.

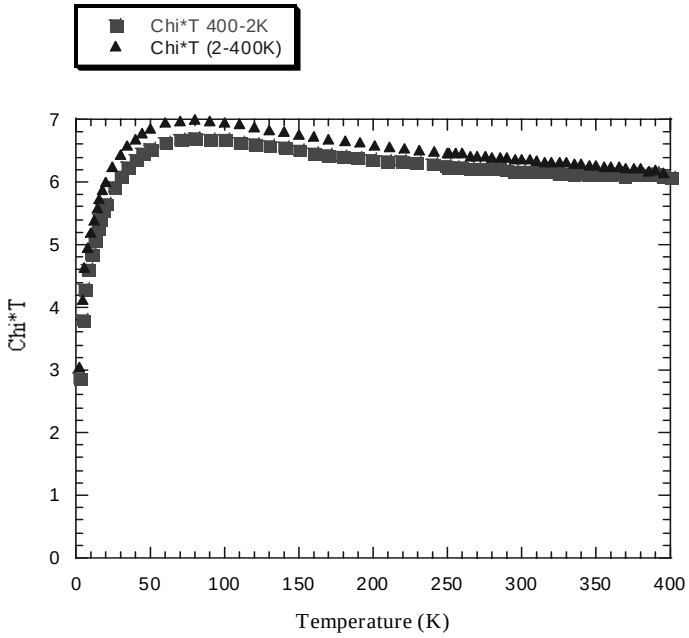

Figure III.28. Variable SQUID magnetic data of **(3.8)**.

Figure III.28 also suggests that the two spins are ferromagnetically coupled due to the increase in the χ_{para} as the temperature is lowered. However, the magnetic data is not well understood for cobalt complexes so it is virtually impossible to extract the magnitude of the exchange coupling.

The use of an even less electronegative metal center such as manganese was the next attempt to obtain a stable complex from which we could possibly obtain the magnitude of the exchange coupling between the unpaired electron spins. Scheme III.5 shows the attempt to produce the complex $(Tp^{Cum,\ Me}Mn)_2$-*t*-Bu, **(3.9)**.

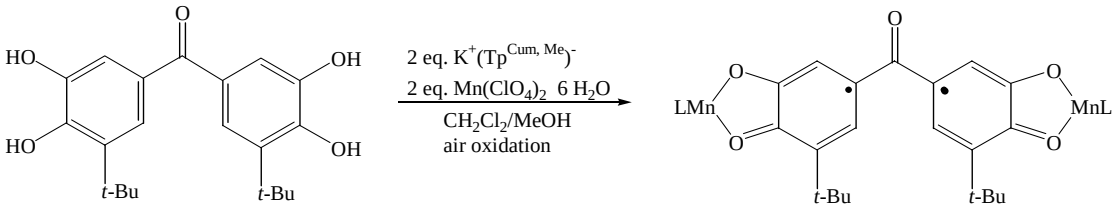

3.3 **3.9**

Scheme III.5. Attempted synthesis of **(3.9)**.

Upon crystallization, a mixture of white precipitate and brown precipitate were obtained but no crystals. The white precipitate is most likely potassium perchlorate as indicated by the IR stretching between 1080-1150cm^{-1}.[3.17] The brown precipitate shows IR stretching between 1420-1480cm^{-1} (indicative to semiquinone C-O stretching) and a lack of O-H and quinone stretching. UV-vis studies done on complex **(3.9)** show the semiquinone $n \rightarrow \pi^*$ transition between 12,000 and 14,000cm^{-1}, as shown in Figure III.29.

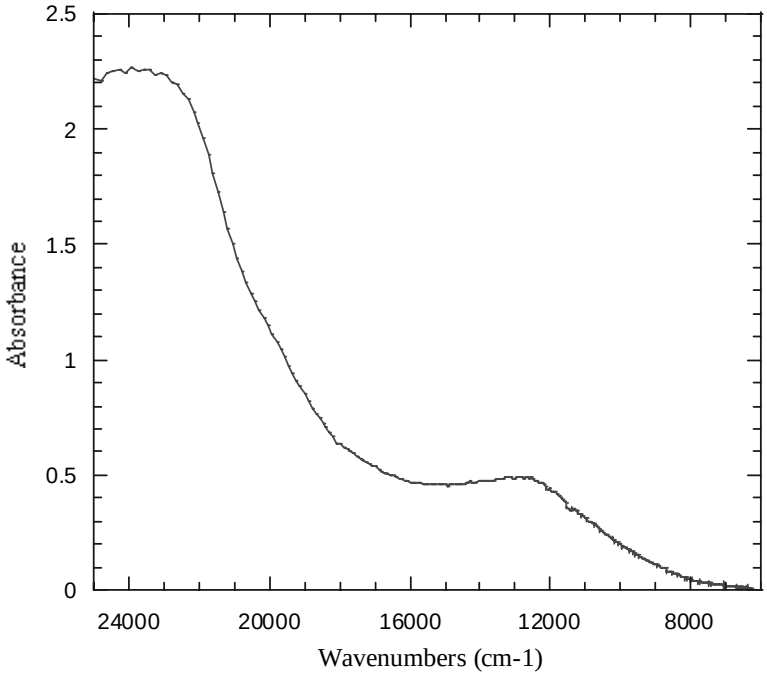

Figure III.29. UV-Vis spectrum of **(3.9)** with semiquinone n $\rightarrow$ π^* transition.

Magnetic studies were attempted with the small amount of brown precipitate recovered from the crystallization. Again, the coupling between the manganese unpaired electrons and the electrons of the semiquinone are antiferromagnetically coupled. If we assume the two electron spins of the semiquinones are ferromagnetically coupled then the saturation magnetization plot should saturate to about eight Bohr magnetons. The saturation magnetization studies suggest the two electron spins are ferromagnetically coupled, as shown in Figure III.30.

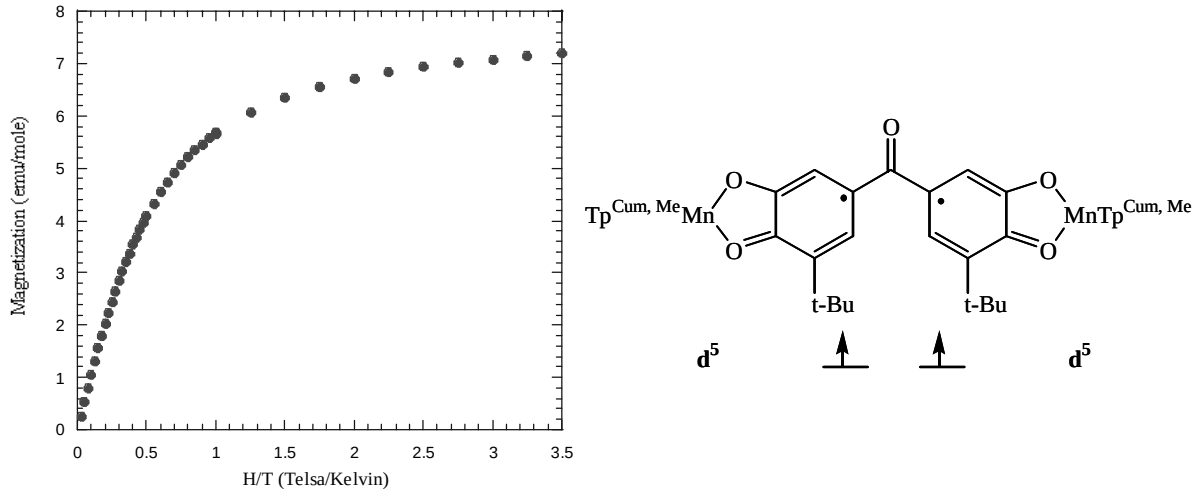

Figure III.30. Saturation magnetization data of **(3.9)** suggests ferromagnetic coupling between to the two electron spins.

Unfortunately, attempts to obtain variable temperature magnetic data on complex **(3.9)** were unsuccessful due to the small amount of material obtained during crystallization. Several attempts to bring up more material did not produce the desired saturation magnetization as shown in Figure III.30.

The final approach at obtaining the magnitude of the exchange coupling between the two electron spins of the bis-semiquinone involved attaching a stronger electron-donating group to the dioxolene rings. This should increase the oxidizability of the bis-catechol making it easier to chelate **LZn(OH)**. The bis-catechol **(3.16)** was successfully synthesized as shown in Scheme III.6.

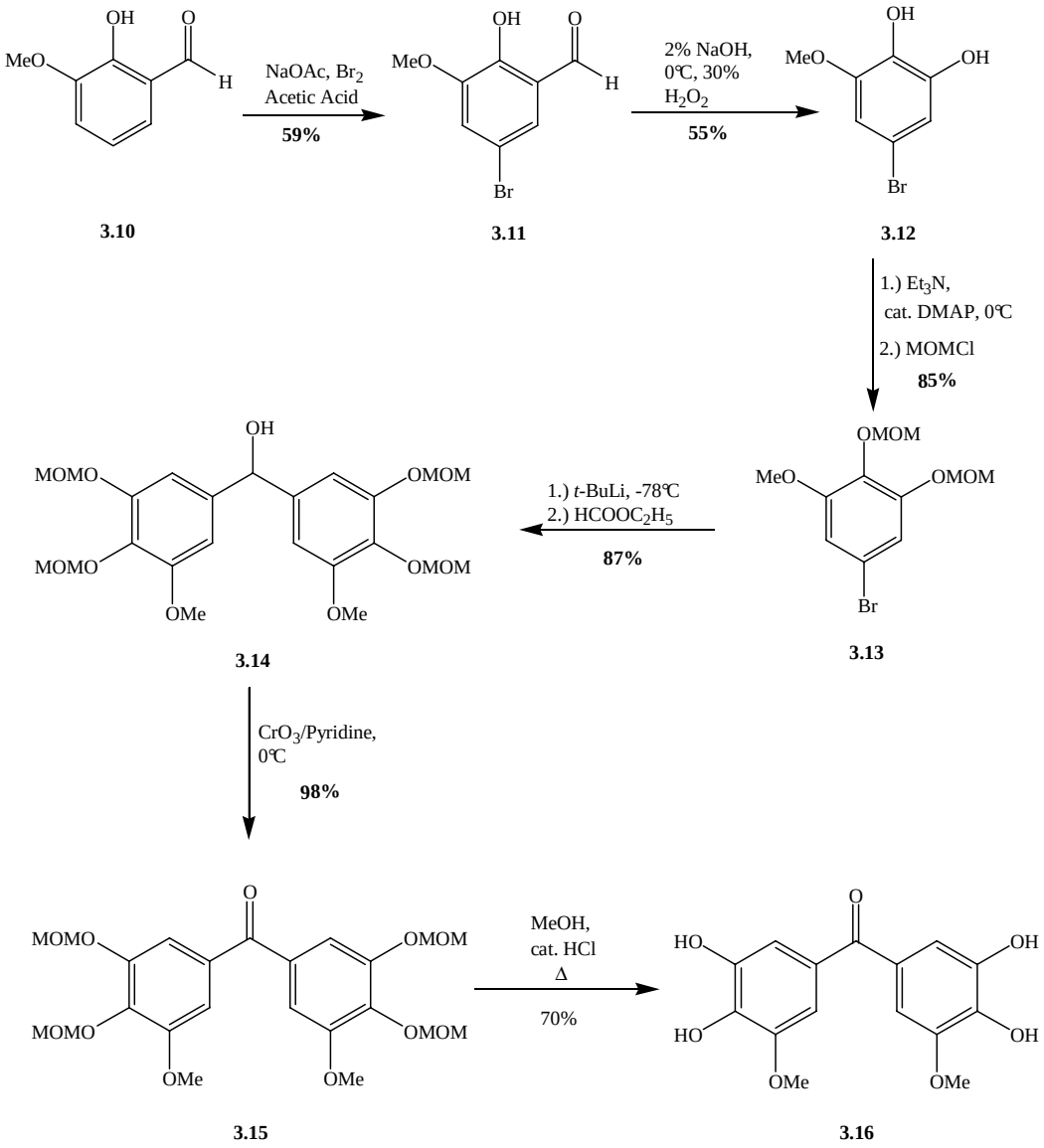

Scheme III.6. Synthesis of bis-catechol **(3.16)**.

The synthesis of the bis-catechol **(3.16)** starts with the bromination of the commercially available **(3.10)** to give **(3.11)**. Molecule **(3.11)** undergoes the Dakin reaction[3.18] to produce the catechol **(3.12)**, which is then protected with methoxymethyl ether

(MOM) groups to give **(3.13)**. One equivalent of compound **(3.13)** is converted to the aryllithium reagent using two equivalent of *t*-BuLi, upon which half an equivalent of ethyl formate is added to produce **(3.14)**. Oxidation of **(3.14)** with Collin's reagent gives the subsequent carbinol **(3.15)**, which is then deprotected using a catalytic amount of concentrated hydrochloric acid in methanol to obtain the bis-catechol **(3.16)**.

The bis-catechol **(3.16)** is then reacted with two equivalents of **LZn(OH)** to give the complex $(Tp^{Cum,\ Me}Zn)_2$-OMe, **(3.17)**, as shown in Scheme III.7. From the lack of fine structure in the EPR at 77K, the appearance of O-H stretching in the IR at 3420 cm^{-1}, and lack in appearance of C-O semiquinone stretching we concluded that complex **(3.17)** was not obtained. The green/white precipitate was then set-up for recrystallization; however, the solution underwent a color change from green to brown overnight. Several attempts to obtain crystals were unsuccessful leading us to believe that complex **(3.17)** is unstable in solution.

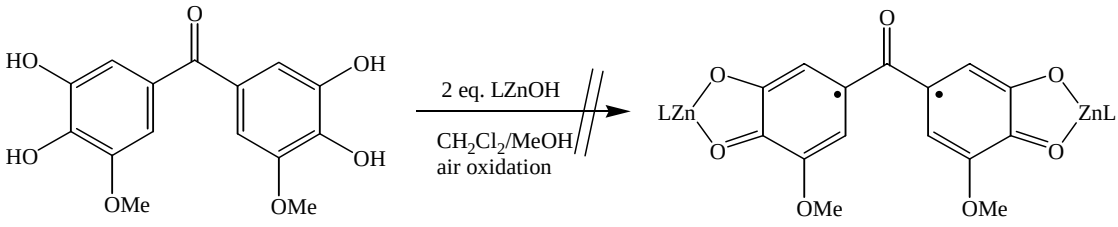

3.16 **3.17**

Scheme III.7. Attempted synthesis of complex **(3.17)**.

Upon oxidation of **(3.17)** with PbO_2 the triplet species grew in intensity while the monoradical/double quantum transition decreased in intensity, as shown in Figure III.31.

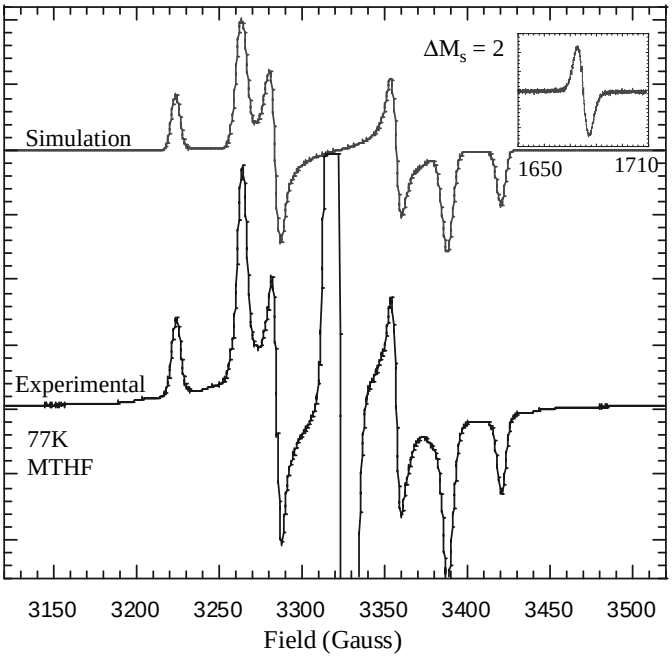

Figure III.31. Experimental EPR spectrum (77K; MTHF) of bis-semiquinone **(3.17)** (bottom) and the $\Delta M_s = 2$ transition near half field (inset). Simulated EPR spectrum with $|\mathbf{D}/hc| = 0.00919 cm^{-1}$ and $|\mathbf{E}/hc| = 0.000804 cm^{-1}$.

Due to the growing $\Delta M_s = 2$ transition near half field, and unsuccessful attempt to obtain pure **(3.17),** variable temperature EPR studies were done, Figure III.32. The Curie Law plot shows a linear relationship, $\mathbf{J} \geq 0$, which suggests that the two electron spins are

ferromagnetically coupled or there is a degeneracy of the singlet and triplet states. Unfortunately, the magnitude of the exchange coupling cannot be measured.

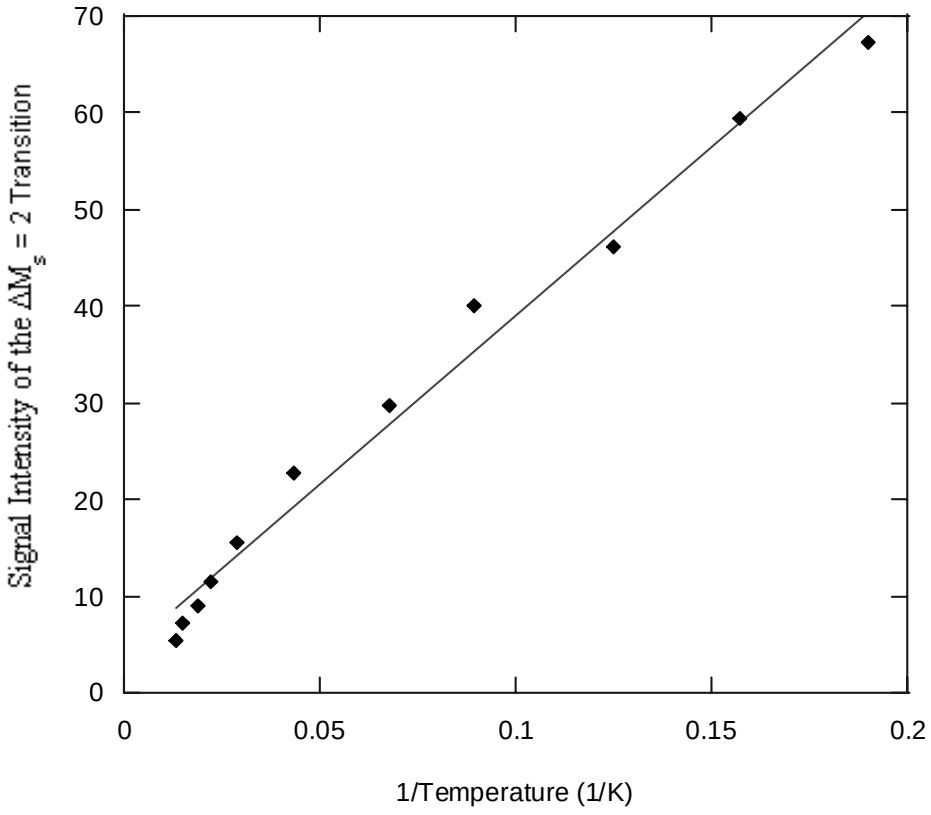

Figure III.32. Variable EPR studies on a mixture of **(3.17)** suggests ferromagnetic coupling of the two electron spins.

Even with several attempts to use radical anion semiquinones to couple two electrons spins through a carbonyl-linker, we were unsuccessful in obtaining the magnitude of the exchange coupling. We believe that the two electron spins are ferromagnetically coupled from the series of data obtained but synthetic and crystallization techniques need to be overcome. Several techniques are underway in the Shultz group to produce pure metal-ligand ions to ensure effective chelation.

Chapter III References.

3.1 Salem, L. *Molecular Orbital Theory of Conjugated Systems*; W.A. Benjamin Inc.: New York, 1966.

3.2 Shaad, L. J.; Hess, B. A. *J. Org. Chem.* **1981**, *46*, 1909. Hirano, T.; Kumagai, T.; Miyashi, T. *J. Org. Chem.* **1991**, *56*, 1907. Matlin, A. R.; Lahti, P. M.; Appella, D. *J. Am. Chem. Soc.* **1999**, *121*, 2164. Osamura, Y.; Borden, W. T.; Morokuma, K. *J. Am. Chem. Soc.* **1984**, *106*, 5112. Ichimura, A. S.; Lahti, P. M.; Matlin, A. R.; *J. Am. Chem. Soc.* **1990**, *112*, 2868. Coolidge, M. B.; Yamashita, K.; Morokuma, K.; Borden, W. T. *J. Am. Chem. Soc.* **1990**, *112*, 1751. Powell, H. K.; Borden, W. T. *J. Org. Chem.* **1995**, *60*, 2654. Borden, W. T. *Diradicals*; John Willey and Sons: New York, 1982

3.3 Shultz, D. A.; Sandberg, K. A. *J. Phys. Org. Chem.* **1998**, *11*, 819.

3.4 Ruf, M.; Vahrenkamp, H. *Inorg. Chem.* **1996**, *35*, 6571.

3.5 Pierpont, C.G.; Yee, G.T.; Groner, M.D. Noll, B.C.; Ruf, M. *Inorg. Chem.* **1997**, *36*, 4860.

3.6 Shultz, D. A.; Bodnar, S. H.; Kumar, R. K.; Kampf, J. W. *J. Am. Chem. Soc.*

1999, *121*, 10664. Shultz, D. A.; Bodnar, S. H.; Kampf, J. W. *Chem. Commun.* **2001**, 93.

Shultz, D.A.; Dei, A.; Lee, H.; Sorace, L.; *Inorg. Chem.* **2001**, *40*, 408.

3.7 Shultz, D. A.; Bodnar, S. H.; Vostrikova, K. E.; Koo, H.; Whangbo, M.;

Kirk, M. L.; Depperman, E. C.; Kampf, J. W. *J. Am. Chem. Soc.* **2003**.

3.8 Benelli, C.; Gatteschi, D.; Pardi, L. *Inorg. Chem.* **1990**, *29*, 3409.

3.9 Dowd, P. *J. Am. Chem. Soc.* **1966**, *88*, 2587. Dixon,D. A.; Dunning, T. A.;

Eades, R. A.; Kleier, D. A. *J. Am. Chem. Soc.* **1981**, *103*, 2878.

3.10 Shultz, D. A. *Synthetic Metals* **2001**, *122*, 495.

3.11 Bodnar, S. H.; *Ph.D. Dissertation*, N. C. State, 2002**.**

3.12 Shultz, D. A.; Lee, H.; Fico, R. M. *Tetrahedron* **1999**, *55*, 12079.

Shultz, D. A.; Boal, A. K.; Lee, H.; Farmer, G. T.; *J. Org. Chem.* **1999**, *64*, 4386. Shultz, D. A.; Boal, A. K.; Lee, H.; Farmer, G. T.; *J. Org. Chem.* **1998**, *63*, 9462.

3.13 Shultz, D. A.; Bodnar, S. H.; Kampf, J. W.; *Chem. Commun.* **2001**, 93.

3.14 Shultz, D. A.; Bodnar, S. H.; Kumar, R. K.; Lee, H., Kampf, J. W.;

Inorg. Chem. **2001**, *40*, 546.

3.15 Lahti, P. M.; Ling, C.; Minato, M.; Willigen, H. *J. Am. Chem. Soc.* **1992**, *114*, 9959.

3.16 Brüker *WINEPR SimFonia*, 1.25 shareware version; Brüker Analytische

Messtechnik GmbH: Rheinstetten, Germany, 1996.

3.17 Lutz, H. D.; Becker, R. A.; Eckers, W.; Hölscher, B.; Berthold, H. J. S*pectrochimica*

Acta. **1983**, *39A*, 7.

3.18 March, J. *Advanced Organic Chemistry; Reaction, Mechanisms, and Structure*;

John Wiley & Sons: New York, 1992.

EXPERIMENTALS

All chemicals were purchased from Aldrich chemical company unless otherwise stated. Methylene Chloride was distilled over CaH_2, tetrahydrofuran was distilled over sodium metal with a benzophenone indicator, methanol was distilled over CaH_2, ethyl formate was distilled over CaH_2, and pyridine was distilled over CaH_2.

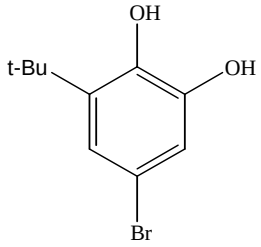

3-*tert*-butyl-4,5-dihydroxy-bromobenzene. A stirred solution of 3-*tert*-butyl-4,5-dimethoxy-bromobenzene (1.05 g, 3.84 mmol) in dry CH_2Cl_2 was cooled to -78°C. Boron tribromide (1.82 mL, 19.22 mmol) was added dropwise to the solution. The solution was let to stir for one hour at -78°C then for 19 hours at room temperature. The mixture was poured over ice into a saturated sodium chloride solution, extracted, and dried over Na_2SO_4. The mixture was concentrated and put under vacuum for one hour. No purification due to instability in air for long periods of time (0.766g crude).

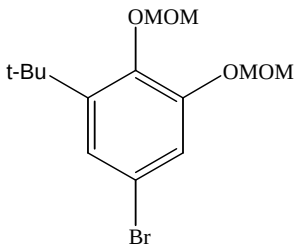

(3.1)

5-Bromo-1-*tert*-butyl-2,3-bis-methoxymethoxy-benzene (3.1). Molecule (**3.1)** was previously synthesized and characterized.[E.1] A stirred solution of 3-*tert*-butyl-4,5-dihydroxy-bromobenzene (0.766 g, 3.13 mmol) and DMAP (0.114 g, 0.94 mmol) in dry CH_2Cl_2 was cooled to O°C. Hunig's base (3.27 mL, 18.77 mmol) was added dropwise to the solution. After an hour, chloromethyl methyl ether (0.95 mL, 12.52 mmol) was added dropwise to the solution. The mixture was let to stir at O°C for an hour then warmed to room temperature to reflux for overnight under N_2. The mixture was quenched with a saturated sodium chloride solution, extracted, then dried over Na_2SO_4. The sample was purified using radial chromatography (SiO_2, 30-40% ethyl ether/petroleum ether containing 1% TEA) to give a yellow oil (0.434 g, 42%). ^{1}H NMR ($CDCl_3$) δ (ppm): 7.18 (d, 1H, J = 2Hz), 7.10 (d, 1H, J = 2.4Hz), 5.16 (s, 2H), 5.15 (s, 2H), 3.64 (s, 3H), 3.50 (s, 3H), 1.39 (s, 9H). ^{13}C NMR ($CDCl_3$) δ (ppm): 151.04, 145.40, 145.39, 123.86, 120.87, 117.98, 115.86, 115.07, 99.24, 95.62, 57.83, 56.59, 30.55, 30.53.

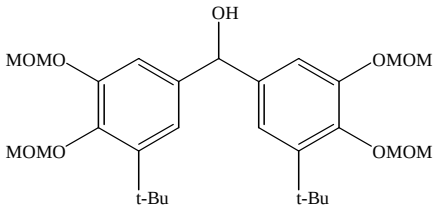

(3.6)

Bis-(*3-tert*-butyl-4,5-bis-methoxymethoxy-phenyl)-methanol (3.6). Molecule **(3.6)** was previously synthesized and characterized.[E.1] A stirred solution of **(3.1)** (2.07 g, 6.23 mmol) in dry THF was cooled to -78°C. *Tert*-butyllithium (1.7 M, 7.3 mL) was added dropwise to the solution. After an hour, ethyl formate (0.25 mL, 3.12 mmol) was added to the mixture dropwise. The mixture was warmed to room temperature and stirred overnight under N_2. The mixture was quenched with saturated sodium chloride solution and extracted with ethyl ether then dried over Na_2SO_4. The sample was purified using radial chromatography (SiO_2, 30-100% ethyl ether/petroleum ether containing 1% TEA) to give a yellow oil (1.54 g, 92%). ^{1}H NMR ($CDCl_3$) δ (ppm): 7.07 (d, 2H, *J* = 2Hz), 7.02 (d, 2H, *J* = 2Hz), 5.68 (d, 1H, *J* = 3.2Hz), 5.18 (s, 4H), 5.15 (s, 4H), 3.64 (s, 6H), 3.48 (s, 6H), ?.??(s, 1H), 1.39 (s, 18H). ^{13}C NMR ($CDCl_3$) δ (ppm): 150.26, 145.40, 143.45, 138.63, 119.07, 113.19, 99.18, 95.57, 76.50, 57.76, 56.50, 35.44, 30.71. IR (film from CH_2Cl_2) ν (cm^{-1}): 3458.

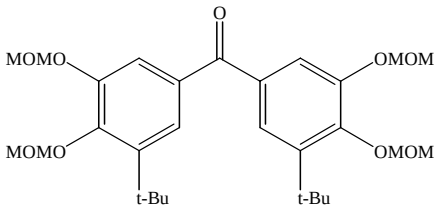

(3.7)

Bis-(3-*tert*-butyl-4,5-bis-methoxymethoxy-phenyl)-methanone (3.7). Molecule **(3.7)** was previously synthesized and characterized.[E.1] A solution with CrO_3 (1.57 g, 15.66 mmol) and pyridine (2.52 mL, 31.32 mmol) in dry CH_2Cl_2 was coolded to O°C. After 30 minutes, a solution of **(3.6)** (1.40 g, 2.61 mmol) was cannulated into the CrO_3/pyridine mixture and stirred for two hours at room temperature. The reaction mixture was poured into a 1M NaOH solution, and the organic layer was extracted. The organic layer was then washed with saturated NaCl solution, extracted, then dried over Na_2SO_4. The sample was purified using radial chromatography (SiO_2, 20-50% ethyl ether/petroleum ether containing 1% TEA) to give a brown-white solid (1.15 g, 82%). ^{1}H NMR ($CDCl_3$) δ (ppm): 7.51 (d, 2H, J = 2Hz), 7.50 (d, 2H, J = 2Hz), 5.31 (s, 4H), 5.21 (s, 4H), 3.67 (s, 6H), 3.51 (s, 6H), 1.43 (s, 18H). ^{13}C NMR ($CDCl_3$) δ (ppm): 194.85, 150.07, 149.69, 143.03, 132.39, 123.69, 116.34, 99.41, 95.50, 57.95, 56.71, 35.55, 30.56. IR (film from CH_2Cl_2) ν (cm^{-1}): 1648.

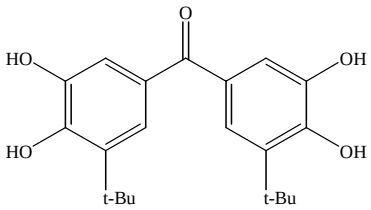

(3.3)

Bis-(3-*tert*-butyl-4,5-dihydroxy-phenyl)-methanone (3.3). Molecule **(3.3)** was previously synthesized and characterized.[E.1] A stirred solution of **(3.7)** (0.098 g, 0.20 mmol) in dry methonal was let to stir for ten minutes. Four drops of concentrated hydrochloric acid was added to the mixture then refluxed for 19hours under N_2. ^{1}H NMR ($(CD_3)_2CO$) δ (ppm): 7.31 (d, 2H, *J* = 2Hz), 7.29 (d, 2H, *J* = 2Hz), 1.42 (s, 18H). ^{13}C NMR (CD_3OD) δ (ppm): 197.29, 149.21, 144.68, 135.02, 128.36, 121.86, 114.00, 34.53, 28.66.

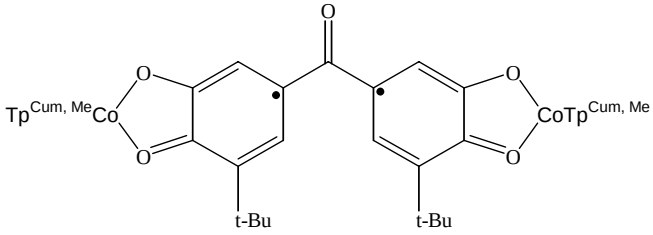

(Tp$^{Cum, Me}$Co)2-*t*-Bu

Cobalt(II)-bis-semiquinone ((Tp$^{Cum, Me}$Co)$_2$*t*-Bu), (3.8). A stirred solution of potassium tris-(3-*p*-cumenyl-5-methyl-pyrazolyl)borate (0.094g, 0.111mmol) and cobalt perchlorate hexahydrate (0.040g, 0.111mmol) in dry CH_2Cl_2 and nitrogen saturated MeOH was let to stir

for 20 minutes. Upon addition of **(3.3)** (0.020g, 0.056mmol) the solution turned sea blue in color. After an hour, triethylamine (0.1mL) was added to the solution that turned dark green. Air was bubbled through the solution for 20 hours, then filtered to obtain a dark green powder (0.04 g, 84% by weight). Upon crystallization from CH_2Cl_2/MeOH obtained green square crystals (0.0035 g, 7%). IR (film from CH_2Cl_2) ν (cm^{-1}): 2958, 2539, 1548, 1519, 1434.

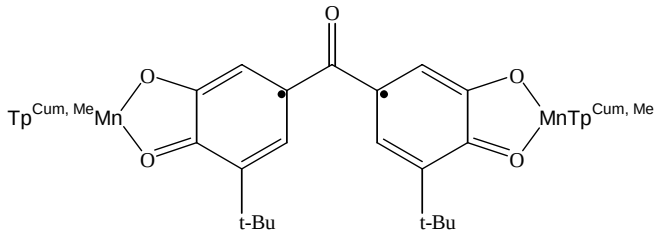

(Tp$^{Cum, Me}$Mn)2-*t*-Bu

Mn(II)-bis-semiquinone ((Tp^{Cum,Me}Mn)$_2$*t*-Bu), (3.9). A stirred solution of potassium tris-(3-*p*-cumenyl-5-methyl-pyrazolyl)borate (0.094 g, 0.111 mmol) and manganese perchlorate hexahydrate (0.040 g, 0.111 mmol) in dry CH_2Cl_2 and nitrogen saturated MeOH was let to stir for 20 minutes. Upon addition of **(3.3)** (0.020 g, 0.056 mmol) the solution turned brown in color. After one hour, triethylamine (0.1 mL) was added to the solution which turned dark green-brown. Air was bubbled through the solution for 20 hours, then filtered to obtain a dark green powder. Upon crystallization from CH_2Cl_2/MeOH obtained brown/green material (0.012 g, 8%). IR (film from CH_2Cl_2) ν (cm^{-1}): 2957, 2558, 1549, 1520, 1427.

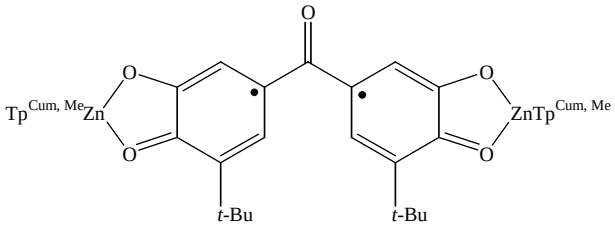

(Tp$^{Cum, Me}$Zn)2-*t*-Bu

Zn(II)-bis-semiquinone ((Tp$^{Cum, Me}$Zn)$_2$-*t*-Bu). A stirred solution of zinc hydroxide potassium tris-(3-*p*-cumenyl-5-methyl-pyrazolyl)borate (0.02 g, 0.03 mmol) and **5b** (0.053 g, 0.15 mmol) in dry CH_2Cl_2 and nitrogen saturated MeOH stirred for one hour. Air was bubbled through the mixture for one day then filtered to give a light green precipitate (0.025 g, 97% by weight). IR (film from CH_2Cl_2) ν (cm^{-1}): 3420, 2958, 2543, 1625, 1518, 1426.

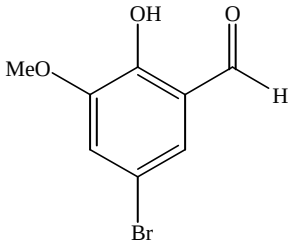

(3.11)

5-Bromo-2-hydroxy-3-methoxy-benzaldehyde (3.11). A stirred solution of o-vanillan (11.10g, 72.96mmol) and sodium acetate (9.1g, 110.89 mmol) in glacial acetic acid was let to stir at room temperature for 30 minutes. Bromine (3.94 mL, 76.60 mmol) was added dropwise to the solution. After an hour, the solution was evaporated to dryness and the yellow-white solid was redissolved in CH_2Cl_2. The organic layer was then extracted from deionized water and dried over Na_2SO_4. The sample was recrystallized from acetic acid/water to give yellow needle-like crystals (10.02 g, 59%). ^{1}H NMR ($CDCl_3$) δ (ppm):

11.02 (s, 1H), 9.86 (s, 1H), 7.32 (d, 1H, *J* = 2.4Hz), 7.18 (d, 1H, *J* = 1.6Hz), 3.92 (s, 3H). ^{13}C NMR ($CDCl_3$) δ (ppm): 195.63, 151.14, 149.53, 126.35, 121.54, 120.99, 119.79, 118.12, 111.28, 56.77. IR (film from CH_2Cl_2) ν (cm^{-1}): 2359, 1651.

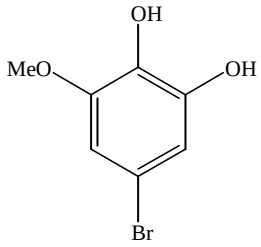

(3.12)

5-Bromo-3-methoxy-benzene-1,2-diol (3.12). A stirred solution of **(3.11)** (9.699g, 38.26mmol) in 2% sodium hydroxide (459 mL, 114 mmol) solution was cooled to 0°C. After 20 minutes, 30% hydrogen peroxide (21.69 mL, 266 mmol) solution was added dropwise to the reaction mixture. After 90 minutes, 12M HCl was added to the flask and the mixture was extracted four times with methylene chloride. The organic layer was then extracted from saturated Na_2SO_3 two times and then dried over Na_2SO_4. The sample was evaporated to dryness to give a brown-white solid (4.60g, 55%). ^1H NMR ($CDCl_3$) δ (ppm): 6.77 (d, 1H, *J* = 2.4Hz), 6.61 (d, 1H, *J* = 2.4Hz), 5.39 (s, 1H), 5.35 (s, 1H), 3.86 (s, 3H). ^{13}C NMR ($CDCl_3$) δ (ppm): 147.78, 144.79, 131.99, 112.66, 112.04, 107.31, 56.67. IR (film from CH_2Cl_2) ν (cm^{-1}): 3412.

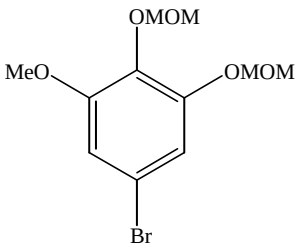

(3.13)

3-methoxy-4,5-bis-methoxymethoxy-bromobenzene (3.13). A stirred solution of **(3.12)** (4.60 g, 21.01 mmol) and DMAP (0.77 g, 6.3 mmol) in dry CH_2Cl_2 was cooled to 0°C. Hunig's base (22 mL, 126.04 mmol) was added dropwise to the mixture. After an hour chloromethyl methyl ether (6.4 mL, 84.03 mmol) was added dropwise to the mixture. The mixture was let to stir for an hour at 0°C then warmed to room temperature to reflux overnight under N_2. The mixture was quenched with a saturated sodium chloride solution and the organic layer was extracted then dried over Na_2SO_4. The sample was purified using radial chromatography (SiO_2, 15% ethyl ether/petroleum ether containing 1% TEA) to give a yellow liquid (5.45 g, 85%). ^{1}H NMR ($CDCl_3$) δ (ppm): 6.96 (d, 1H, *J* = 2.4), 6.75 (d, 1H, *J* = 2.4), 5.16 (s, 2H), 5.08 (s, 2H), 3.82 (s, 3H), 3.58 (s, 3H), 3.49 (s, 3H). ^{13}C NMR ($CDCl_3$) δ (ppm): 154.23, 151.79, 135.00, 116.56, 112.80, 110.07, 98.41, 95.51, 57.25, 56.41, 56.33. Anal. Calcd for $C_{11}H_{15}O_5Br$: C, 43.02; H, 4.92. Found: C, 43.54; H, 4.92.

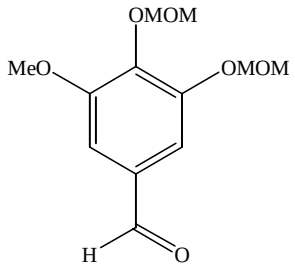

3-Methoxy-4,5-bis-methoxymethoxy-benzaldehyde. A stirred solution of **(3.13)** (0.083 g, 0.272 mmol) in dry THF was cooled to -78°C. A 1.7M solution of *tert*-butyllithium (0.32 mL, 0.545 mmol) was added dropwise to the solution. After an hour, dimethylformamide (0.21 L, 2.7 2mmol) was added dropwise to the mixture. The mixture was let to stir for an hour at -78°C then warmed to room temperature to stir for 22 hours under N_2. The mixture was quenched with saturated sodium chloride solution and extracted three times with ethyl ether then dried over Na_2SO_4. The sample was purified using radial chromatography (SiO_2, 10%-100% ethyl ether/petroleum ether containing 1% TEA) to give a yellow oil (0.046 g, 25%). ^{1}H NMR ($CDCl_3$) δ (ppm): 9.86 (s, 1H), 7.34 (d, 1H, J = 2Hz), 7.19 (d, 1H, J = 2Hz), 5.27 (s,2H), 5.23 (s, 2H), 3.92 (s, 3H), 3.61 (s, 3H), 3.51 (s, 3H).

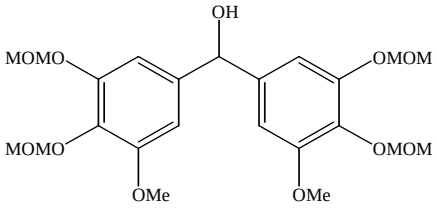

(3.14)

Bis-(3-methoxy-4,5-bis-methoxymethoxy-phenyl)-methanol (3.14). A stirred solution of **(3.13)** (4.75 g, 15.49 mmol) in dry THF was cooled to -78°C. *Tert*-butyllithium (1.7 M, 18.22 mL) was added dropwise to the solution over an hour period. After an hour, ethyl formate (0.63 mL, 7.75 mmol) was added to the mixture dropwise. After an hour, the mixture was let warm to room temperature and stirred overnight. The solution was quenched with saturated sodium chloride and extracted with ethyl ether then dried over Na_2SO_4. The sample was purifed using radial chromatography (SiO_2, 30-90% ethyl ether/petroleum ether containing 1% TEA) to give a light yellow oil (3.17 g, 85%). ^{1}H NMR ($CDCl_3$) δ (ppm): 6.83 (d, 2H, *J* = 2Hz), 6.66 (d, 2H, *J* = 1.6Hz), 5.66 (s, 1H), 5.17 (d, 4H, *J* = 2Hz), 5.11 (s, 4H), 3.814(s, 6H), 3.60 (s, 6H), 3.482(s, 6H), 2.44 (s, 1H). ^{13}C NMR ($CDCl_3$) δ (ppm): 153.34, 150.64, 140.76, 134.64, 107.73, 104.55, 98.35, 95.344, 75.40, 56.95, 56.10, 55.90. IR (film from CH_2Cl_2) ν (cm^{-1}): 3454. Anal. Calcd for $C_{23}H_{32}O_{11}$: C, 57.02; H, 6.66. Found: C, 56.93; H, 6.71.

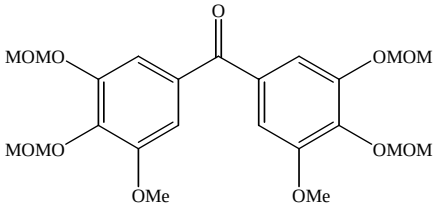

(3.15)

Bis-(3-methoxy-4,5-bis-methoxymethoxy-phenyl)-methanone (3.15). A solution with CrO_3 (2.97 g, 29.74 mmol) and pyridine (4.79 mL, 59.74 mmol) in dry CH_2Cl_2 was let to stir for 30 minutes at O°C. A solution of **(3.14)** (2.40 g, 4.96 mmol) was cannulated into the CrO_3/pyridine mixture and stirred for 90 minutes at room temperature. The reaction mixture was poured into a 1M NaOH solution, and the organic layer was extracted. The organic layer was then washed with a saturated NaCl solution, extracted, and dried over Na_2SO_4. The sample was purified using radial chromatography (SiO_2, 30-40% ethyl ether/petroleum ether containing 1% TEA) to give a white crystalline solid (2.35 g, 98%). ^{1}H NMR ($CDCl_3$) δ (ppm): 7.27 (d, 2H, *J* = 1.6Hz), 7.17 (d, 2H, *J* = 2Hz), 5.24 (s, 4H), 5.22 (s, 4H), 3.90 (s, 6H), 3.63 (s, 6H), 3.49 (s, 6H). ^{13}C NMR ($CDCl_3$): 194.12, 153.53, 150.42, 139.66, 133.12, 112.12, 108.23, 98.56, 95.44, 57.47, 56.5, 56.40. IR (film from CH_2Cl_2) ν (cm^{-1}): 1650. Anal. Calcd for $C_{23}H_{30}O_{11}$: C, 57.26; H, 6.27. Found: C, 57.62; H, 6.33.

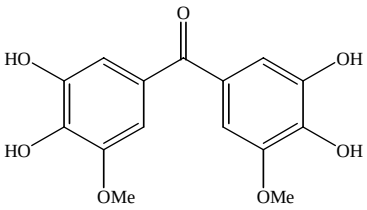

(3.16)

Bis-(3,4-dihydroxy-5-methoxy-phenyl)-methanone (3.16). A stirred solution of **(3.15)** (0.098 g, 0.20 mmol) in dry MeOH was let to stir for ten minutes. Four drops of concentrated hydrochloric acid was added to the mixture then refluxed for 19hours under N_2. The methanol was evaporated off to give a green film. ^{1}H NMR (CD_3OD) δ (ppm): 6.97 (d, 2H, J = 2.1Hz), 6.94 (d, 2H, J = 2.1Hz), 3.88 (s, 6H). ^{13}C NMR (CD_3OD): 196.07, 147.97, 144.80, 139.13, 128.52, 112.01, 105.59, 55.50. MS: $C_{15}H_{14}O_7$ calcd M + 1 mass 307.1. obsd 307.08.[E.2]

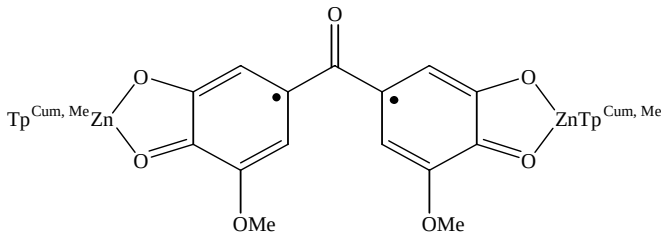

((Tp$^{Cum, Me}$Zn)$_2$OMe)

Zn(II)-bis-semiquinone ((Tp$^{Cum, Me}$Zn)$_2$OMe), (3.17). A stirred solution of potassium tris(-3-*p*-cumenyl-5-methyl-pyrazolyl)borate (0.222 g, 0.35 mmol) and zinc perchlorate hexahydrate (0.129 g, 0.35 mmol)in dry CH_2Cl_2 and nitrogen saturated MeOH was let to stir for ten minutes. A stirred solution of **(3.16)** (0.053 g, 0.17 mmol) in dry methylene chloride and nitrogen saturated methanol with four drops of triethlyamine was cannulated into the reaction mixture. Air was bubbled through the mixture for 24 hours then filtered to give a light green precipitate (0.230 g, 81% by weight).

Experimental References

E.1 Shultz, D. A., Bodnar, S. H., Kumar, R. K., Lee, H., Kampf, J. W., *Inorg. Chem.*, **2001**, *40*, 546.

E.2 Mass spectra were obtained at the Mass Sepctrometry Laboratory for Biotechnology. Partial funding for the Facility was obtained from the North Carolina Biotechnology Center and National Science Foundation.